STUDY OF STRUCTURAL INTEGRITY OF INTERSTELLAR SPACECRAFT REACTION CHAMBER AND THRUST STRUCTURE IN SUPPORT OF PROJECT ICARUS

by

SRIKANTH K. REDDY

A thesis submitted to the

Graduate School-New Brunswick

Rutgers, The State University of New Jersey

in partial fulfillment of the requirements

for the degree of

Master of Science

Graduate Program in Mechanical and Aerospace Engineering

Written under the direction of

Dr. Haym Benaroya

and approved by

_____

_____

_____

New Brunswick, New Jersey

January, 2014

ABSTRACT OF THE THESIS

STUDY OF STRUCTURAL INTEGRITY OF INTERSTELLAR SPACECRAFT REACTION CHAMBER AND THRUST STRUCTURE IN SUPPORT OF PROJECT ICARUS

By Srikanth K. Reddy

Thesis Director: Dr. Haym Benaroya

This thesis supports studies of the international effort of Project Icarus, dedicated to the unmanned, interstellar exploration of nearby stellar systems within the next century. The target system is 5.9 light years away, with a required velocity of 12% the speed of light. This study primarily focuses on the structural analysis of the reaction chamber and supporting structure of the Icarus interstellar spacecraft, which will be powered by nuclear fusion reactions to achieve the required velocity and time-frame for the mission. First, a computational finite element analysis is conducted on the reaction chamber in terms of loading, vibration, and fatigue. Different configurations and assumptions are studied for the reaction chamber as well. Present-day manufacturing considerations are also taken into account, with a modest extrapolation for future manufacturing technologies that are currently not in existence. Next, the thrust supporting structure for the reaction chamber is incorporated into the analysis. This study serves as a precursor for the multi-level analysis into the eventual detailed design and production of an interstellar spacecraft, and is the first such study.

Acknowledgements

Dedication

To those who stand between us and harm's way on a daily basis, asking for nothing in return. Especially to those brothers and sisters-in-arms that made the ultimate sacrifice in defending our freedom. To the hope of all nations coexisting peacefully in the exploration and settlement of the cosmos, however foolishly optimistic, one can hope.

Table of Contents

Lists of Tables

List of Figures

1. Thesis Introduction

1.1 Motivation

The goal of this thesis is the study of the detailed design and manufacture of the reaction chamber and supporting thrust structure of the Project Icarus interstellar spacecraft. Project Daedalus [1] was a trade study published in 1978 proving the feasibility of interstellar travel (with a linear extrapolation of technologies that were currently not in existence at the time but seen to be developed within the next century). Project Icarus is treated as the detailed design and analysis of Project Daedalus, incorporating present-day technologies to a decades old study. This thesis specifically addresses the structural properties, namely the strength, stiffness, and elasticity of the reaction chamber and supporting thrust structure, providing the first such study of this chamber and structure.

A computational approach is taken in analyzing the reaction chamber. The finite element method is utilized to study responses to various types of loading on different possible configurations of the reaction chamber. Specifically, thermal loading in terms of resultant forces encountered from inertial confinement fusion (ICF) is explored. This resultant loading is analyzed for operational loading (tensile) and failure loading (compressive). However, effects from the radiation and the deep space environment on the chamber are not explored. Frequency analysis is also performed to study the natural modes of the chamber. The resultant loading from ICF and frequency analysis are performed on a singular shell model, as opposed to multiple shell configurations. Static loading is explored, but dynamic considerations dependent on the frequency and load are not analyzed in this study. This analysis is computationally analyzed from the 'ground

up', meaning that the properties of the reaction chamber are studied computationally by itself, before more features are added to the model. Thus, the gross behavior of the reaction chamber can be studied before complexities are added to the analysis.

The pursuit of interstellar travel may seem to some as too far reaching. However, it should be noted that the U.S. manned mission to the Moon started in its roots as a trade study.

1.2 Contribution to Icarus

As there are a myriad of different teams working on many aspects of Icarus (navigation, target star, fuel acquisition, nuclear fusion reactions, etc.), this thesis is intended to be a long-standing contribution in the specific design of the reaction chamber and thrust structure. A critical analysis is performed about assumptions taken during Project Daedalus, and preliminary assumptions taken during Project Icarus. Daedalus presented many theoretical calculations without rigorous examination, as it was a trade study to prove feasibility. For the first time, these assumptions are explored more rigorously from a mathematical and computational viewpoint, and a new set of assumptions are utilized when necessary to provide a robust support structure for the Icarus spacecraft that has taken into account all loading expected to be encountered.

Project Icarus is still in the very early design phase, and as such, various configurations of the starship are still being discussed. This thesis focuses on a certain configuration that may be used by the Icarus team. As parameters change (i.e., pulse repetition rate of firing of the nuclear fuel pellets), the Icarus team may view this analysis before making any structural changes to the reaction chamber or thrust structure. With the

detailed analysis backing this design, it may be used to enhance/eliminate other potential starship configurations as necessary.

Specifically, this thesis is the first computational study of the thrust structure. A static loading analysis of the reaction chamber is performed first. Then, a finite element model of the reaction chamber and thrust structure is created along with a discussion of the FEM methodology. This study is a foundation for future development. The finite element model includes assembly level displacement, stress, and frequency analyses. Finally, manufacturing methodologies and considerations are developed and discussed.

For the Project Icarus team, this thesis directly contributes to the following work modules: 3.0 Vehicle Configuration, 7.0 Structure and Materials, and 17.0 Vehicle Assembly. This analysis is conducted in the English system of units, and as Icarus is an international effort, care must be taken in conversions between unit systems (S.I. and English).

1.3 Outline

Chapter 2 starts with the basic design of the reaction chamber by itself, as a simple hemispherical model. A closed form approximate analysis is performed for comparison. No details are added to the reaction chamber at this stage in order to study the basic behavior of the reaction chamber as a base point. Present day materials are researched and specified for this model. The material properties are specified to the simulation.

Chapter 3 presents a closed form approximate solution and a finite element analysis of this model. The model is assumed to be fixed at the bottom of the reaction

chamber, and this assumption is carried through the various studies of this chapter. Tensile loading, compressive loading, and frequency analysis are performed on this configuration.

Chapter 4 introduces the pellet injector interface structure and the condition of the reaction chamber being fixed at this interface (top). A mixed mesh assembly analysis is conducted, modeling of the reaction chamber by shell elements and the pellet injector interface by solid elements. Tensile and compressive loading, as well as frequency analysis are performed on this new assembly.

Chapter 5 incorporates an integrally backed thrust structure to the assembly. This consists of 12 lateral braces and one bottom brace that would be attached directly to the reaction chamber. A shell mesh analysis is conducted of the reaction chamber, pellet injector interface, and thrust structure using shell elements. Tensile loading, compressive loading, and a modal analysis are performed on this assembly configuration.

Chapter 6 presents the addition of the induction loop, field coils (1 to 4), and the support tubular struts to the field coils. There are 12 tubular struts between the field coils for support, made from titanium. A mixed solid/shell analysis is conducted with surfaces converted into shells. The additional induction loop and field coils are treated as mid-surface shells. The tubular struts are treated as solids with surfaces treated as shells. Tensile and compressive loading, as well as a modal analysis, are performed on this final assembly configuration.

Chapter 7 presents a rendering of what a partial first stage assembly of this spacecraft may look like with all the analyzed components. A concept of what the parabolic reflector may look like is included. The chapter also describes a concept for

course-correction using actuators, showing the interface between the thrust structure and the parabolic reflector. The pellet injector and interface to the parabolic reflector is also added. This assembly is represented as a solid model for conceptual representation only (without any analysis performed on the additional parts).

Chapter 8 outlines manufacturing considerations, both present-day and linearly extrapolated future, that must be taken into account during the production of this starship. It also outlines any testing considerations that may be prudent to take in this endeavor.

The last chapter, Chapter 9, outlines recommendations for future work. As Project Icarus is aimed at production of an interstellar starship within the next century, assumptions and configurations must be regularly updated as technologies emerge.

2. Icarus Vehicle Configuration and Properties

2.1 Icarus Vehicle Configuration and Properties

The Icarus starship currently has a couple of favored designs and configurations, created by artists, architects, engineers, physicists, and those interested in interstellar travel. The design and configuration for the Icarus interstellar spacecraft used in this thesis is based on the original configuration from Project Daedalus. Figure 1 shows an isometric view of the spacecraft [2].
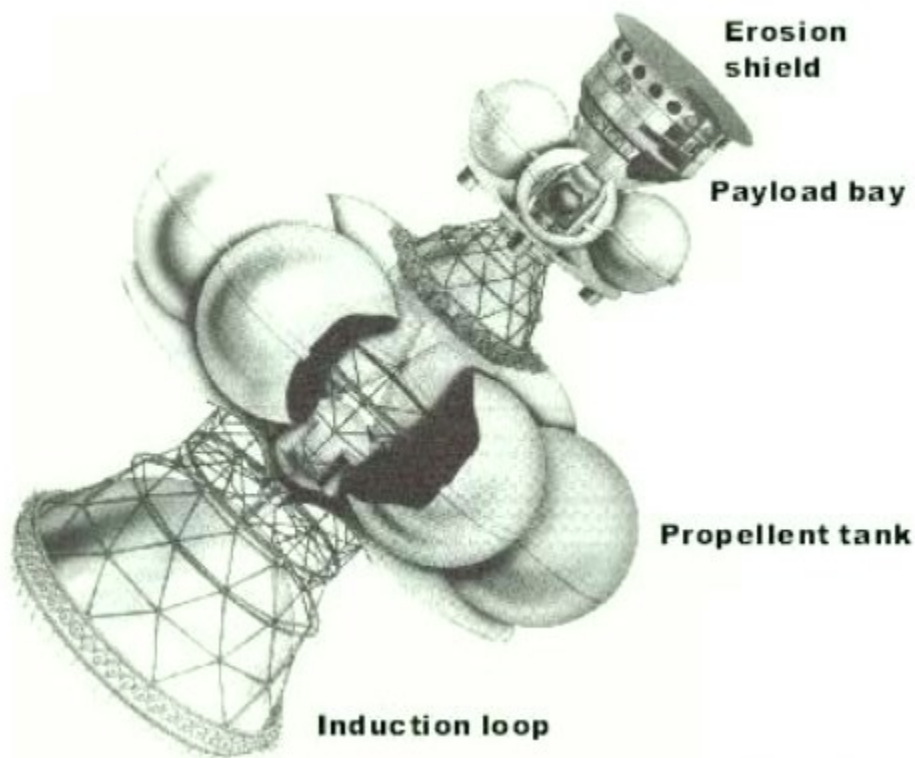
Figure 1: Isometric View of Icarus Interstellar Spacecraft used in Study

The Icarus starship consists of two stages, each with a separate reaction chamber and supporting structure. The first stage reaction chamber and thrust structure is studied in this thesis, as it experiences more severe loading and will be more challenging to

manufacture. The second stage reaction chamber and supporting structure is a scaled-down model of the first stage reaction chamber. Figure 2 shows a plan view of the first stage configuration from the original Project Daedalus configuration [1].
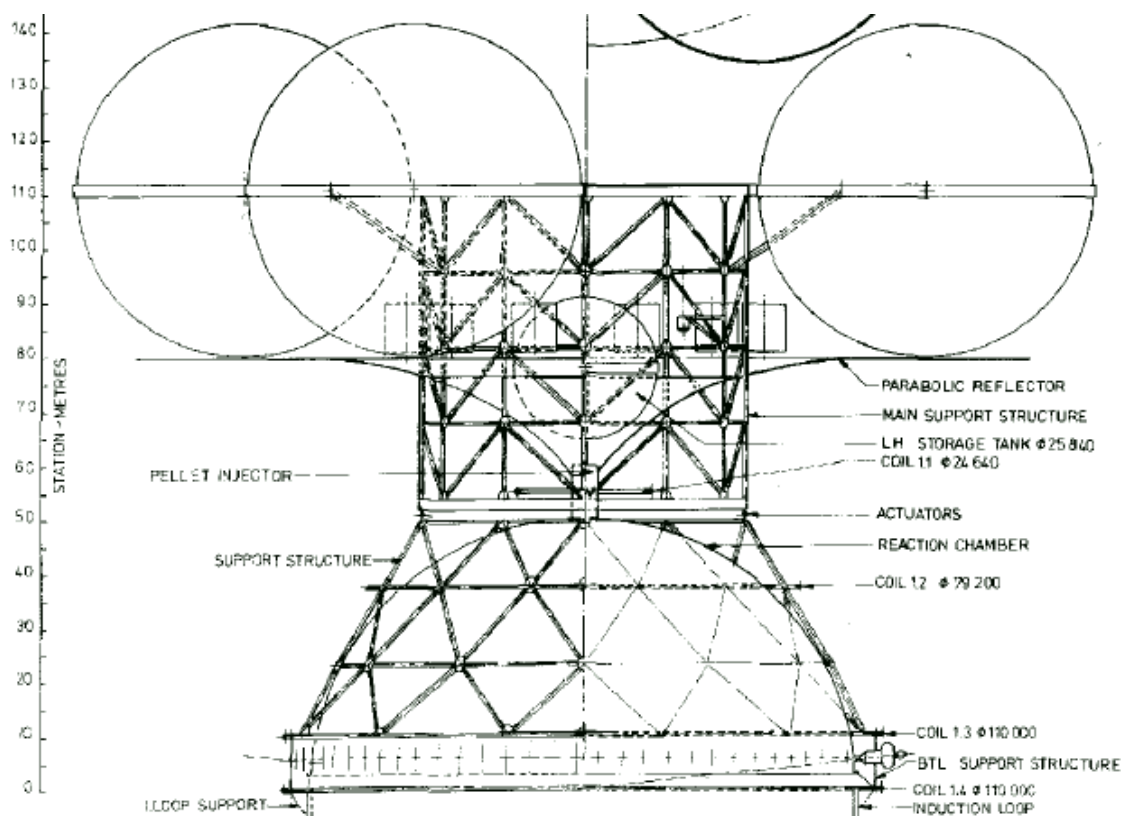
Figure 2: Icarus Starship First Stage Plan View

The reaction chamber and support structure can be clearly seen in this view. The relativistic electron beam generator and induction loop can be seen at the bottom of the reaction chamber in the plan view. This is where the finite element representation is rigidly fixed in the subsequent studies of this chapter. In Figure 2, this fixed boundary condition is around the periphery of the reaction chamber between coils 1.4 and the induction loop.

2.2 Material Choices

The next step after choosing the preferred starship configuration for a starting

point of the analysis was to research and specify a material for the reaction chamber. The

reaction chamber must have a low density for weight savings and fuel consumption

considerations. It must also have a high temperature capability as it is estimated that the

operating temperature of the reaction chamber would be near 1600 K, with the

temperature of deep space being close to absolute zero (0 K), and a very high electrical

conductivity to transmit the radiation from the nuclear fusion reactions into thrust [1].

Titanium-Zirconium-Molybdenum (TZM) alloy (also known as Molybdenum TZM,

Molybdenum TMZ, or TMZ alloy) was one of the materials of interest from the Daedalus

study. Figure 3 shows a rendering by the artist Adrian Mann of the proposed inertial

confinement fusion reaction.
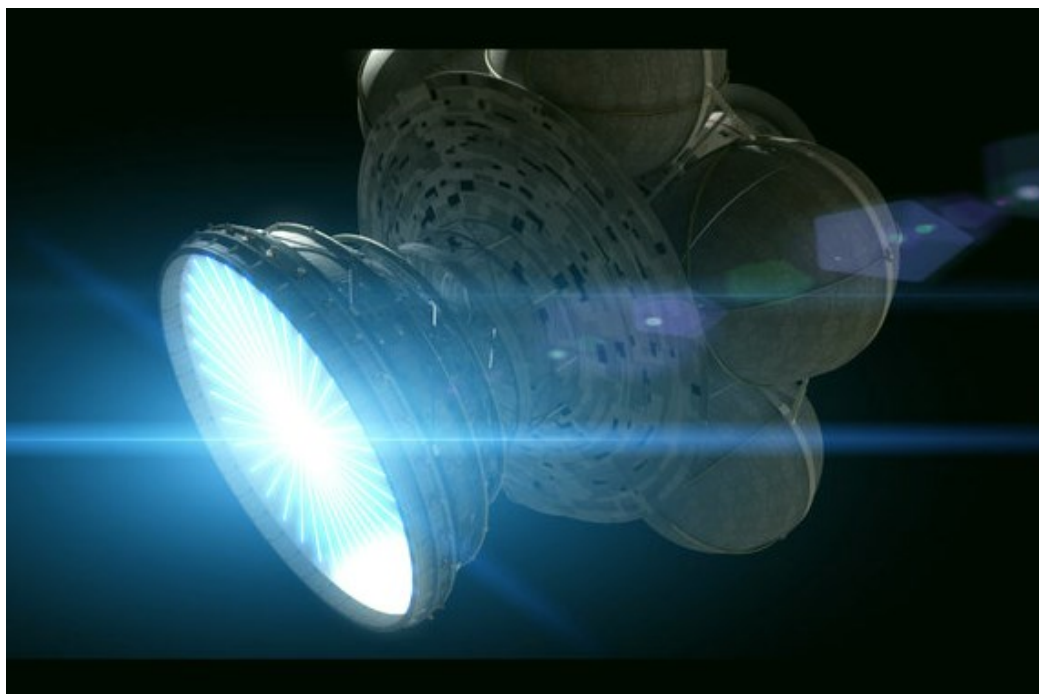
Figure 3: Artist Rendering of ICF

Materials development and research has come a long way from when the Project Daedalus study was published. After some research into comparable materials for the reaction chamber with the above characteristics, TZM alloy was chosen by the Rutgers team as a suitable initial alloy. The next step was to find commercially available TZM alloys, governed by manufacturing specifications (ASTM, ASM, MIL-STD, etc.). This would be used as a baseline if present-day materials would be suitable for the starship reaction chamber, or if additional research is necessary for a TZM alloy of different composition, or an entirely different alloy all together. This analysis will reveal whether the material is suitable or not, and in what aspects the properties might need refinement (higher temperature capability, stronger yield strength, etc.).

It is found that there is a commercial grade TZM available, governed by ASTM B386 and ASTM B387 [5, 6]. These two specifications correlate to the different forms of TZM that are commercially procurable in the following forms: plate, sheet, strip, foil, bar, rod, and wire. ASTM B386 would be the specification of interest that applies to plate, sheet, strip, and foil. Various alloy compositions are included in ASTM B386, and Type 363 and Type 364 would be the initial forms of interest for the reaction chamber. Type 363 is vacuum arc-cast with 0.5% titanium, 0.1% zirconium, and the balance molybdenum. Type 364 is powder metallurgy with 0.5% titanium, 0.1% zirconium, and the balance molybdenum [5]. The impact of production processes (vacuum arc-cast versus powder metallurgy) will be explored later in this thesis. For our immediate purposes, these two forms have the same chemical composition and mechanical properties for use in the analysis. The modulus of elasticity for TZM is 46 million psi.

For comparison, the modulus of elasticity for aluminum is 10 million psi and 30 million psi for carbon steel.

2.3 Structure Geometry and Mass

Initial reaction chamber properties were explored by the Daedalus team with preliminary calculations in Project Daedalus, including estimated thickness of the reaction chamber wall. The wall thickness is specified as 1.09 mm for the first stage reaction chamber [1]. The diameter of the reaction chamber is 100 meters [1]. We have adopted these values in this study.

Figure 4 shows a solid model of the reaction chamber built to these parameters, utilizing SolidWorks [7].
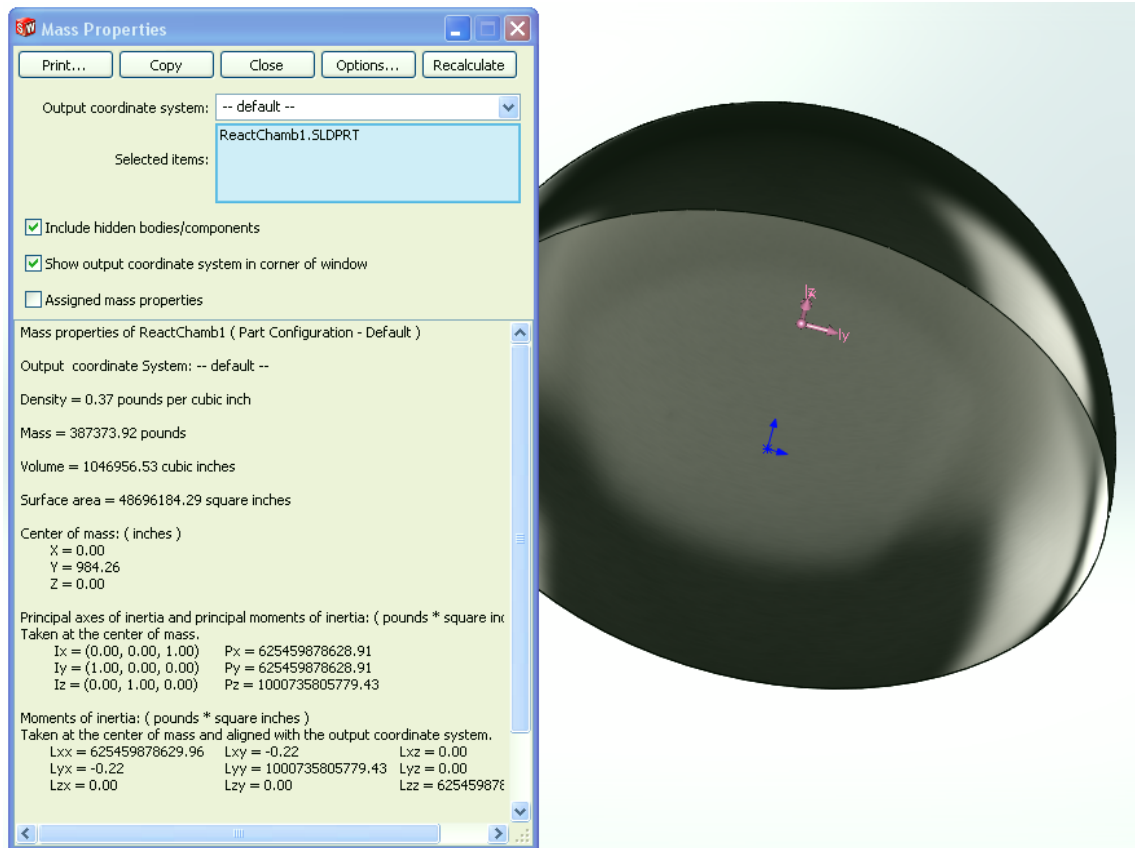
Figure 4: Reaction Chamber Solid Model

The calculated mass using SolidWorks mass properties at the specified wall thickness and diameter is 387,374 pounds. This differs from the weight calculated in Daedalus, which is 218.7 tonnes, or 482,151 pounds [1]. In Daedalus, the normal operating mode for the reaction chamber results in the chamber being in tension. If a fuel pellet fails to ignite, it is postulated that the reaction chamber will go into a compressive mode. It is feared that the dynamic stresses that result from this quick tensile to compressive mode will tear the reaction chamber given the small thickness of the wall. A preliminary design is constructed with a double walled chamber, held by internal ties and pressurized as to prevent the reaction chamber from going into compression [1]. This design and assumption will be investigated later in the thesis, but for preliminary calculations and investigations, the reaction chamber is modeled as a solid one-wall hemisphere. This double-wall and tie structure assumed in Daedalus accounts for the weight difference between the Daedalus calculated reaction chamber weight compared to the weight calculated in this model.

3. Reaction Chamber Finite Element Model Fixed at the Ignition Coil Interface (Bottom)

3.1 Closed Form Approximate Solution for Hemispherical Reaction Chamber

Consider a hemisphere fixed at its base as the model for the reaction chamber. The reaction chamber with an internal tensile load from the nuclear fuel detonation is modeled by membrane stresses in a thin-walled pressure vessel. More specifically, it is a uniform internal pressure with a tangential edge support around the bottom periphery of the reaction chamber. Figure 5 depicts a stress element in this hemispherical reaction chamber [17].
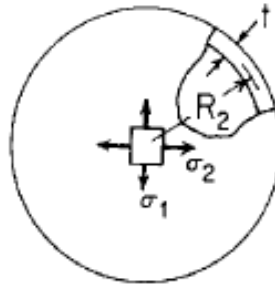
Figure 5: Stress Element of Hemisphere

Equation (3.1) is a statement of the thin-walled condition,

$$\frac{R_2}{t} > 10 \qquad (3.1)$$

For the reaction chamber, this ratio is 45,780. Figure 6 shows the direction of the loading compared with the geometry of the hemisphere.

Figure 6: Stress Relationships to Geometry of Reaction Chamber

Equation (3.2) is for the principal stress of this hemisphere,

$$\sigma_1 = \sigma_2 = \frac{qR_2}{2t} \qquad (3.2)$$

For the reaction chamber, this results in a principal stress of 3189 psi.

This stress from the closed form solution will be compared to the results from the finite element model of the reaction chamber in this chapter. For subsequent chapters where more structural elements and interfaces are analyzed and added to the finite element representations, a closed form solution would be not possible.

3.2 Finite Element Software Background

The finite element models in this thesis assume that all the materials within the model comply with Hooke's law, with stress being linearly proportional to strain, as shown in Figure 7.

Figure 7: Hooke's Law

All loading in our study induce linear responses. All boundary conditions are fixed during the load application. The loads remain constant after reaching their full magnitude [16].

Equation (3.3) is used by the Simulation software to calculate the constant displacements and stresses,

$$[K]\{u\} = \{f\} \qquad (3.3)$$

[K] represents the stiffness matrix, with {u} representing the displacement vector and {f} representing the force vector.

In this thesis, and in industry, the von Mises stress, σ_{vm}, is commonly used as the design parameter to verify that a design is safe. This is represented in Equation (3.4),

$$\sigma_{vm} < \sigma_y \qquad (3.4)$$

The von Mises stress is required to be below the yield limit of the material. This is the methodology used in this thesis. The calculation of the von Mises stress by the Simulation software is based on Equation (3.5),

$$\sigma_{vm} = \sqrt{\{(\sigma_1 - \sigma_2)^2 + (\sigma_2 - \sigma_3)^2 + (\sigma_1 - \sigma_3)^2\}} \qquad (3.5)$$

This is represented in terms of the principal stresses.

3.2.1 Discretization Procedure (Meshing)

Shell and solid elements are both used in this study for different components. The shell elements consist of parabolic, triangular elements. Figure 8 shows a representation of this element.
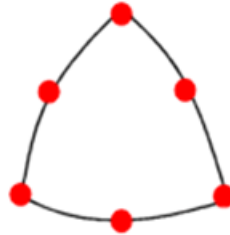
Figure 8: Parabolic, Triangular Shell Element

Each node has six degrees of freedom, three translation and three rotation. The parabolic

displacement function of the shell element allows the analyst to better map the geometry

of the structure. Shell elements are two-dimensional elements that can resist membrane

and bending loads. They are limited in interpretations of shear stresses. The thin shell

formulation in the software is used when the thickness-to-span ratio is less than 0.05. The

thin shell formulation treats bending as predominant and shear as negligible across the

thickness. In models with an interface between solid and shell elements, a mixed mesh is

used and preprocessing contact conditions are explicitly specified to constrain the

rotational degrees of freedom.

Shell surfaces may be created as mid-surface planes or as user specified surfaces

that are converted into shells by the software. In this thesis, mid-surface planes are used,

where two parallel planes are selected and a two-dimensional mid-surface plane is

created. The rendering of loads on the mid-surface plane are shown on the outside of the

surface, as opposed to directly on the surface that was chosen for the loading.

The solid element is comprised of parabolic, second-order, tetrahedral elements.

Figure 9 shows this element.
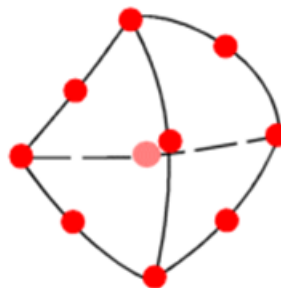
Figure 9: Parabolic, Second-Order, Tetrahedral Solid Element

This element consists of four corner nodes and six mid-side nodes. Each node has three

degrees of freedom in the translational directions. These elements provide better

mathematical approximations and represent curved boundaries more accurately than first-order elements.

3.3 Reaction Chamber Finite Element Model for Static Loading

Developing a finite element model of this reaction chamber, with a wall thickness of 0.043 inches and a diameter of 3937 inches poses many computational complexities. The thickness to radius ratio is 2.18×10^{-5}, or 2.18×10^{-3}%. It is good practice to have at least two elements spanning a thickness to correctly envelope part geometry. At the reaction chamber's thickness, a symmetrical portion of the solid model will result in hundreds of thousands of elements, and millions of degrees of freedom for the simulation. This is assuming symmetry of the loading and geometry of the reaction chamber (i.e., cutting the reaction chamber into a portion and using symmetry conditions). A full-scale reaction chamber would have exponentially more elements and degrees of freedom, and would take excessively long to develop and analyze. As such, models fitting the geometry of the reaction chamber are recommended to be evaluated as shell elements because the small thickness compared to radius would require a very small element size to span the thickness. This small element size would be unnecessary in the other directions as their dimensions are much greater. Shell elements are two-dimensional elements capable of resisting membrane and bending loads. Table 1 shows a summary of the details of the Reaction Chamber.

Reaction Chamber Details					
Weight (lbs)	Diameter (in)	Wall Thickness (in)	Material	Elastic Modulus (ksi)	Poisson Ratio
387374	3937	0.043	TZM Alloy	46000	0.38

Table 1: Reaction Chamber Details

Figure 10 shows the finite element model of the reaction chamber modeled in shell elements.
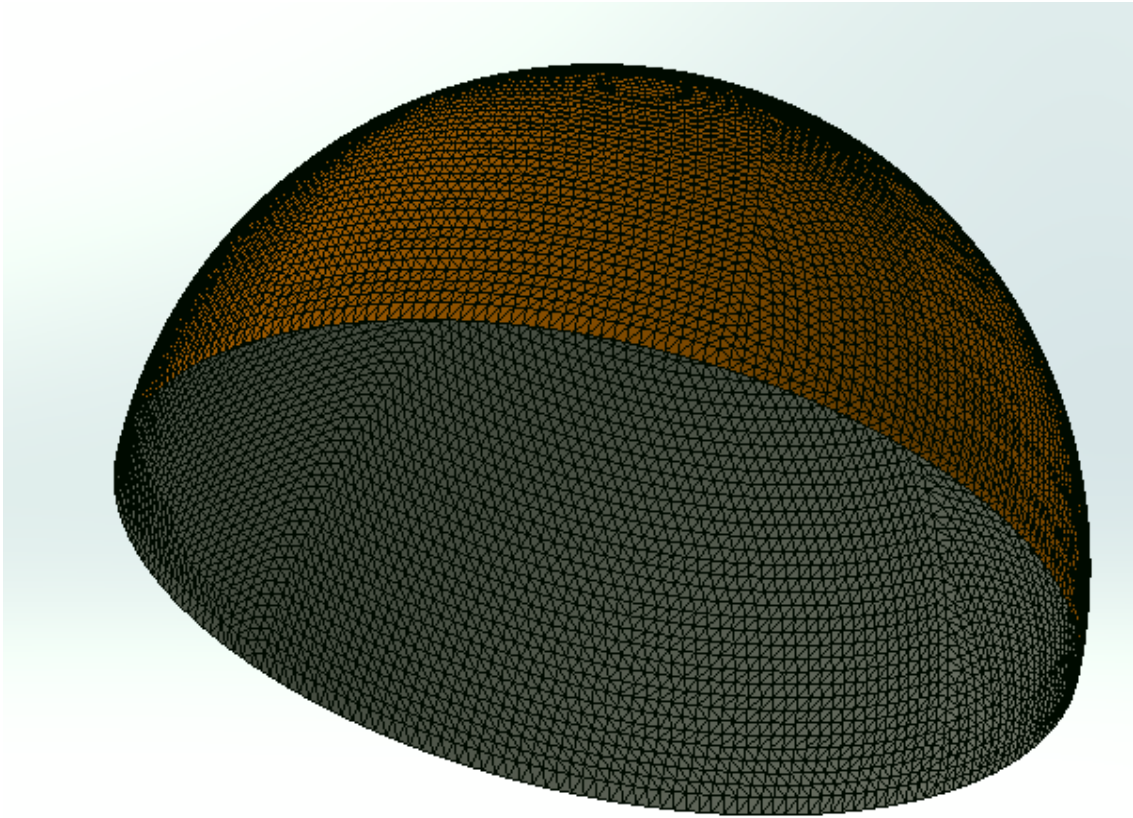
Figure 10: Finite Element Model of Reaction Chamber in Shell Elements

The utilization of shell elements results in 17,369 elements and 34,974 nodes, which is substantially less than attempting to use solid elements. The global mesh size is 52.89 inches. Since shell elements are treated as two-dimensional elements as opposed to three-dimensional solid tetrahedral elements, the reduction in magnitude of elements and nodes does not decrease accuracy. Rather, the analyst is able to assign more elements to properly span the rest of the geometry as opposed to redirecting elements to unnecessarily span the thickness.

3.3.1 Static Tensile (Operational) Loading

     The reaction chamber being in tension is considered the normal operating load on

the reaction chamber. Figure 11 shows the boundary conditions applied to the finite

element model using the SolidWorks Simulation [7] finite element analysis software

package.
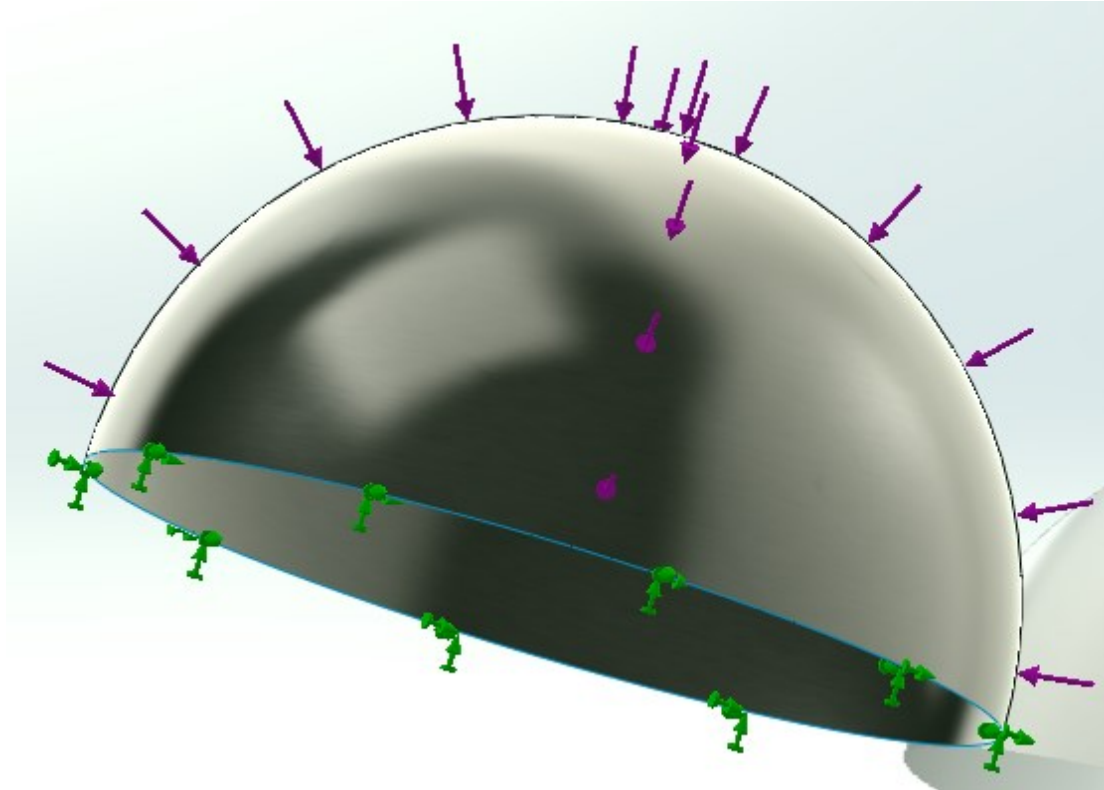
Figure 11: Static Tensile FEM Boundary Conditions

The green arrows represent a rigidly fixed boundary condition at the interface to the field

coils (bottom). This is rigidly fixed in all axes, assuming no translation or rotation at that

interface.

     The magenta arrows represent the tensile load of 1.696 million pounds-force

(pressure of 0.139 psi), as calculated in Daedalus as the equivalent thrust force from the

nuclear fusion reactions [1]. Shell elements do not allow the selection of a face for the

loading, as shell elements are treated as two-dimensional elements. Solid elements, on the other hand, will allow the selection of a specific face. The real-life loading on the reaction chamber would more accurately be represented by loading on the reaction chamber inner face, but the model chosen here is considered accurate to study the reaction chamber behavior.

The element size close to the fixed boundary condition around the periphery of the bottom of the reaction chamber should be small enough to capture the large moment gradients at the fixed end [17]. The gradient of the moment is proportional to Equation (3.6),

$$\sqrt{rt} \quad (3.6)$$

Therefore, if we were interested in the details at the boundary, our elements need to be of dimension on the order of 5% of 9.2 inches, or 0.5 inches. This mesh size was determined iteratively for the model until the moment gradients were captured appropriately. But since this section is preliminary to the actual model of interest, we do not enforce this mesh size.

The simulation model has 207,024 degrees of freedom. Resultant stresses are plotted as von Mises. Figure 12 shows the resultant von Mises stress plot.
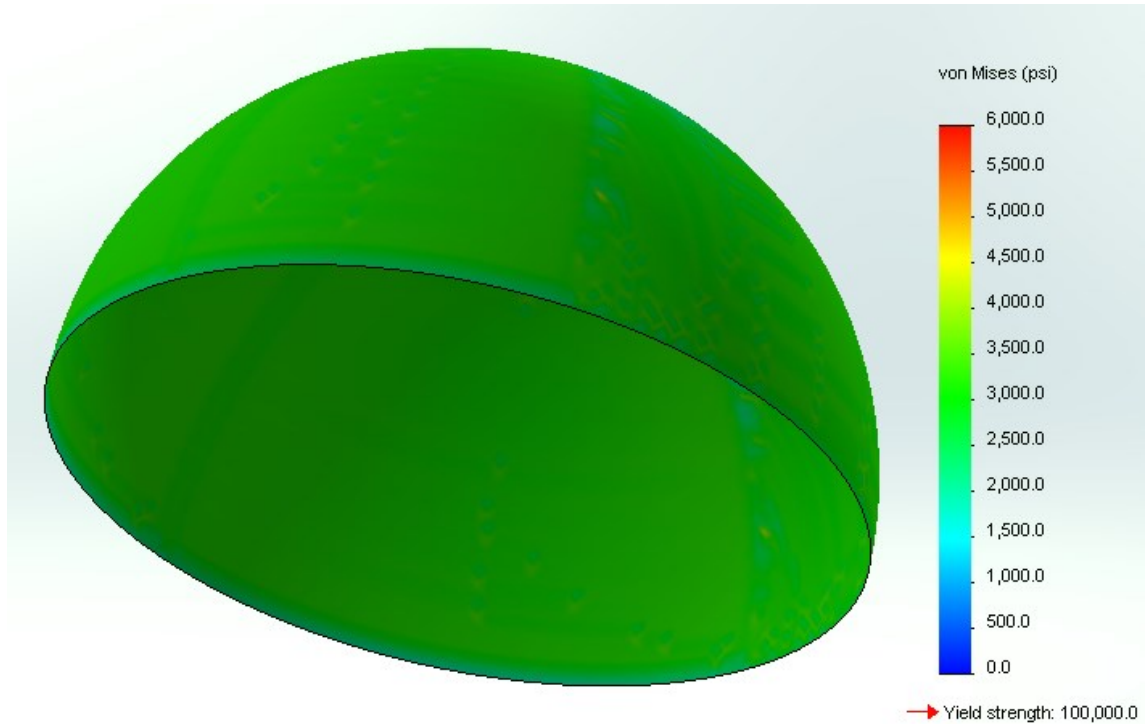
Figure 12: von Mises Stress for Static Tensile Loading

The average stress is 3087 psi. This compares to an average stress of 3189 psi from the closed form solution, providing good correlation with the finite element model. As a reference point, the yield strength of TZM Type 363/364 per ASTM B386 is 100 ksi at 0.2% offset, with ultimate tensile strength being 120 ksi [5]. The maximum stress is well under the yield strength of the specified form of TZM.

Displacement under loading is also studied. Figure 13 shows the URES displacement (SolidWorks term for resultant) under this tensile load.
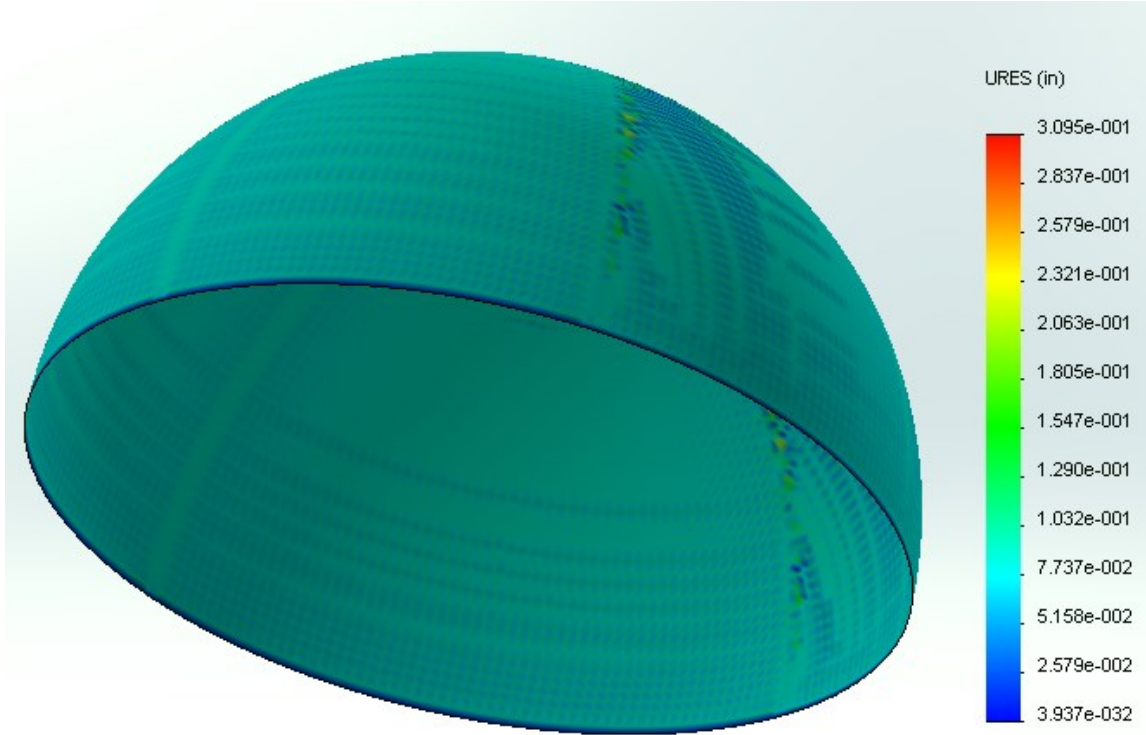
Figure 13: URES (Resultant) Displacement under Static Tensile Loading

The average resultant displacement is 0.076 inches, which is minimal given the scale of the reaction chamber. Also the resultant stresses are under the yield limit. As such, no plastic deformation results in the static tensile case.

3.3.2 Static Compressive (Ignition Failure) Loading

If a fuel pellet fails to ignite, the reaction chamber will go into compression and possible buckling. A closed form approximate solution is presented below to calculate the critical buckling load. Equation (3.7) shows the critical buckling load for a complete shell [19].

$$K_c = \frac{2E}{\sqrt{3(1-v^2)}} \left(\frac{h}{R}\right)^2 \qquad (3.7)$$

Equation (3.8) shows the critical buckling load for a hemisphere.

$$P_{cr} = \left(.14 + \frac{3.2}{\lambda^2}\right) K_C \qquad (3.8)$$

Equation (3.9) is for the λ^2 term.

$$\lambda^2 = \sqrt{12(1-v^2)} * \frac{R}{h} * 4(\sin\left(\frac{\pi}{4}\right))^2 \qquad (3.9)$$

The $\frac{3.2}{\lambda^2}$ term becomes negligible in this equation. The critical buckling load for the

hemispherical reaction chamber equals 0.0039 psi. This is compared to the pressure of

0.139 psi under operational loading. The bracing structure proposed in this thesis will not

only help with the thrust loads, but will also help with support against the buckling load.

The buckling load will dynamically stress the thin wall of the reaction chamber in the

opposite direction of the operational loading, possibly tearing apart the reaction chamber

wall. This possibility and its consequences are first studied here in the static scenario, to

observe resultant stresses. Figure 14 shows the boundary conditions applied to this finite

element model.
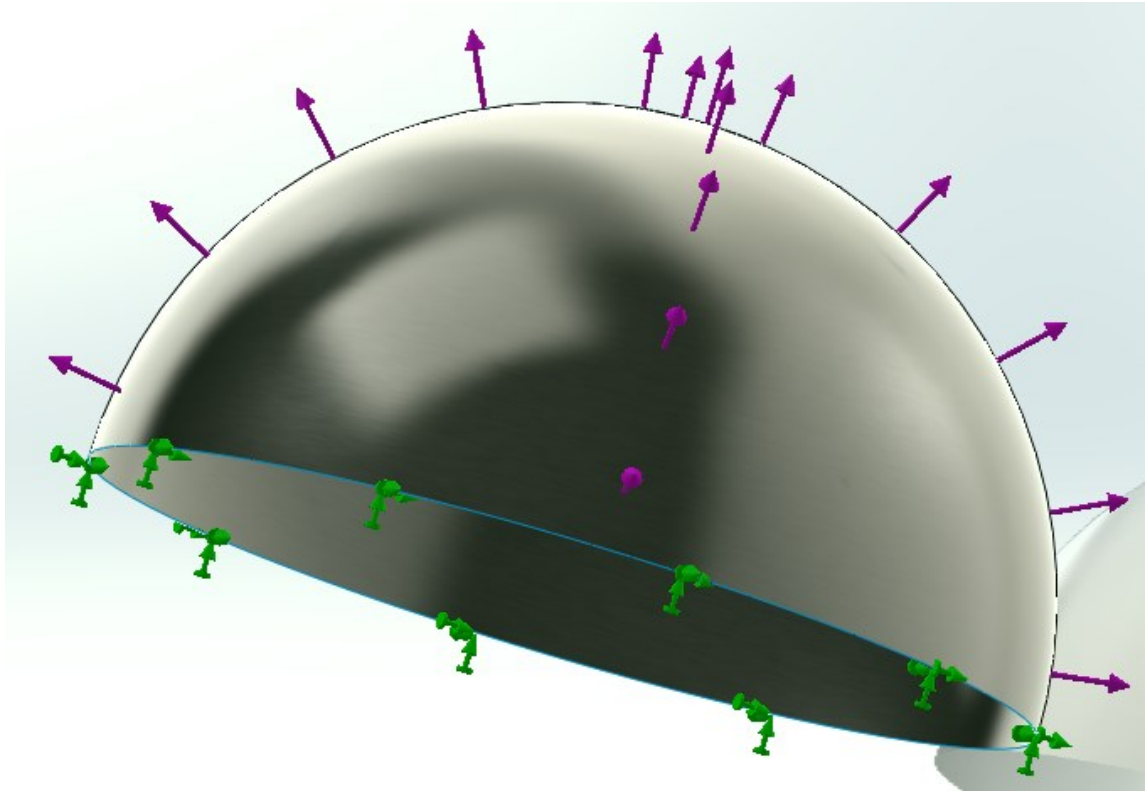
Figure 14: Static Compressive FEM Boundary Conditions

The green arrows represent the bottom of the reaction chamber being rigidly fixed, using the same assumptions in the static tensile case of section 3.3.1. The magenta arrows represent 1.696 million pounds-force compressive load, as an equal and opposite scale load of the tensile case.

This simulation also results in 207,024 degrees of freedom as did the static tensile case. Figure 15 shows the resultant von Mises stress plot.
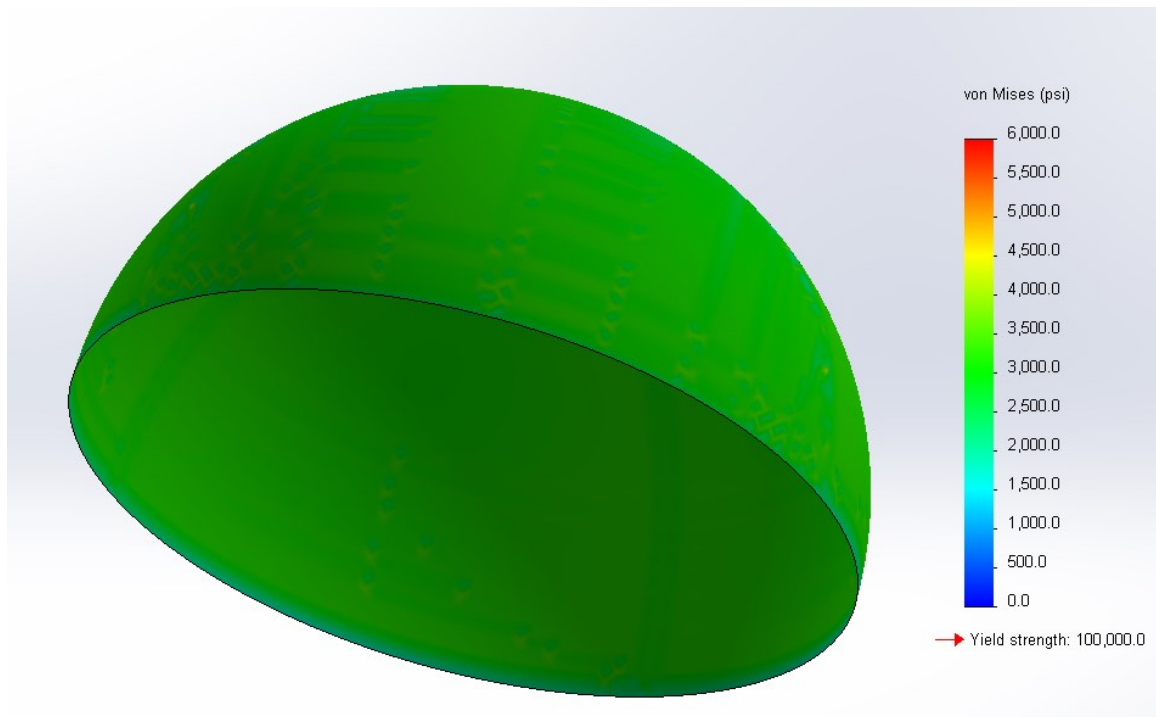
Figure 15: von Mises Stress for Static Compressive Loading

The average von Mises stress is 3087 psi, which is expected from the equal and opposite loading of the tensile case. This stress is also well under the yield limit of TZM.

The resultant displacement under loading is shown in Figure 16.
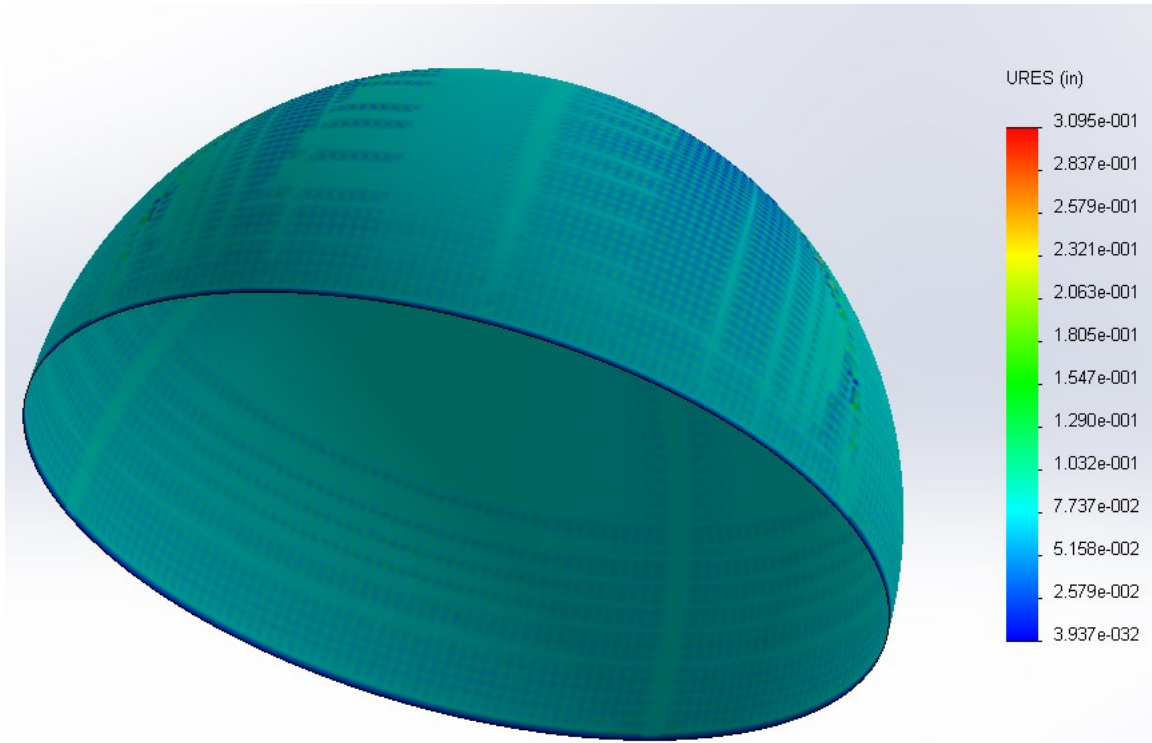
Figure 16: URES (Resultant) Displacement under Static Compressive Loading

The average resultant displacement is 0.076 inches, which is also minimal. No

plastic deformation occurs in the static compressive model either. In the subsequent

sections, a frequency analysis is performed of the reaction chamber.

3.4 Reaction Chamber Finite Element Model for Frequency Analysis

The natural modes and frequencies of the reaction chamber are very important

when designing the fuel pellet firing repetition rate, currently specified as 250 Hz [1].

The preliminary calculations from Project Daedalus calculate the lowest natural

frequency of the reaction chamber as 20.4 Hz [1]. The modes are explored

computationally, using different boundary assumptions. The finite element model for the

frequency analyses of this section resolve with 56,214 degrees of freedom.

3.4.1 Frequency with Fixed Condition

The reaction chamber is assumed fixed at the bottom here and for all the studies in this chapter. This fixture condition was used to recreate the Daedalus team's assumptions in their modal analysis. The finite element model for frequency analysis is run iteratively, and the first thirty modes are retained to study the behavior of the structure. Figure 17 shows the mesh, boundary condition, and natural frequency results of the first four modes.
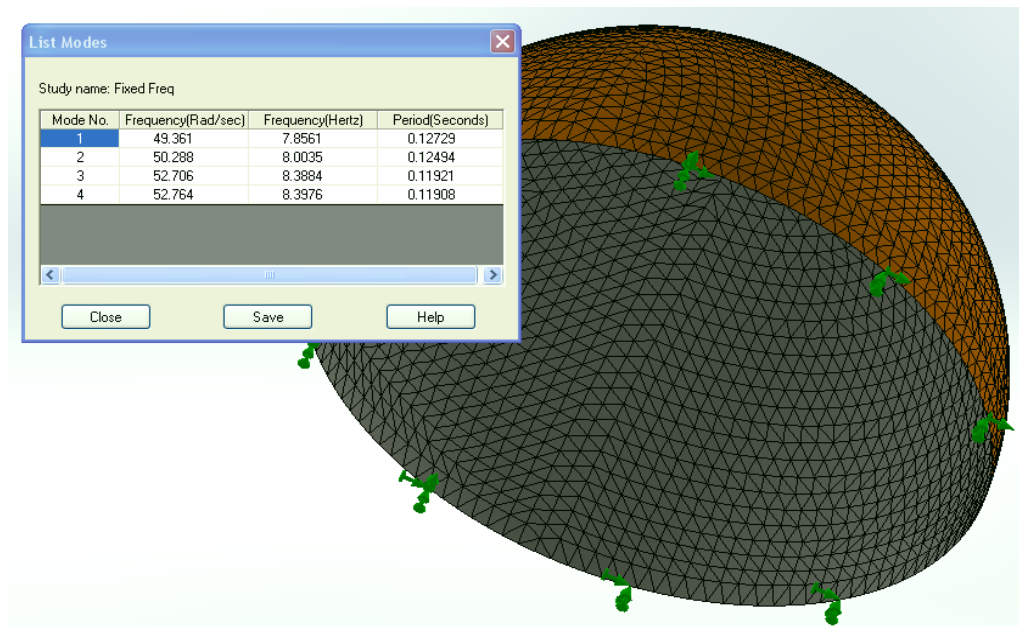
Figure 17: Natural Frequency Analysis of Reaction Chamber Fixed at Ignition Coil Interface

The first natural frequency is 7.86 Hz, with the second natural frequency as 8.00 Hz, and the third natural frequency as 8.39 Hz. Table 2 shows the natural frequency results of the first thirty modes for this configuration.

Mode No.	Frequency (Hz)	Mode No.	Frequency (Hz)	Mode No.	Frequency (Hz)
1	7.8561	11	9.0866	21	9.6987
2	8.0035	12	9.1314	22	9.8127
3	8.3884	13	9.1657	23	9.8152
4	8.3976	14	9.2118	24	9.9105
5	8.4892	15	9.2698	25	9.9194
6	8.6436	16	9.3042	26	9.9309
7	8.7179	17	9.3234	27	9.9711
8	8.7774	18	9.4633	28	10.033
9	8.9369	19	9.4727	29	10.088
10	8.9839	20	9.5375	30	10.135

Table 2: Modal Analysis Natural Frequency Results of Reaction Chamber Fixed at Ignition Coil Interface

The first natural frequency calculated in Daedalus differs by a factor of more than two from the computationally calculated natural frequency. This may be due to different assumptions, but will have to be thoroughly explored before considering reducing the firing pellet repetition rate, as to avoid any resonance behavior.

3.4.2 Frequency with Fixed Condition including Operational Loading

The first thirty modes are also explored with the operational tensile load of 1.696 million pounds-force. Given the estimated 250 Hz firing rate, it is important to study the modes of the structure under the operational loads.

Figure 18 lists the frequencies of the first four modes for this model, and shows the mesh and boundary conditions on the model. As in Section 3.3.1, the model remains fixed at the bottom. The magenta arrows represent the tensile load placed on the reaction chamber.
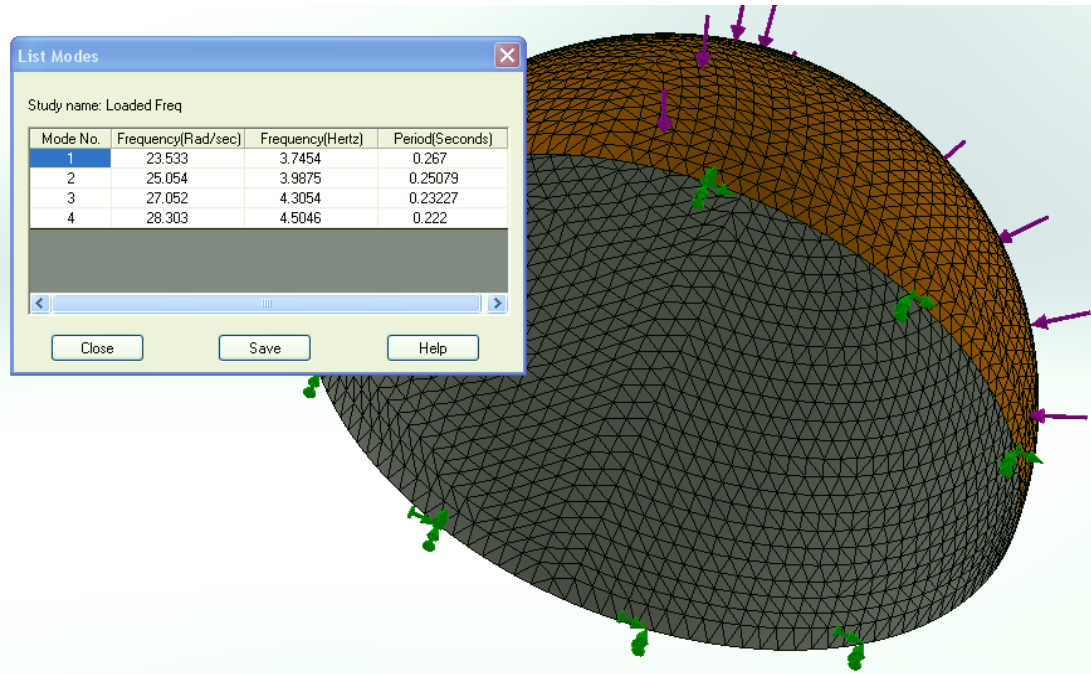
Figure 18: Frequency Analysis of Reaction Chamber Fixed at Ignition Coil Interface with Operational Loading

The first mode is at the frequency 3.75 Hz, with the second mode's frequency as 3.99 Hz, and the third mode's frequency as 4.31 Hz. Table 3 lists the natural frequency results of the first thirty modes for this configuration.

Mode No.	Frequency (Hz)	Mode No.	Frequency (Hz)	Mode No.	Frequency (Hz)
1	3.7454	11	5.8712	21	6.4954
2	3.9875	12	5.8800	22	6.5282
3	4.3054	13	5.9225	23	6.5769
4	4.5046	14	6.0721	24	6.6240
5	4.8002	15	6.1149	25	6.6548
6	4.8317	16	6.1724	26	6.7419
7	5.4055	17	6.1845	27	6.7493
8	5.7019	18	6.2327	28	6.7513
9	5.8045	19	6.3592	29	6.7860
10	5.8215	20	6.3890	30	6.7947

Table 3: Modal Analysis Natural Frequency Results of Reaction Chamber Fixed at Ignition Coil Interface with Operational Loading

Comparing the first natural frequency of the reaction chamber being fixed at the bottom to the first mode frequency of the reaction chamber being fixed at the bottom with the operational tensile load, it is seen that frequency with loading is approximately half as much as without loading. This is due to stress stiffening from the tensile loading. If there were compressive loading, stress softening would occur.

The lowest natural frequency without loading is 7.86 Hz. The lowest natural frequency with loading is 3.74 Hz. In future studies, modal analysis models should be compared with loading and without loading for its effect on the structure.

4. Reaction Chamber Finite Element Model Fixed at the Pellet Injector Interface (Top)

4.1 Pellet Injector Interface Thrust Reaction Instability at Nominal Daedalus

Dimensions

The structure of the Icarus starship has a mix of large and small dimensions. In particular, the pellet injector interface has an inner diameter of 1.575 inches and an outer diameter of 3.500 inches. The 1.575 inch inner diameter of the pellet injector is subsequently drilled through the top of the reaction chamber, by which the fuel pellets drop through this interface before being ignited. The schematic of this design from Project Daedalus can be seen in Figure 19.
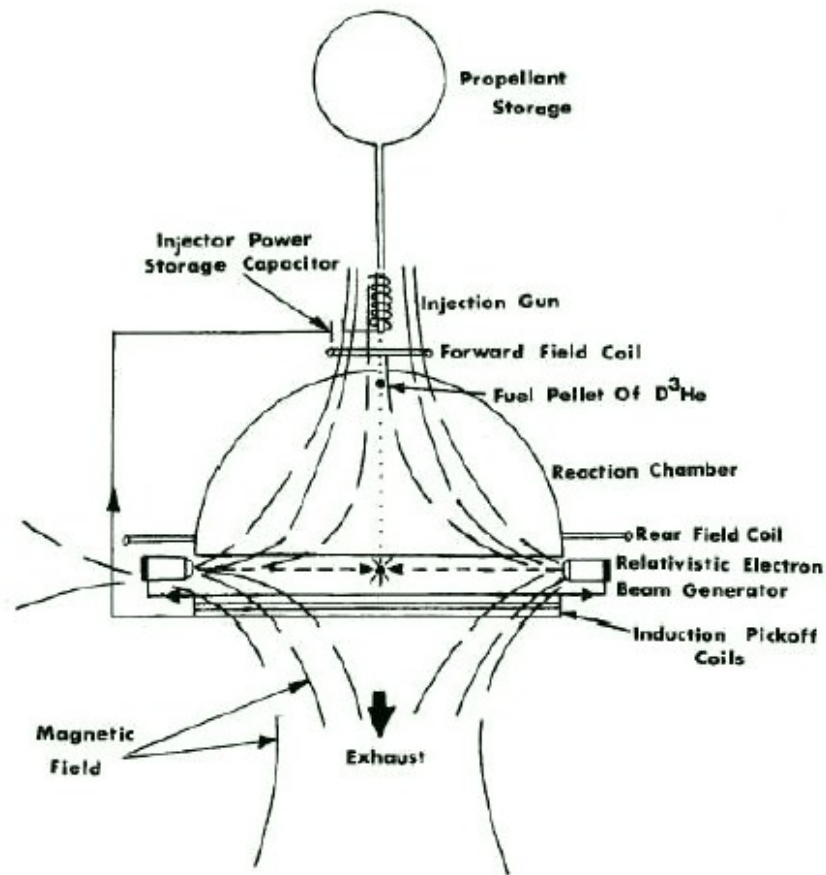
Figure 19: Pellet Injector Operation Schematic

In a static scenario, the large mass of the reaction chamber reacting to the thrust force at this very small interface would clearly lead to high stresses and instability. Figure 20 shows a model of the injector gun and reaction chamber to scale as per the Daedalus starship parameters.
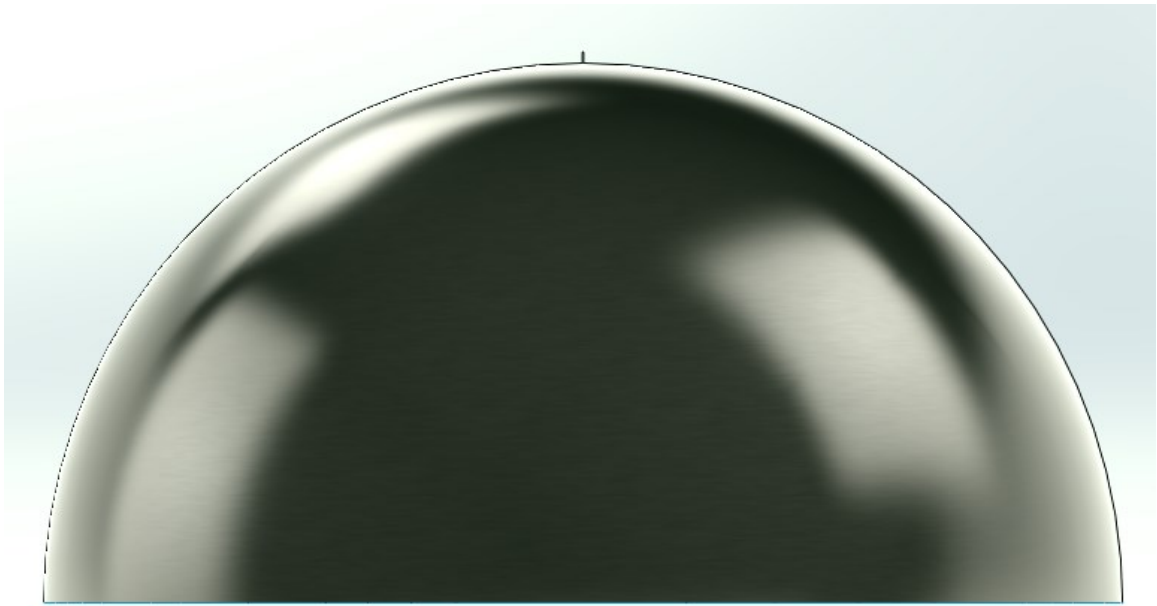
Figure 20: Pellet Injector and Reaction Chamber Interface to Scale per Daedalus Starship Parameters

It can easily be seen from this scale model that the reaction chamber dimensions are vastly greater than the pellet injector dimensions. Figure 21 shows a close-up view of the pellet injector interface to the reaction chamber. It is assumed to be flat where the pellet injector surface interfaces to the reaction chamber, for future manufacturing considerations.
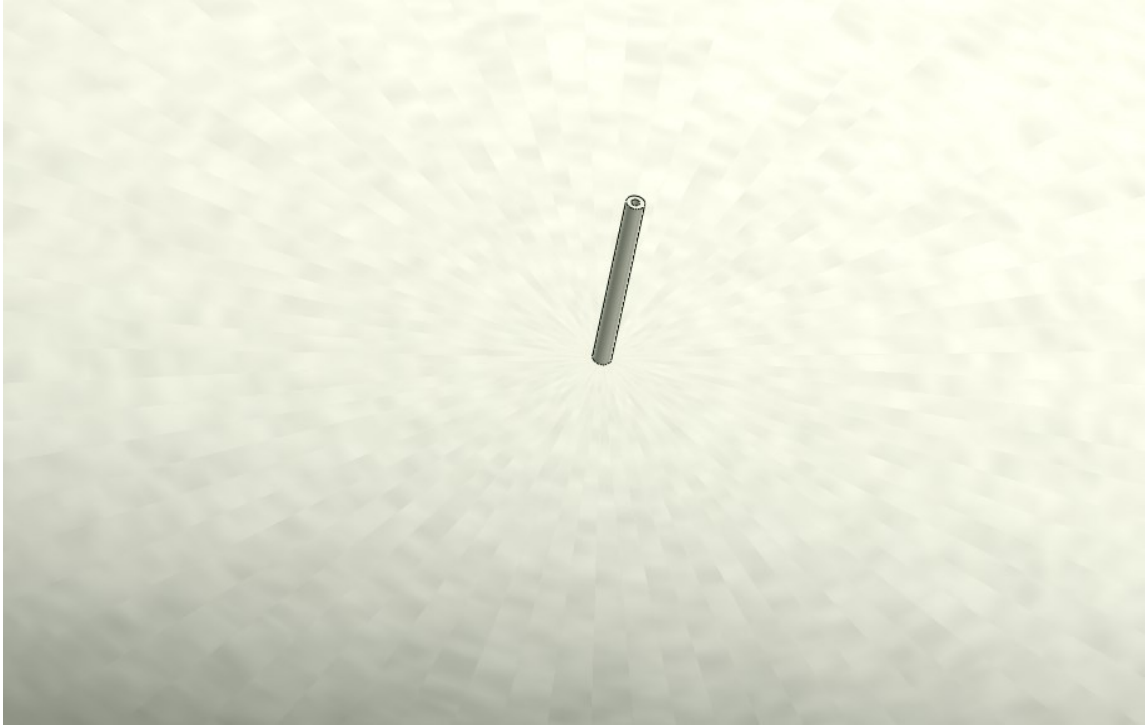
Figure 21: Pellet Injector to Reaction Chamber Interface (Zoomed In View)

The hole for the pellets that can be seen in Figure 21 extends through the reaction

chamber, to enable the pellet to drop through the reaction chamber.

The finite element modeling for this configuration is more complex than that of

the simpler reaction chamber of Chapter 3. This configuration features the reaction

chamber and pellet injector as separate parts, combined together in an assembly. Also, the

pellet injector is modeled as a solid part, as its dimensions do not justify making shell

elements as with the reaction chamber. Figure 22 shows the pellet injector part as a solid

model.
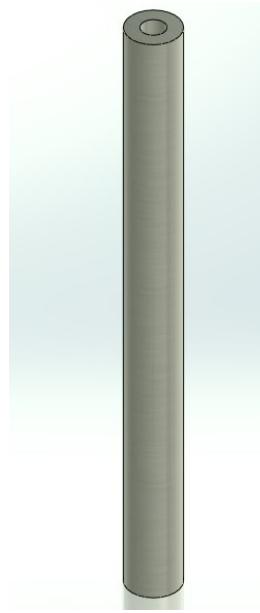
Figure 22: Pellet Injector Solid Model

The pellet injector is extruded to a height of 39.37 inches, or 1 meter, as a starting point.

The reaction chamber is still resolved as a shell model, as its wall thickness to radius ratio is miniscule. For the finite element model, this results in a mixed mesh analysis, with the reaction chamber comprised of shell elements and the pellet injector being solid elements. Figure 23 shows the initial conditions of this study.
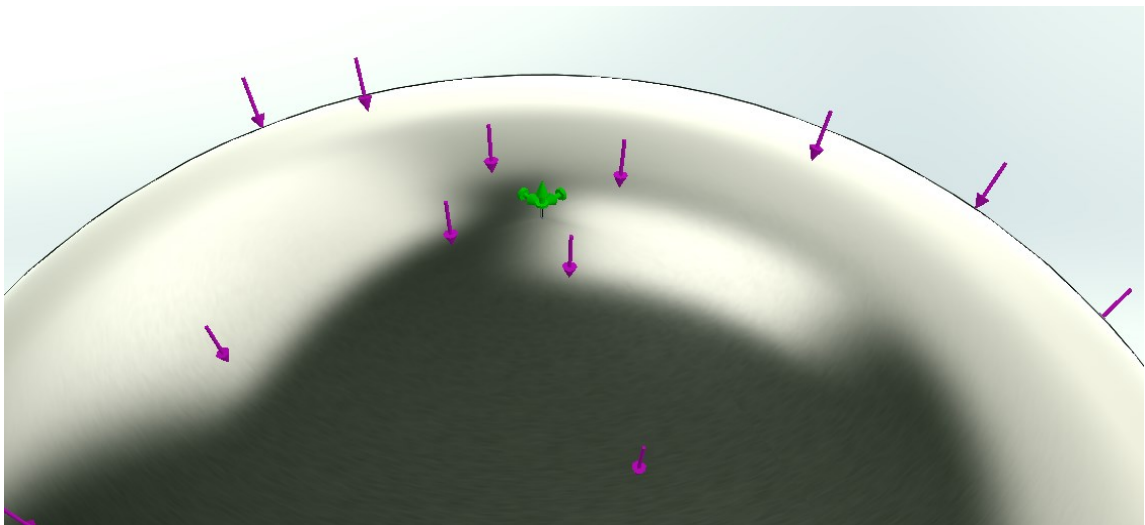
Figure 23: Initial Boundary Conditions of RC and Pellet Injector Assembly Finite Element Model to Daedalus Starship Parameters

The magenta arrows represent the tensile operational load of 1.696 million pounds-force as per the previous study. The green arrows represent the fixed boundary condition, where the pellet injector is fixed on the top face, where it is assumed to interface to the rest of the Icarus structure and convey the thrust force. The pellet injector is assumed fully bonded to the reaction chamber at its respective interface for this study.

A curvature based mesh is utilized with mesh refinement around the pellet injector and interface to the reaction chamber. The mesh refinement is adjusted as the interfaces dimensions are fine compared to the scale of the model, permitting a coarser mesh for the rest of the reaction chamber. Figure 24 shows the mesh of this assembly, zoomed in on the top of the assembly where the pellet injector interfaces to the reaction chamber.
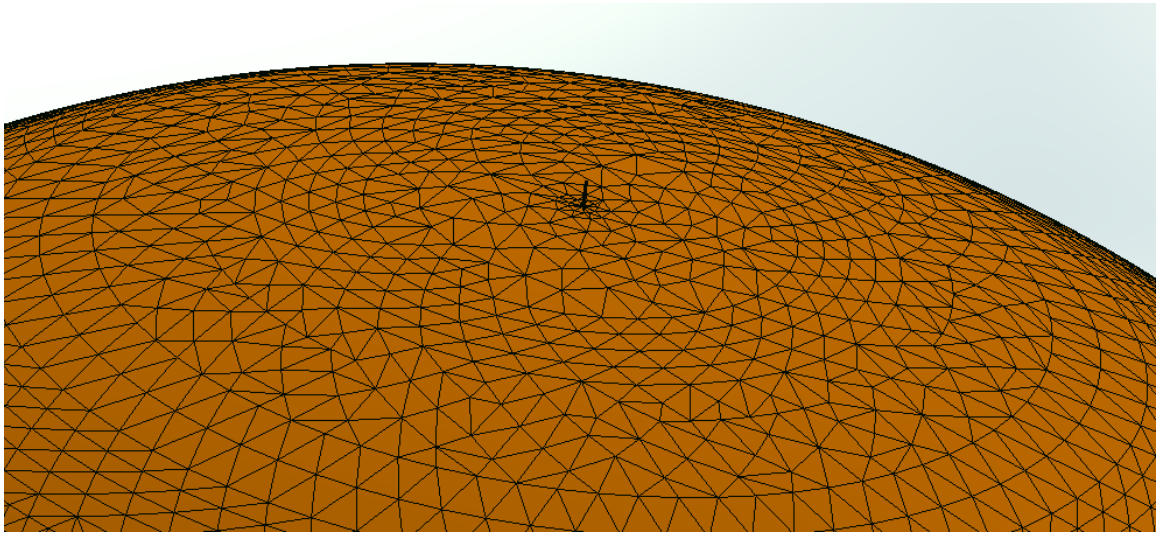
Figure 24: Pellet Injector and RC FEM Mesh at Interface

This model results in 38,098 nodes and 18,964 elements. Figure 25 shows a screenshot of the large displacement error during the solving of the model.
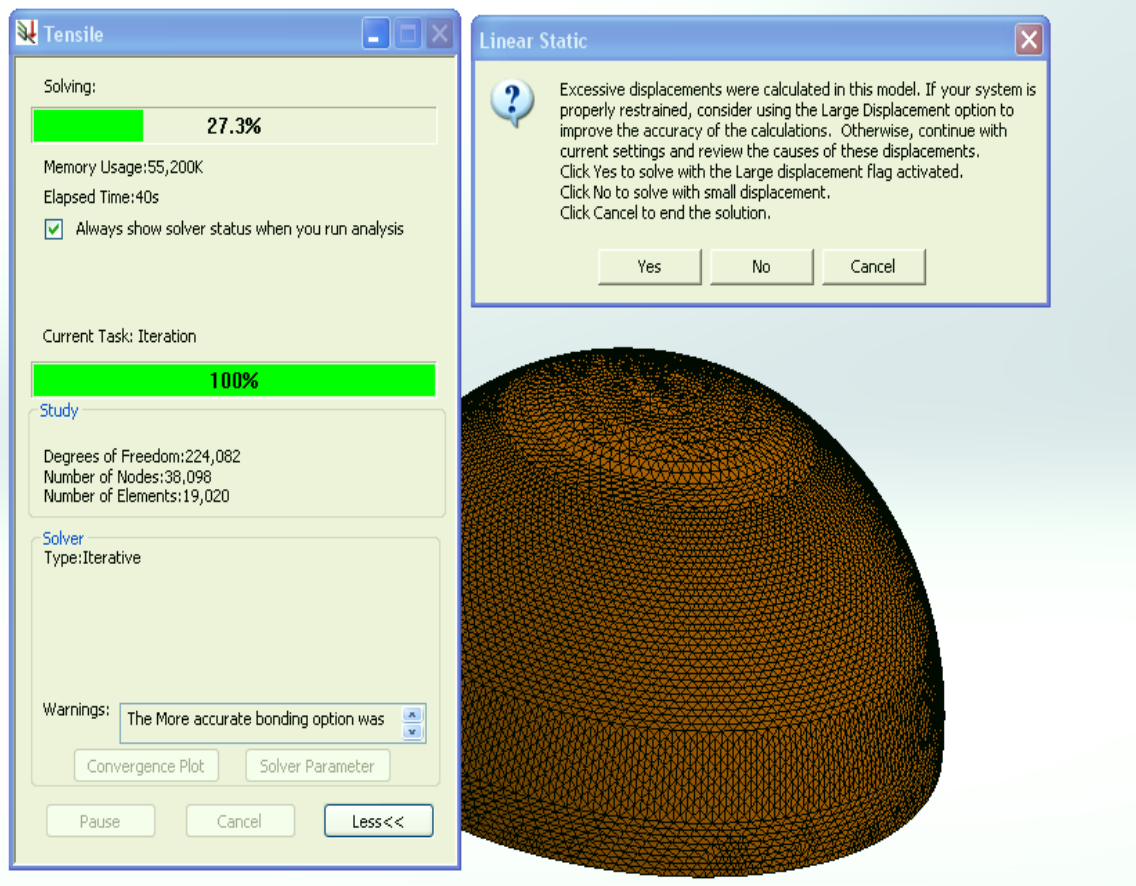
Figure 25: Solver Error for Scale Injector Gun and RC FEM Assembly

This model is solved with the small displacement flag. The small displacement flag in

this FEA software means that the model has insufficient fixture or boundary conditions.

Using the small displacement flag solves the model linearly. Not using the small

displacement flag solves the model nonlinearly. If the assumed loading, fixture and

boundary conditions should result in a linear model, this cautions the analyst to revisit the

design of the model. The stress results will not prove accurate for this solution, but the

stress patterns and displacement patterns are useful tools in determining the instability of

the model. Figure 26 shows a close up view of the von Mises stress results of pellet

injector to reaction chamber interface.
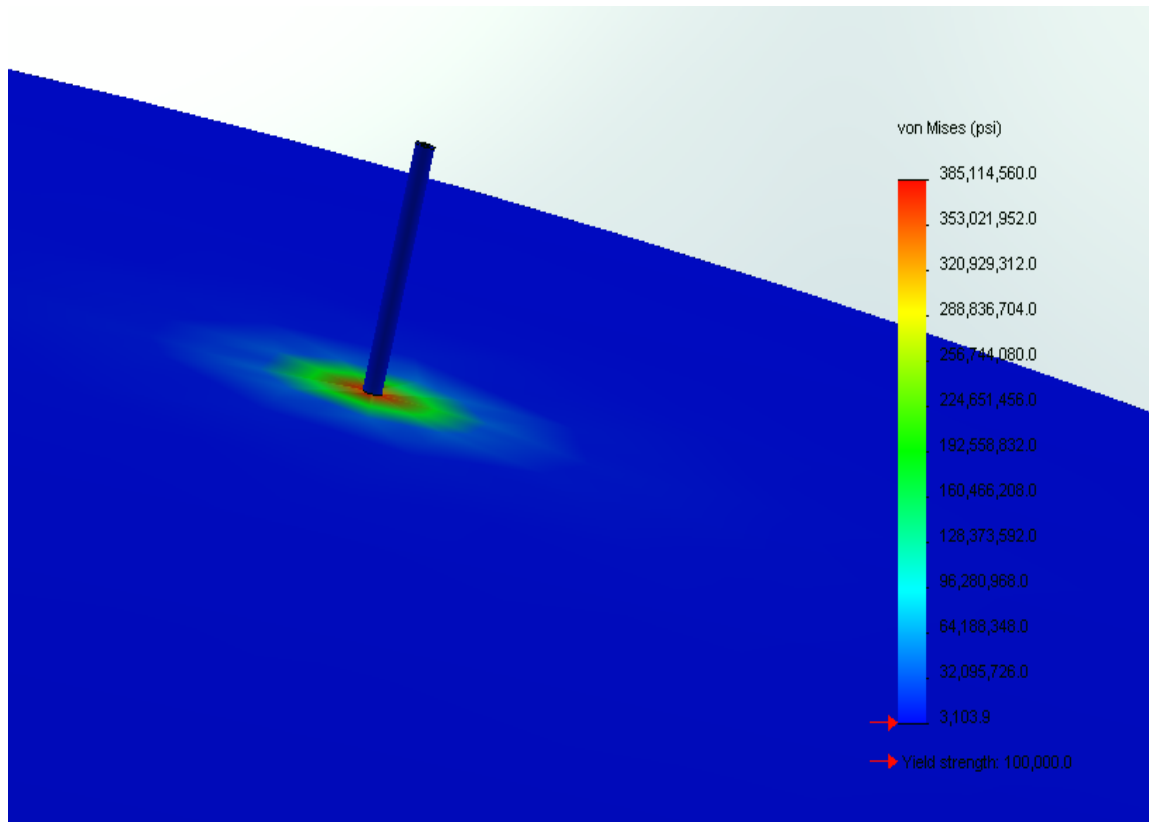
Figure 26: von Mises Stress Results for Pellet Injector and RC Static Tensile FEM

It can be seen that the maximum stress is over 385 million psi. The yield strength of TZM

at Room Temperature is 100,000 psi, so this stress result, if accurate, would suggest a

very high stress concentration at this interface. However, the magnitude of this stress

result cannot be trusted due to the solver error, but the stress patterns are important in

determining this instability. Figure 27 shows the resultant displacement results for this

model.
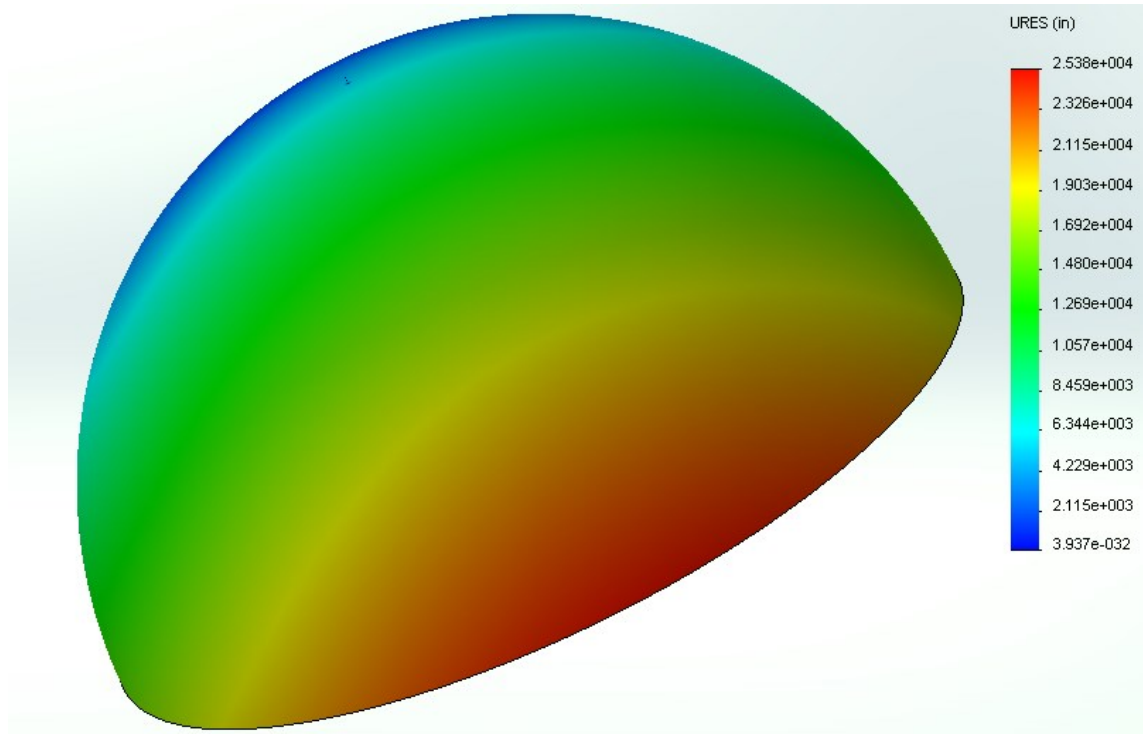
Figure 27: Resultant Displacement of Pellet Injector and RC Static Tensile FEM

The magnitude of the maximum displacement is 25,380 inches. Again, this is studied to

see that fixing a large reaction chamber at a small injector interface produces an unstable

structure. This interface must be modified to stabilize this model. The truss structure

introduced in Chapter 5 stabilizes the structure.

4.2 Pellet Injector Interface Modification to Produce a Stable Structure

The finite element models and simulations are altered iteratively in order to

resolve a stable structure. Figure 28 shows the von Mises stress results with the outer

diameter of the pellet injector interface at 35.00 inches, a factor of 10 greater than the

Daedalus parameters. All the boundary conditions and assumptions are the same as the

previous section. Take note that this model is still structurally unstable with a small

displacement flag (insufficient fixture conditions), but is provided as an intermediate step and result.
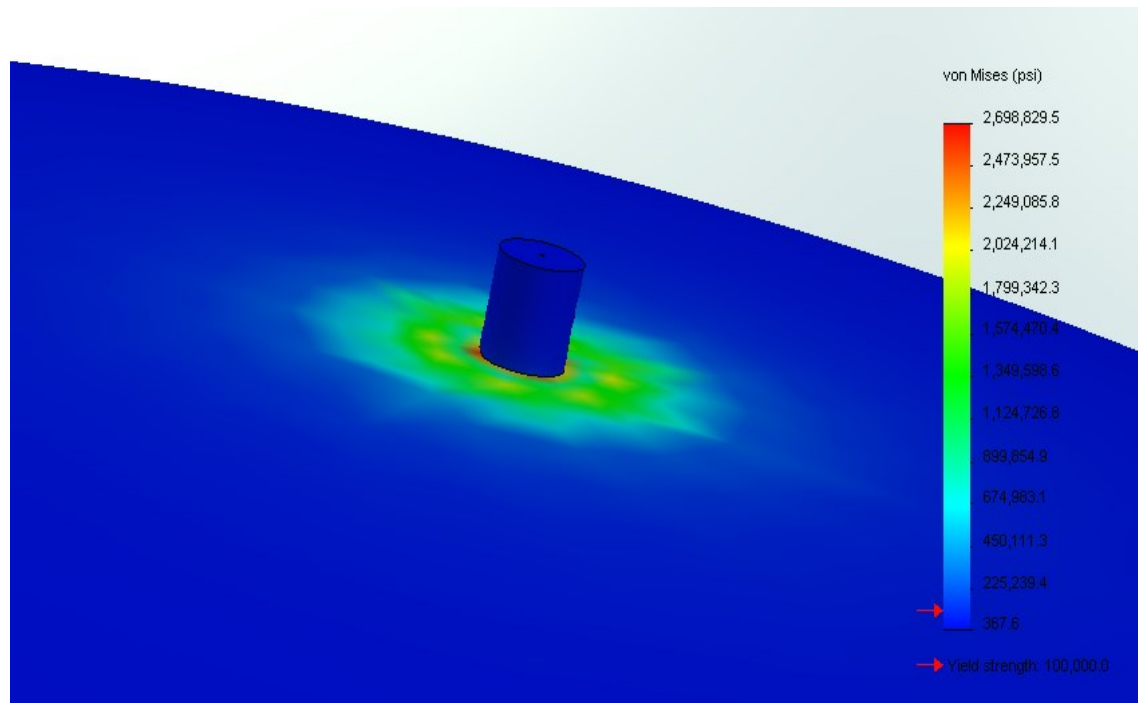
Figure 28: von Mises Stress Result for Pellet Injector Interface OD Increased by Factor of 10

The von Mises stress is over 2.6 million psi, but it can already be seen that the magnitude of stress is decreasing with a larger area reacting the thrust force at the top of the pellet injector interface.

Figure 29 shows the von Mises stress results with the outer diameter of the pellet injector interface at 350.00 inches, a factor of 100 greater than the Daedalus parameters. All the boundary conditions and assumptions are the same as the previous section. Take note that this model is now structurally stable with no solver error.
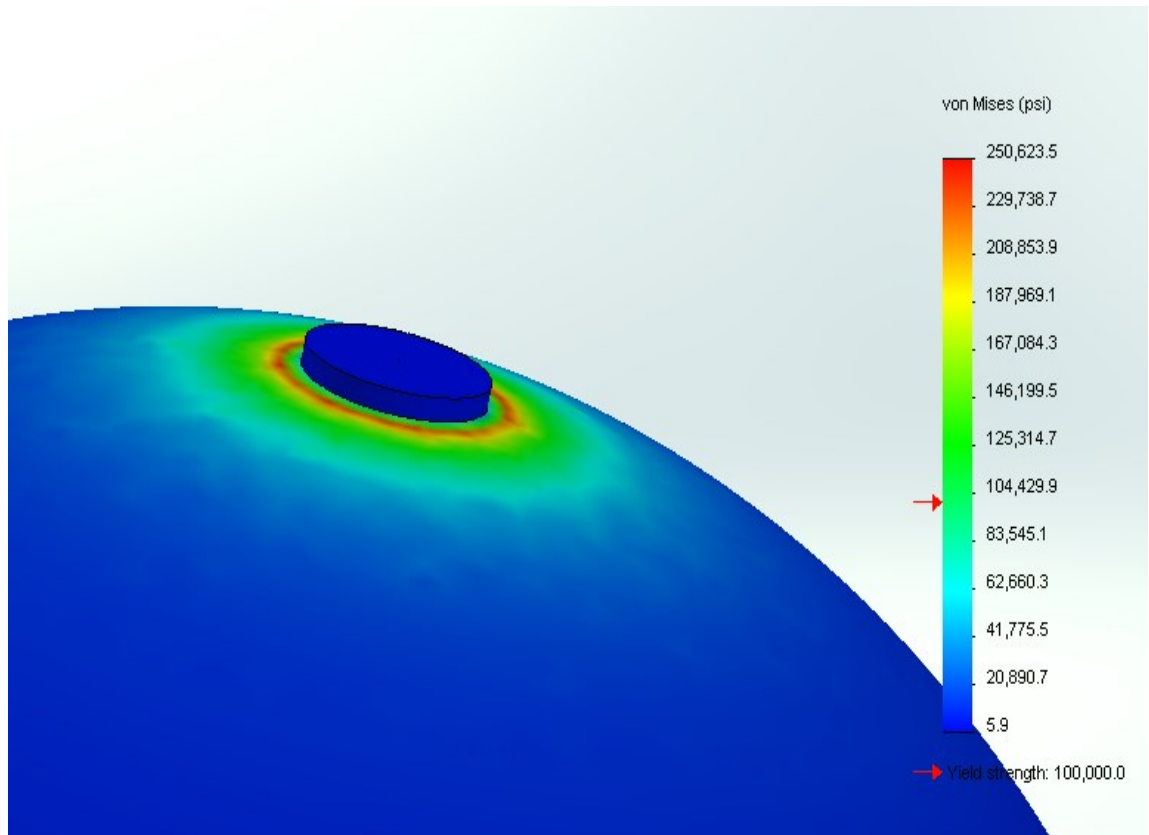
Figure 29: von Mises Stress Result Pellet Injector Interface OD Increased by Factor of 100 (Structurally Stable)

The maximum von Mises stress is seen to be 250,623.5 psi. This is drastically lower than the magnitudes from where the model began. Figure 30 shows the displacement results of this iteration.
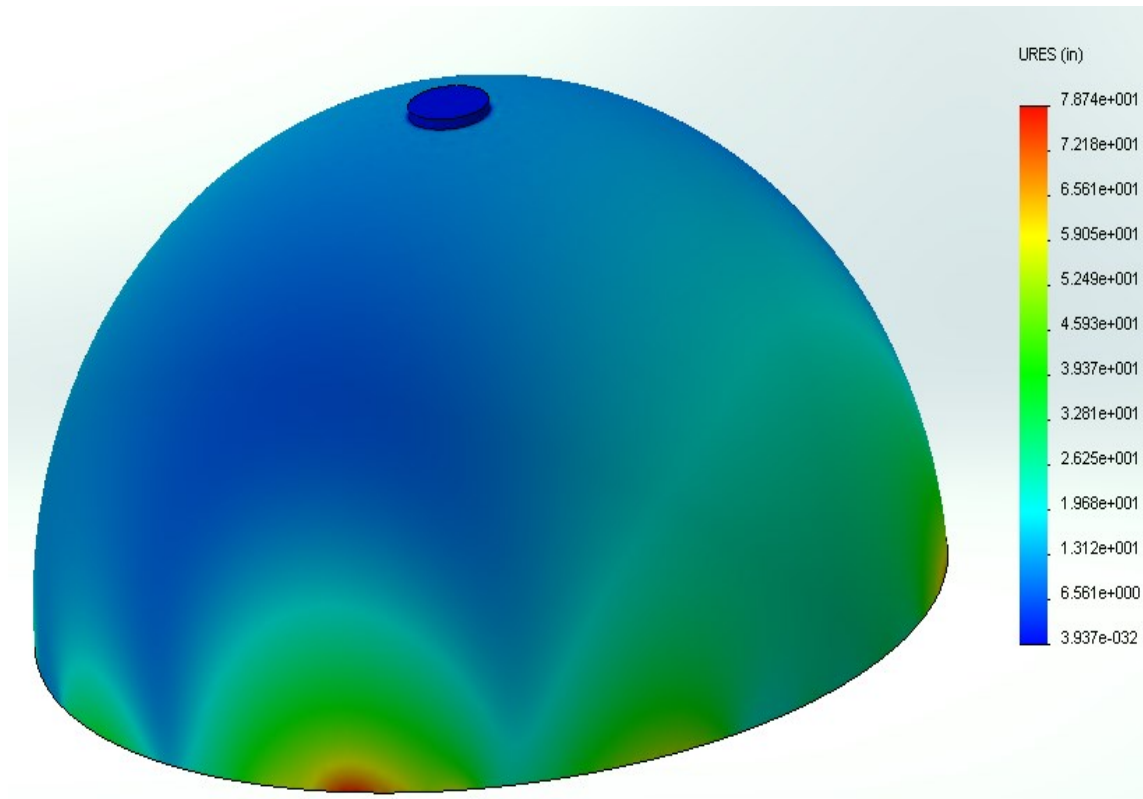
Figure 30: Resultant Displacement of Modified Pellet Injector and RC FEM

The maximum displacement here is seen as 78.7 inches at the bottom of the reaction

chamber.

      The model is solved iteratively varying the outer diameter of the pellet injector

structure until stress results are below the yield limit of TZM. Figure 31 shows the

reaction chamber. The outer diameter of the 'flat spot' on top of the reaction chamber

where the pellet injector interfaces is 700 inches, with the original 1.575 inch hole for

where the pellet drops through.
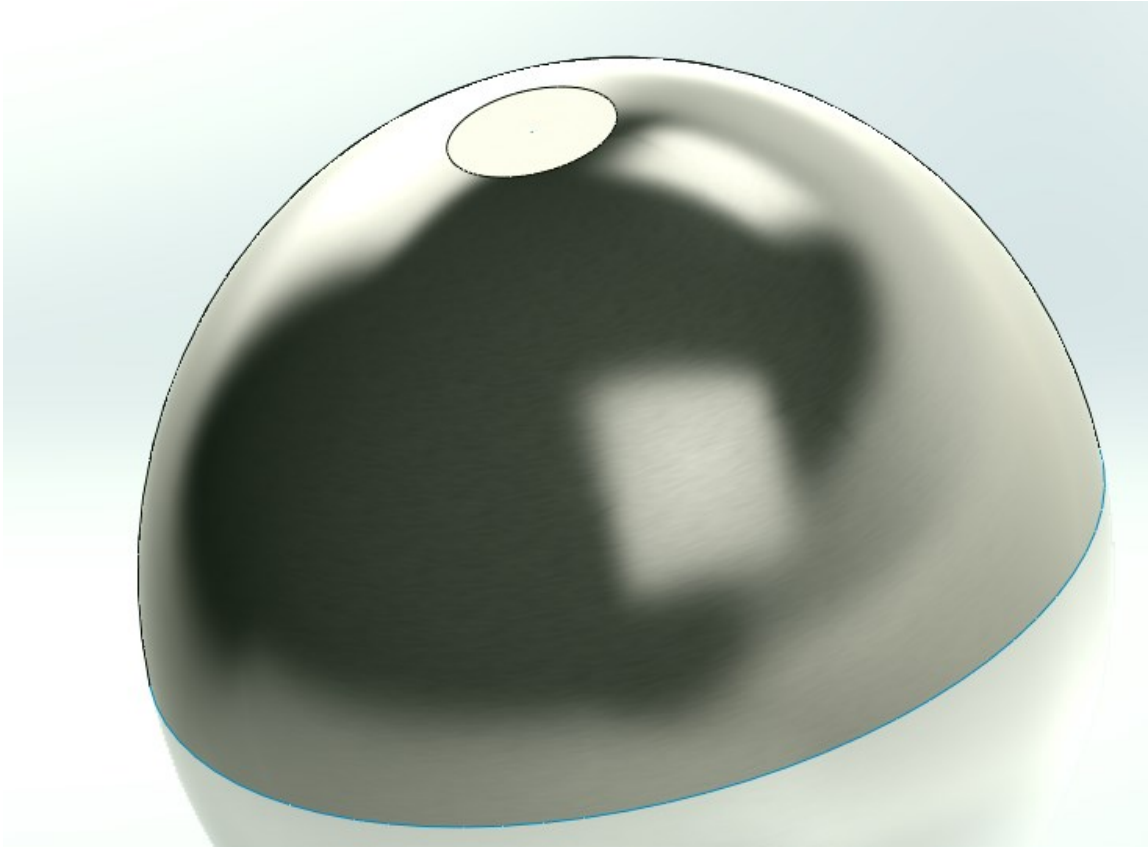
Figure 31: Reaction Chamber with Larger Pellet Injector Interface

Figure 32 shows the pellet injector part. The outer diameter is finalized at 700 inches.

The thickness is settled at a tenth of an inch (0.100), which is about twice the wall

thickness of the reaction chamber. This may be adjusted in subsequent studies

accordingly as detailed design progresses. The initial weight estimate is also provided in

Figure 32.
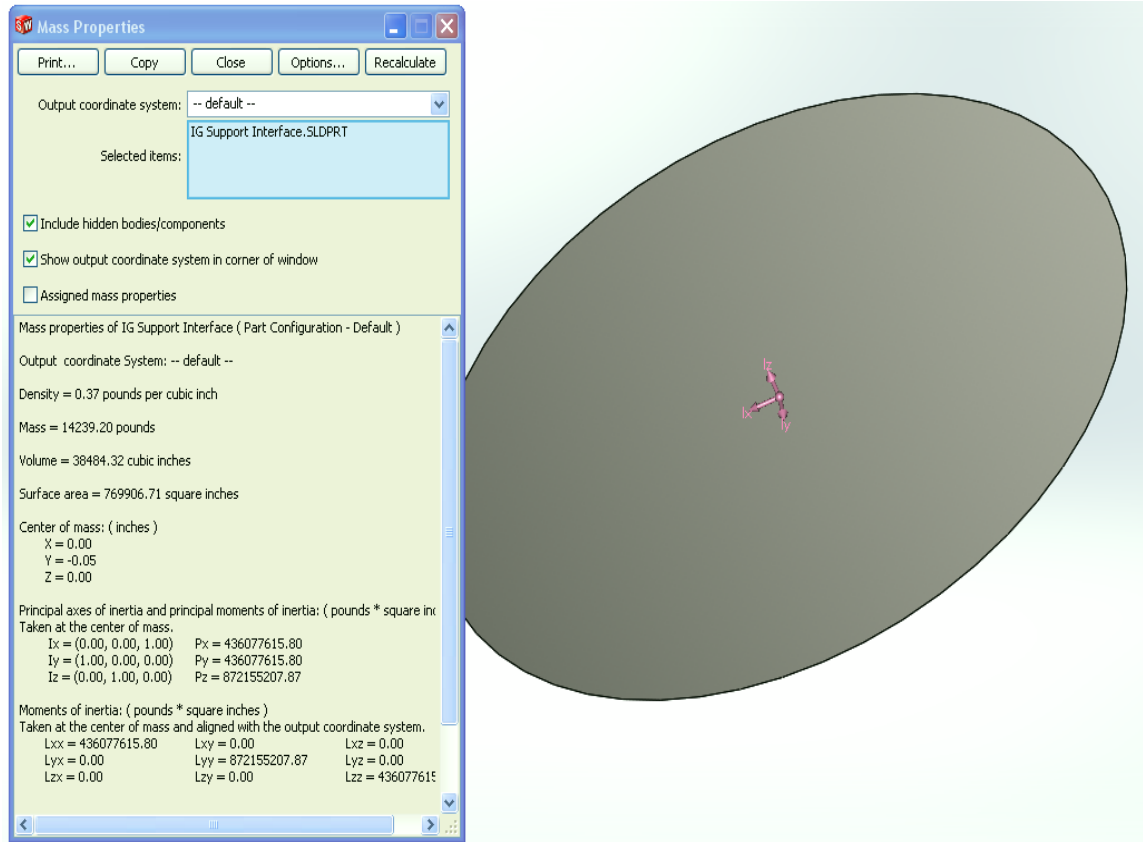
Figure 32: Pellet Injector Solid Model After Final Iteration

The weight of the pellet injector structure is 14,239 pounds. The material for this pellet

injector is assumed to be TZM at this stage, but this may change later with further

analysis. Figure 33 shows an exploded view of the assembly model, so that the interface

between the pellet injector and reaction chamber can clearly be seen.
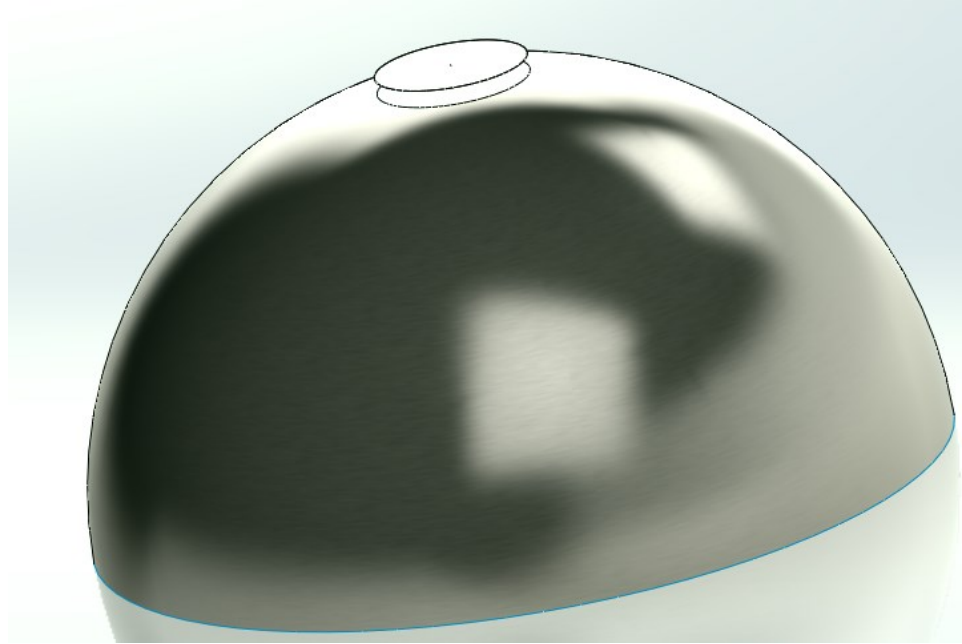
Figure 33: Exploded Assembly View of Pellet Injector to Reaction Chamber

4.3 Reaction Chamber and Pellet Injector Assembly Finite Element Model for Static Loading

The two following subsections explore operational (tensile) and failure (compressive) loading on the reaction chamber and pellet injector structure in the same manner as Chapter 3. The results of these finite element models show the necessity of an integral thrust structure to react the forces on the reaction chamber.

4.3.1 Reaction Chamber and Pellet Injector Assembly Static Tensile (Operational) Loading

For the last configuration of the interface to the pellet injector, a finite element model is developed for the static tensile loading scenario. The next figure, Figure 34, shows the initial boundary conditions with the mesh of the finite element model.
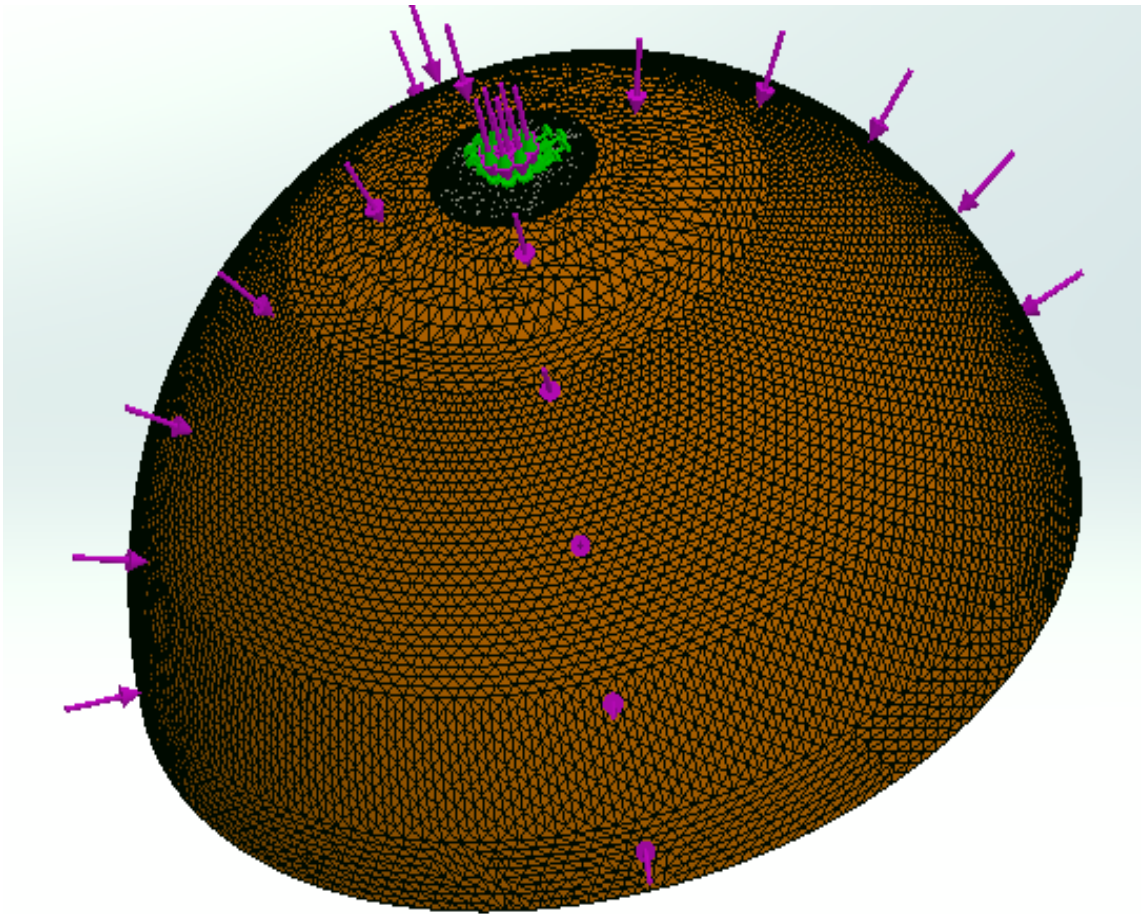
Figure 34: Initial Conditions and Mesh of Injector and RC Interface Tensile Loading Configuration

The magenta arrows represent the tensile load, as per the previous studies. A 1.696 million pounds-force tensile load is still used. The green arrows represent the rigidly fixed condition at the top of the pellet injector interface.

Boundary conditions are always one of the toughest aspects of finite element analysis to represent accurately. Especially with a mixed mesh of solid and shell elements, the boundary conditions between parts and fixed conditions should be isolated for detailed analysis. The inherent difference in degrees-of-freedom of shell and solid elements will produce poor models in the boundary areas of those parts. If this were the final starship configuration, the boundaries between all parts would be isolated for

refined analyses. Also, areas that have mixed shell and solid meshes would be resolved
into a separate model consisting of like meshes for analysis.

The mesh details are 40,310 nodes and 19,920 elements. The degrees of freedom
of this model are 227,307. The von Mises stress results are shown in Figure 35.
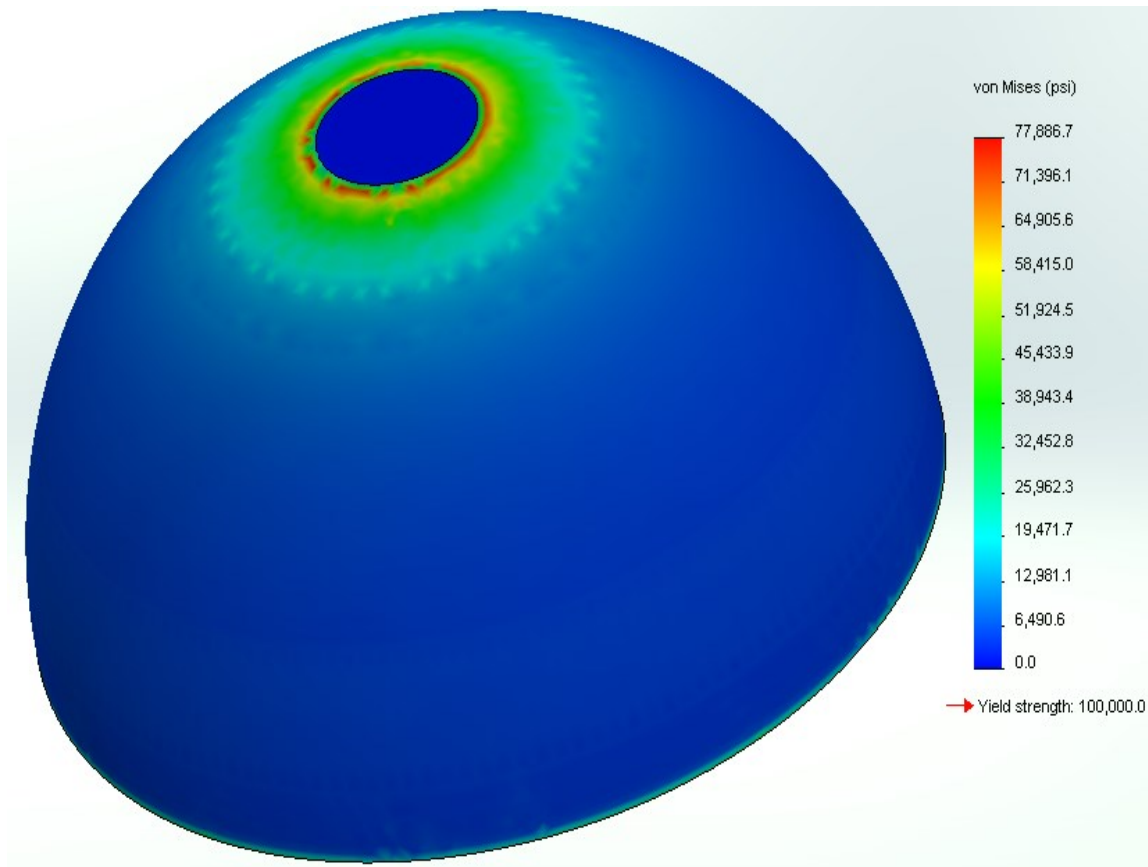
**Figure 35: von Mises Stress Results for Static Tensile FEM of RC and Pellet
Injector Final Iterative Configuration**

The maximum stress is 77,887 psi, which is less than the 0.2% offset yield strength of

TZM (100 ksi) that was tested between 65 and 85 degrees Fahrenheit. Figure 36 shows

the resultant displacement of this model, exploring the areas of the reaction chamber that

are susceptible to higher strain.
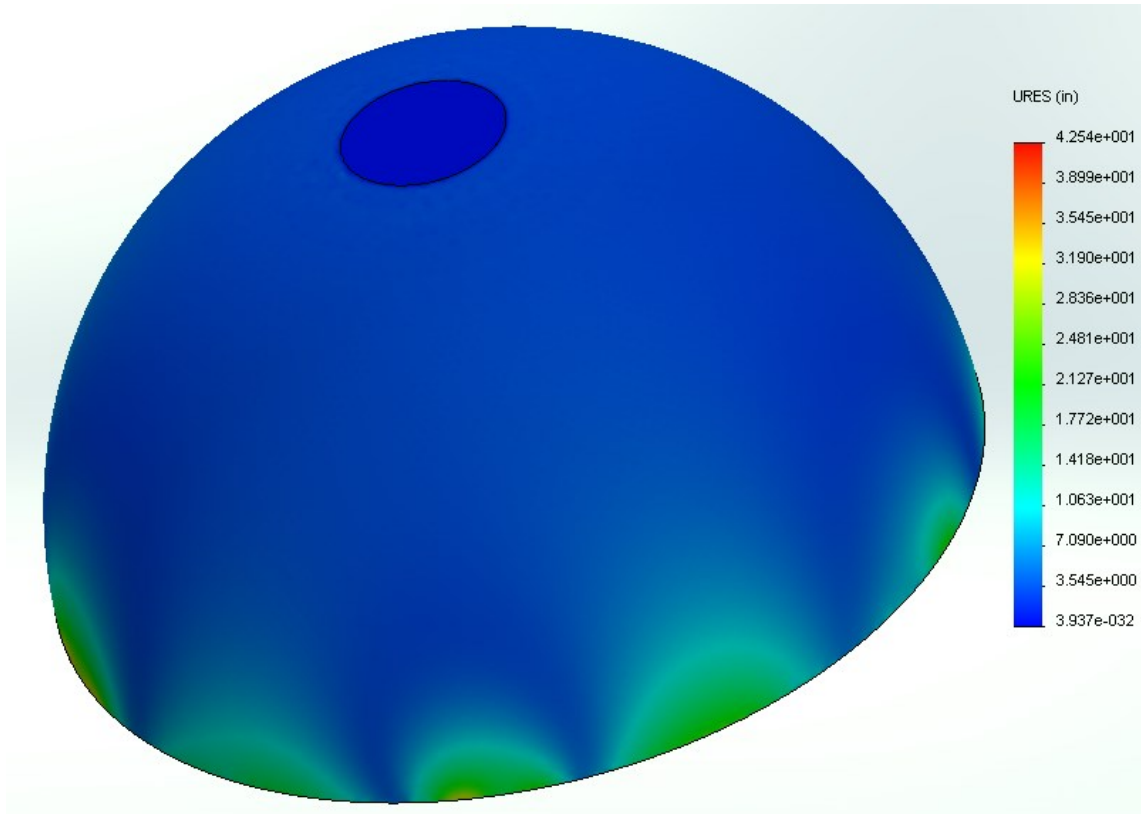
Figure 36: Resultant Displacement for Static Tensile FEM of RC and Pellet Injector Final Iterative Configuration

The maximum displacement is located towards the bottom of the reaction chamber with a value of 42.5 inches. The supporting thrust structure, which will be added in the next chapter to the analysis, is seen to be justified by analyzing these FEM results.

4.3.2 Reaction Chamber and Pellet Injector Assembly Static Compressive (Ignition Failure) Loading

Compressive loading of this structure is now explored, in case any pellet fails to ignite. The next figure, Figure 37, shows the initial set-up conditions of the compressive finite element model.
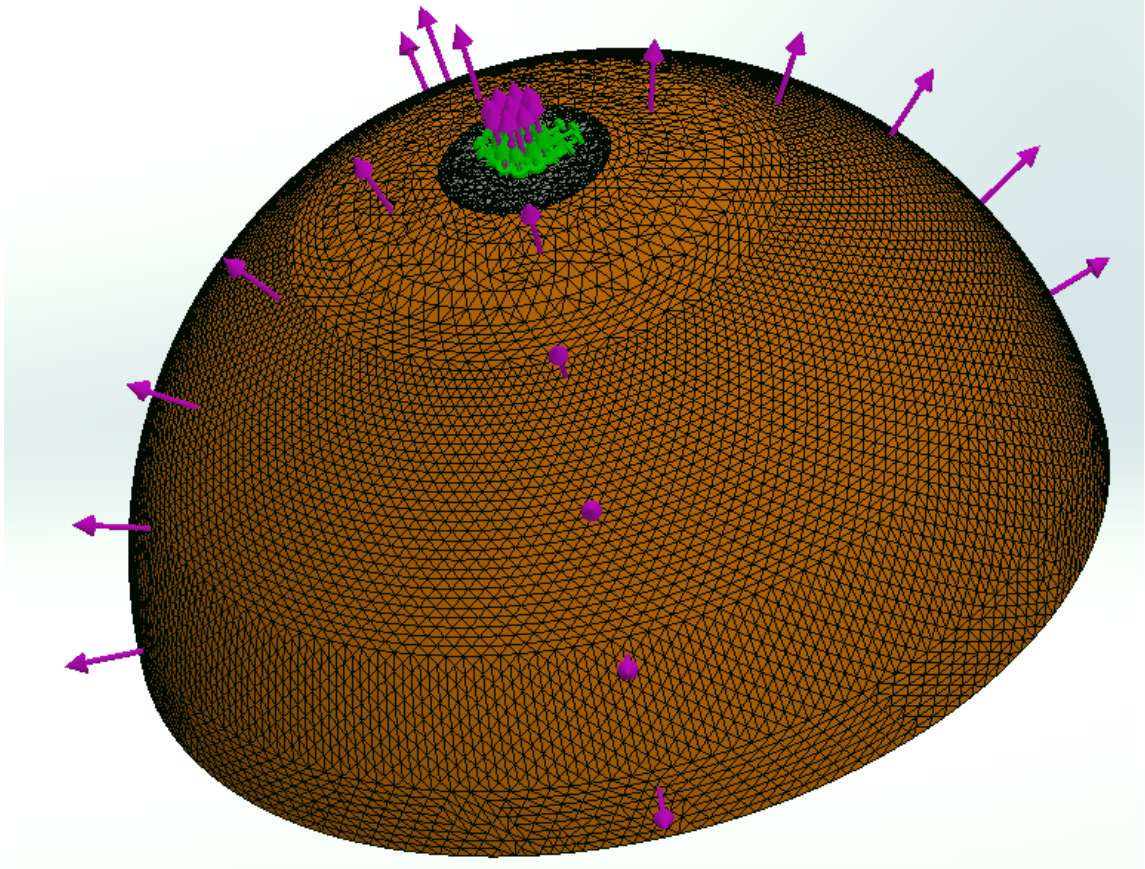
Figure 37: Initial Conditions and Mesh of Injector and RC Interface Compressive Loading Configuration

The mesh details are the same as with the tensile case, with 40,310 nodes and 19,920 elements. The degrees of freedom of this model are 227,307. Figure 38 shows the von Mises stress results for this compressive loading case.
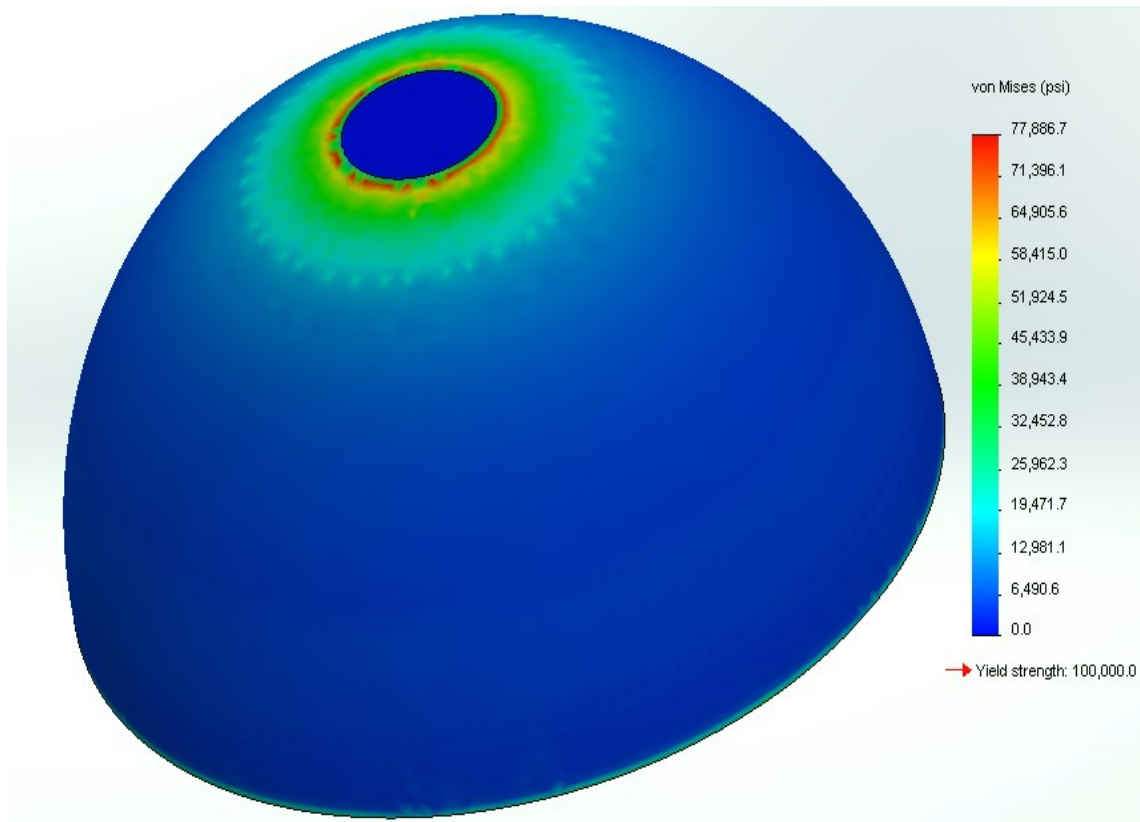
Figure 38: von Mises Stress Results for Static Compressive FEM of RC and Pellet Injector Final Iterative Configuration

The maximum stress in this compressive model is 77,887 psi. This is the same as with the

tensile case. As such, the resultant displacement should also be expected to be the same,

as the loading is equal and opposite. Figure 39 shows the resultant displacement of the

compressive loading case.
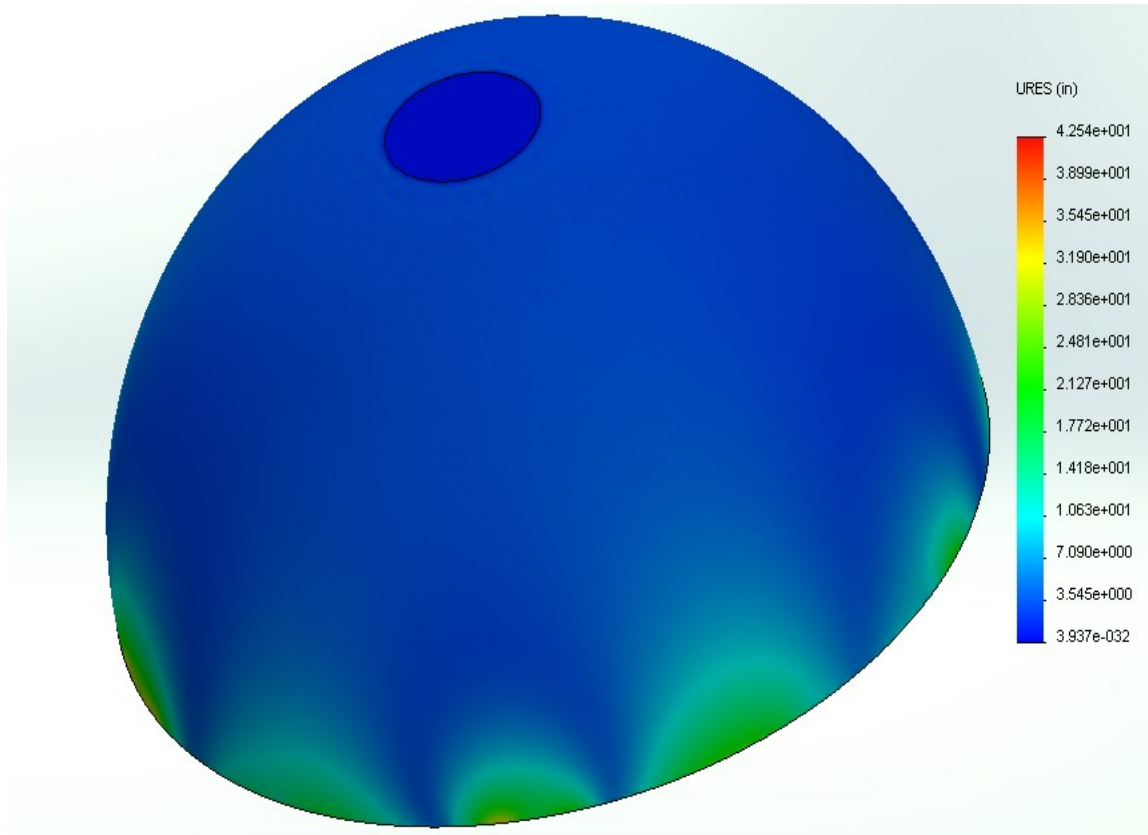
Figure 39: Resultant Displacement for Static Compressive FEM of RC and Pellet Injector Final Iterative Configuration

As expected, the maximum displacement is 42.5 inches. The next figure, Figure 40,

shows a deformed result of the reaction chamber due to this compressive loading. One

would expect that the higher resultant displacement areas, shown in Figure 40 as green,

would deform in the direction of the loading. The deformed result is taken with a

magnification scale of about 10.
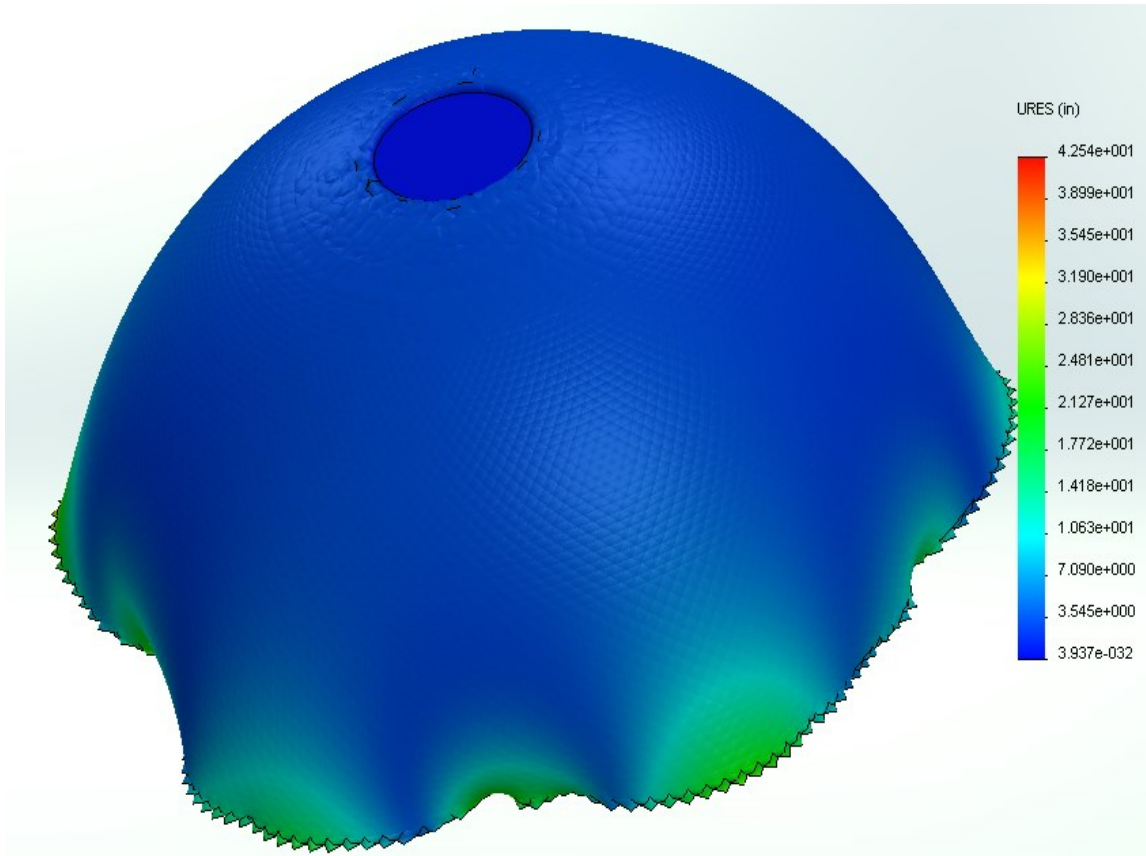
Figure 40: Deformed Resultant Displacement for Static Compressive FEM of RC and Pellet Injector Final Iterative Configuration

As expected, the deformed areas are in the direction of the loading. The compressive

loading case also shows the necessity of a thrust structure integrated on the reaction

chamber, as was the case with the tensile loading.

4.3.3 Reaction Chamber and Pellet Injector Assembly Static Tensile (Operational)

Loading with Thicker Reaction Chamber Wall

After these operational and failure load cases were analyzed, another finite

element model was generated for the static tensile case with a thicker reaction chamber

wall. For all other scenarios in this study, the reaction chamber wall is maintained at

0.043 inches as per the Daedalus parameter. This was not changed as there are other

fields and aspects of Icarus where this thickness is a key to operation. However, the case

in this subsection analyzes increasing the wall thickness by a factor of two (from 0.043 to 0.086 inches) to analyze effect on loading results. Shell thicknesses are assigned in the finite element model initial condition set-up. The initial conditions and mesh are the same as with the two previous cases of this section. The mesh details are 40,310 nodes and 19,920 elements. The degrees of freedom of this model are 227,307. The next figure shows the von Mises stress results for this altered thickness tensile case.
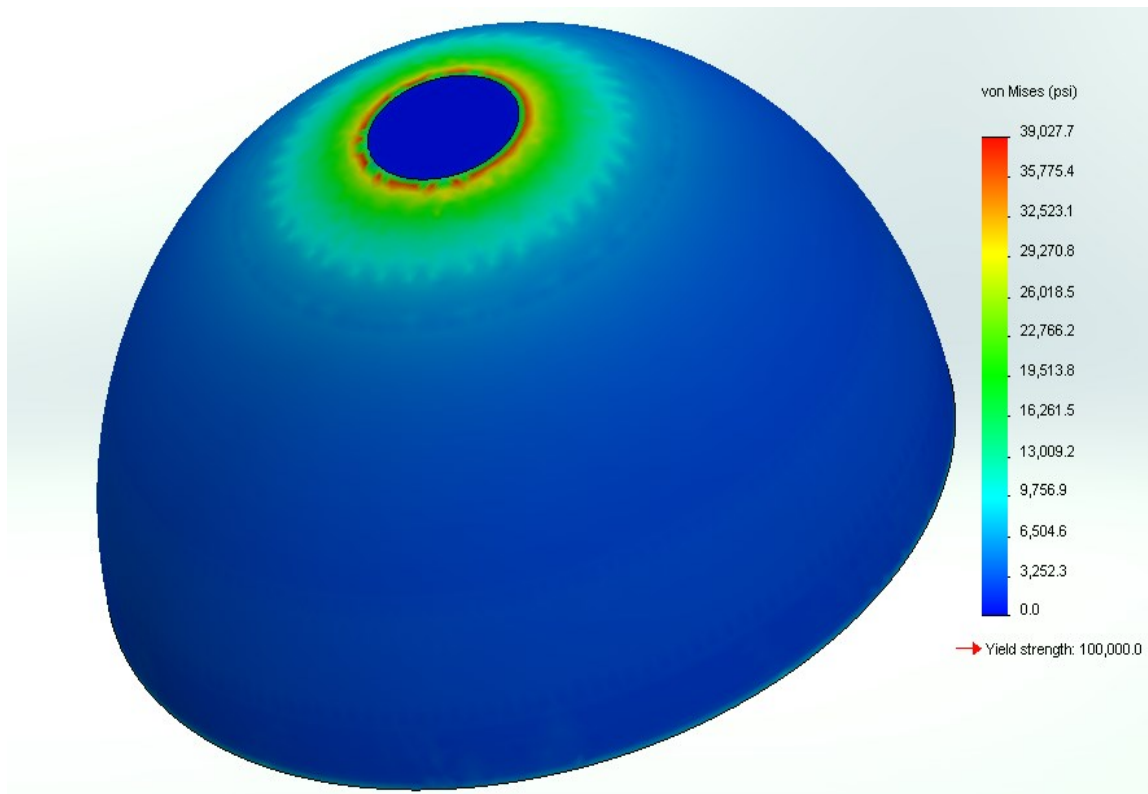
Figure 41: von Mises Stress Results for Static Tensile FEM of RC and Pellet Injector Final Iterative Configuration with Increased Reaction Chamber Wall Thickness

The maximum von Mises stress for this model is 39,028 psi. This is compared to the von Mises stress of 77,867 psi from the Daedalus parameter wall thickness. Increasing the wall thickness by a factor of two decreases the von Mises stress by almost the same factor. For a simple hemispherical model, this result is expected. Equation (3.2) shows

that stress is dependent on the thickness of the hemisphere in the denominator. Thus,

doubling the thickness will subsequently halve the stress. Figure 42 shows the resultant

displacement at this increased wall thickness.
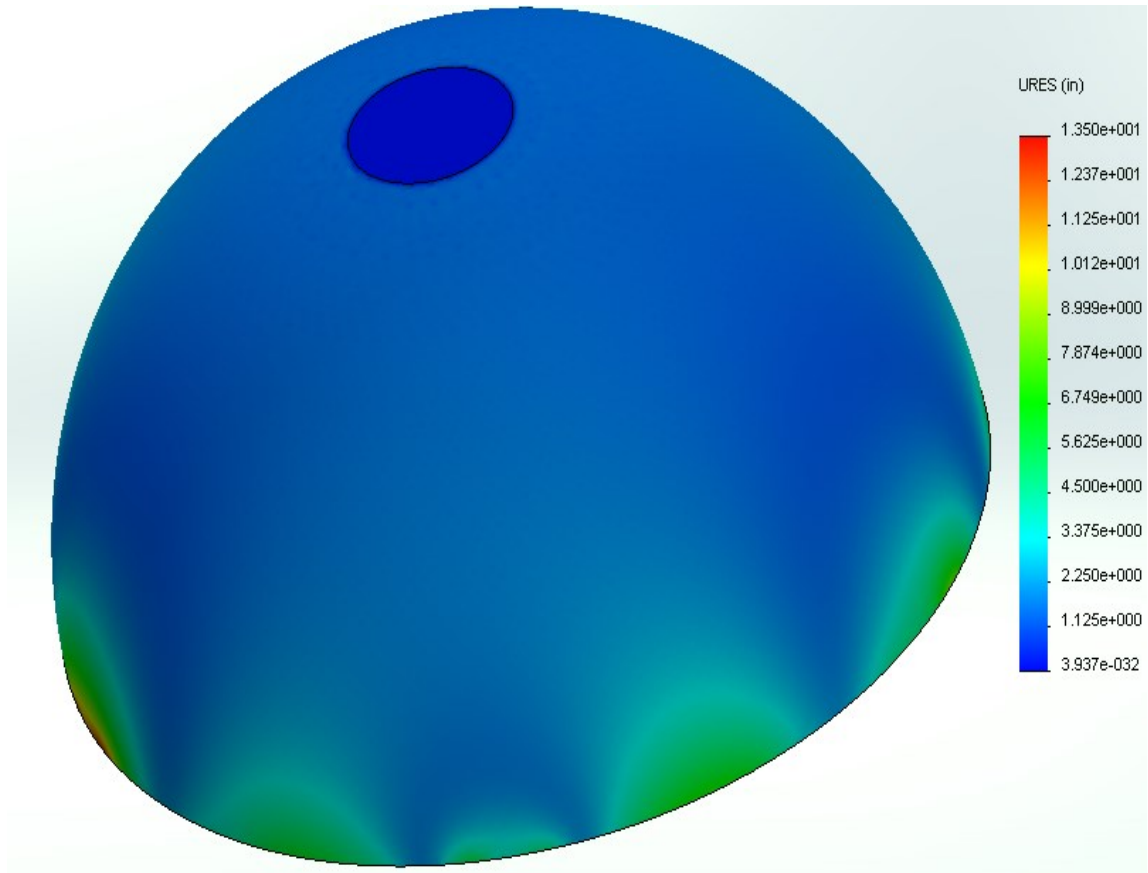
Figure 42: Resultant Displacement for Static Tensile FEM of RC and Pellet Injector Final Iterative Configuration with Increased Reaction Chamber Wall Thickness

The maximum resultant displacement is 13.5 inches. This is compared to 42.5 inches at

the Daedalus parameter wall thickness of 0.043 inches. Increasing the wall thickness by a

factor of two decreases the resultant displacement by a factor of 3.15.

The differences in stress and displacement results by increasing the reaction

chamber wall thickness are significant. For future considerations of the Icarus team, this

wall thickness may be changed iteratively as necessary, factoring in all considerations of

altering the wall thickness. Be cautioned that changing the reaction chamber wall

thickness will have direct implications on other research modules of Icarus. For instance, changing the wall thickness on this structure has direct implications on the electromagnetic field conveyed through the reaction chamber to the external field coils, affecting thrust of the structure.

4.4 Reaction Chamber and Pellet Injector Assembly Finite Element Model for Frequency Analysis

The reaction chamber and pellet injector assembly are analyzed for natural frequencies. Two cases are explored for the assembly's natural frequency: fixed at the ignition coil interface (bottom) as in Chapter 3, and fixed at the pellet injector interface (top), as the structure is now stable in that condition. This finite element model consists of 11,467 nodes, 5,653 elements, and 62,505 degrees of freedom.

4.4.1 Assembly Frequency Fixed at Ignition Coil Interface (Bottom) Condition

The assembly is fixed at the bottom, the same as the fixed end condition in Chapter 3. This is where the ignition coil system is located. Figure 43 shows the fixture condition, mesh, and first four natural frequencies for this model.
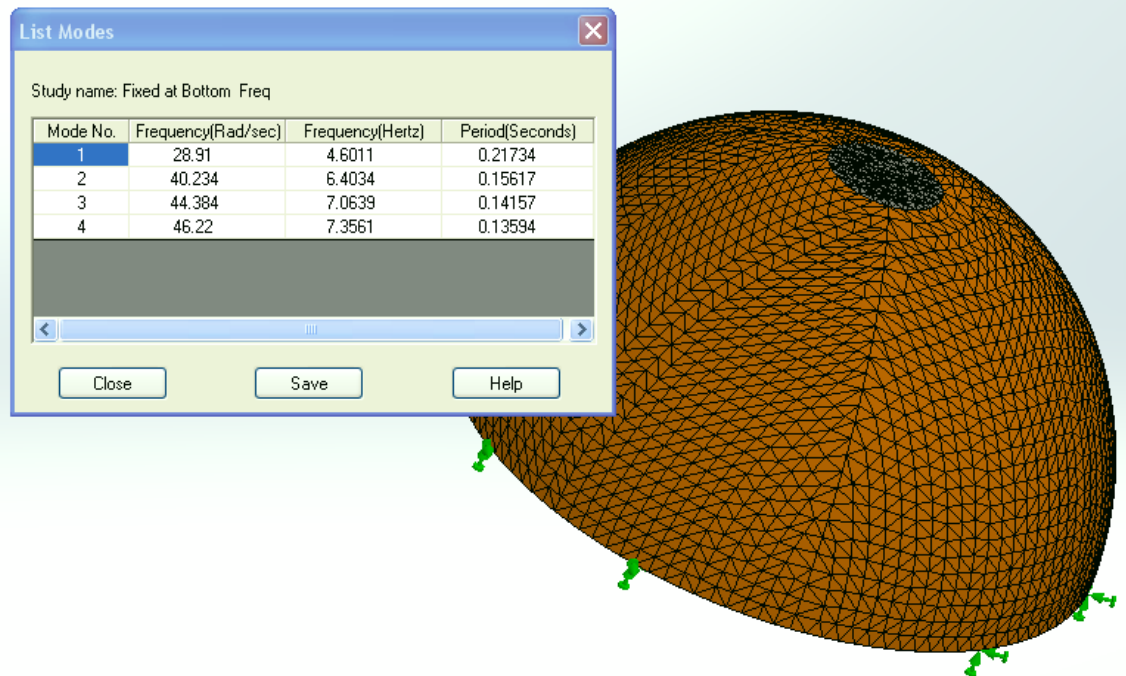
Figure 43: Frequency Analysis of Reaction Chamber and Pellet Injector Assembly Fixed at Ignition Coil Interface (Bottom)

The first natural frequency is 4.60 Hz, with the second natural frequency being 6.40 Hz, and the third natural frequency being 7.06 Hz. Table 4 lists the natural frequencies for the first thirty modes of this configuration.

Mode No.	Frequency (Hz)	Mode No.	Frequency (Hz)	Mode No.	Frequency (Hz)
1	4.6011	11	8.8495	21	9.3719
2	6.4034	12	8.8635	22	9.3858
3	7.0639	13	8.9406	23	9.5838
4	7.3561	14	9.0321	24	9.5852
5	7.9968	15	9.0421	25	9.6783
6	8.3861	16	9.1509	26	9.6912
7	8.4335	17	9.1880	27	9.7391
8	8.5913	18	9.2068	28	9.8195
9	8.6958	19	9.2171	29	9.8721
10	8.7065	20	9.2305	30	10.006

Table 4: Modal Analysis Natural Frequency Results of Reaction Chamber and Pellet Injector Assembly Fixed at Ignition Coil Interface

This compares to 7.86 Hz as the fundamental frequency for the Reaction Chamber by itself fixed on the bottom as per Section 3.4.1. The fundamental frequency of this assembly is 4.60 Hz, and this difference can be explained by the slight geometry change at the top of the reaction chamber to allow for a flat surface at the pellet injector interface, and the addition of the pellet injector interface part itself to this assembly. The added mass and geometry changes account for a change in frequency for this model.

4.4.2 Assembly Frequency Fixed at Pellet Injector Interface (Top) Condition

This finite element model is run with the same mesh conditions as the previous subsection. However, this model is fixed at the top of the pellet injector interface as opposed to the bottom at the ignition coil interface. Figure 44 shows the mesh, initial fixture conditions, and first seven frequency modes for this model.

List Modes

Study name: Fixed at Top Freq

Mode No.	Frequency(Rad/sec)	Frequency(Hertz)	Period(Seconds)
1	0.05722	0.0091068	109.81
2	0.099323	0.015808	63.26
3	0.15432	0.024561	40.716
4	0.2364	0.037624	26.579
5	0.25514	0.040607	24.627
6	0.31291	0.049801	20.08
7	0.36983	0.058861	16.989

Close   Save   Help
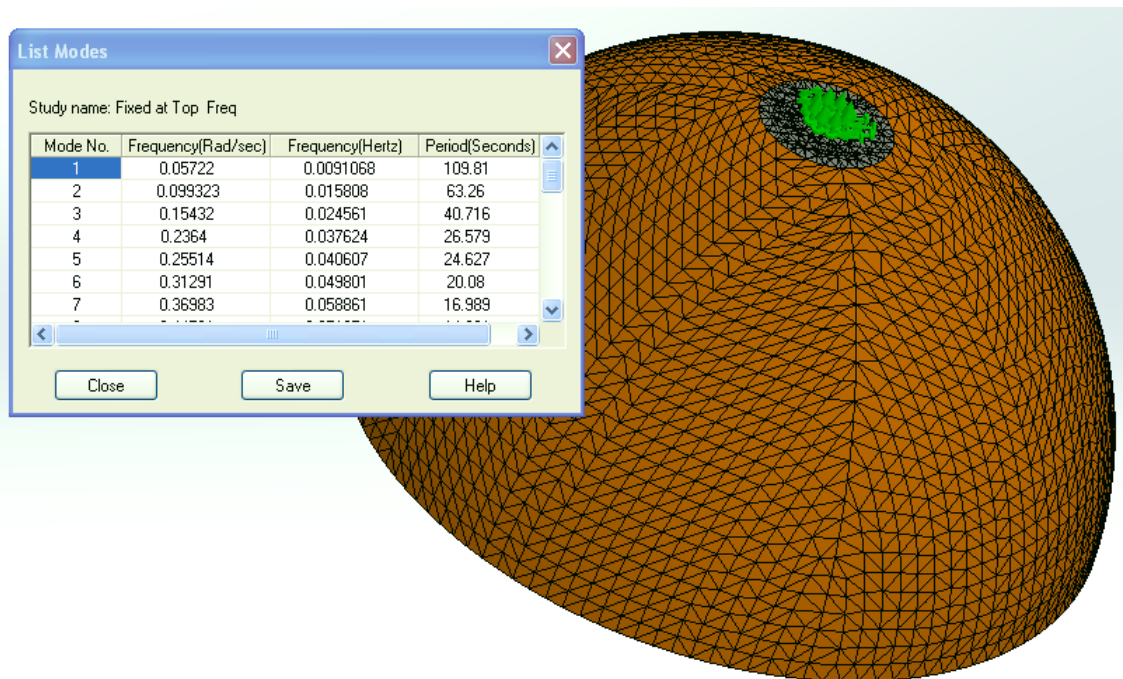
Figure 44: Frequency Analysis of Reaction Chamber and Pellet Injector Assembly Fixed at Pellet Injector Interface (Top)

The first natural frequency is 0.009 Hz, with the second natural frequency being 0.015 Hz, and the third natural frequency being 0.024 Hz. Table 5 lists the natural frequencies for the first thirty modes of this configuration.

Mode No.	Frequency (Hz)	Mode No.	Frequency (Hz)	Mode No.	Frequency (Hz)
1	0.0091	11	0.1007	21	0.2059
2	0.0158	12	0.1127	22	0.2192
3	0.0245	13	0.1265	23	0.2328
4	0.0376	14	0.1329	24	0.2362
5	0.0406	15	0.1429	25	0.2491
6	0.0498	16	0.1566	26	0.2630
7	0.0588	17	0.1718	27	0.2670
8	0.0712	18	0.1727	28	0.2799
9	0.0840	19	0.1865	29	0.2919
10	0.0983	20	0.2020	30	0.2996

Table 5: Modal Analysis Natural Frequency Results of Reaction Chamber and Pellet Injector Assembly Fixed at Pellet Injector Interface

Fixing the reaction chamber assembly at the pellet injector interface drastically reduces the natural frequencies as compared to being fixed at the bottom. Changing the assumed fixture conditions from the periphery of the bottom of the reaction chamber to the top at the pellet injector interface produces two very different models. In the finite element analysis of this spacecraft, assumed fixture conditions have a direct impact on results and should be carefully evaluated.

5. Reaction Chamber, Thrust Structure, and Pellet Injector Interface Finite Element Model Fixed at the Pellet Injector Interface (Top)

5.1 Reaction Chamber, Thrust Structure, and Pellet Injector Interface Shell Model

In this chapter, an integrally-backed thrust structure is added to the Icarus structure. This thrust structure consists of 12 lateral braces and one brace at the bottom of the reaction chamber. Each brace is 3 feet in width at 0.100 inches thick. Figure 45 shows the reaction chamber with the thrust structure and pellet injector interface included.

Figure 45: Reaction Chamber with Thrust Structure Isometric View

The thrust structure addition to the reaction chamber assembly can be seen outlined in blue in this figure. Figure 46 shows an exploded view of the thrust structure and pellet

injector interface separated from the reaction chamber, to show a clear view of these parts.
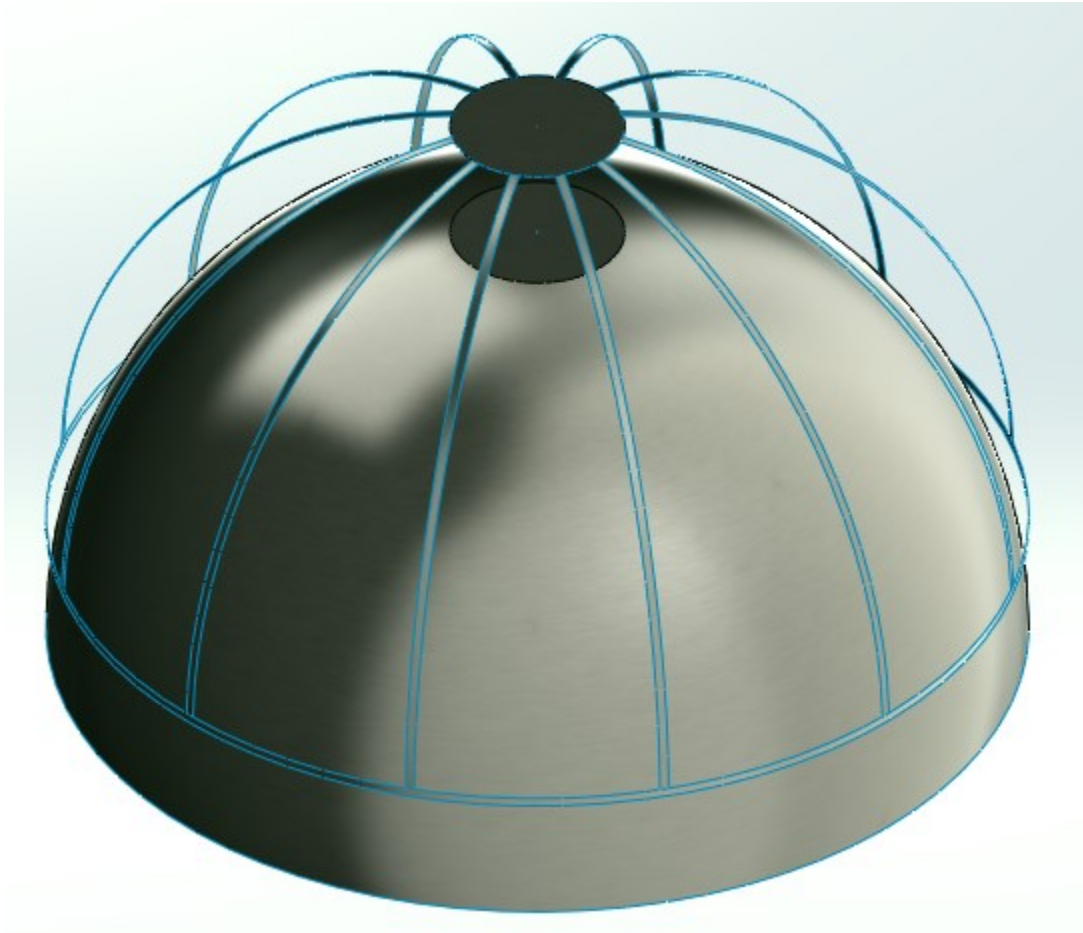
Figure 46: Reaction Chamber with Thrust Structure Exploded View

The figure clearly depicts the interface to the reaction chamber. The braces of the structure are modeled here as Molybdenum TZM, but the material may be changed as design progresses. The addition of the thrust structure provides key support to the operational tensile loading on the reaction chamber, by interfacing directly to the reaction chamber. These braces would be attached to the reaction chamber via electron beam welding, and this will be explored further in the manufacturing chapter.

5.2 Reaction Chamber, Thrust Structure, and Pellet Injector Interface Finite Element Model for Static Loading

With the addition of more parts, the finite element assembly model becomes more complex. The new thrust structure parts are treated as shell elements similar to the reaction chamber, as the thickness is very small compared to its other respective dimensions. Contact conditions have to be explicitly specified to ensure appropriate resolution of the model.

5.2.1 Reaction Chamber, Thrust Structure, and Pellet Injector Assembly Static Tensile (Operational) Loading

The operational loading of this assembly is explored first. One would intuitively expect a decrease of the deformation conditions that were present without the thrust structure in the previous chapter. Figure 47 shows the initial conditions and mesh of this finite element model.
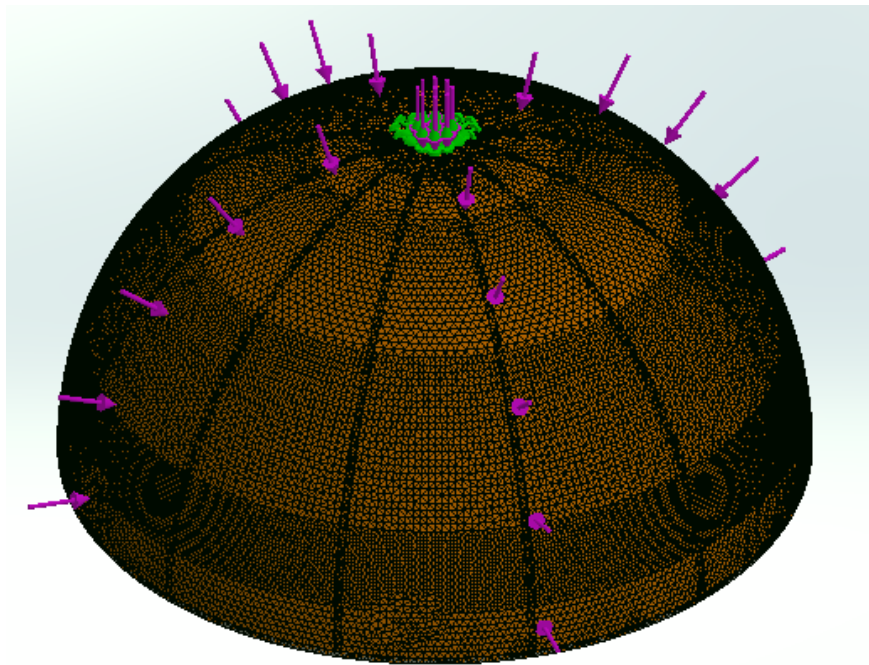
Figure 47: Initial Conditions and Mesh of Thrust Structure and RC Interface Tensile Loading Configuration

The magenta arrows represent the tensile loading on the reaction chamber with the green arrows representing the interface to the pellet injector being a fixed condition. This model consists of 91,320 nodes and 44,760 elements. There are 547,512 degrees of freedom in this model. Figure 48 shows the von Mises resultant stress results from this loading condition.

Figure 48: von Mises Stress Results for Static Tensile FEM of Thrust Structure and Reaction Chamber

The maximum von Mises stress is 80,595 psi, which in under the 0.2% offset yield strength of TZM at room temperature. For this stage of the design, this is considered an acceptable stress (as there are still other elements of the Icarus structure to be added that will affect stress distribution). As the structure becomes more finalized, detailed design will work to reduce this stress to lower levels.

The next figure, Figure 49, shows the resultant displacement from this loading. This model compares to the resultant displacement of just the reaction chamber and pellet injector interface of the last chapter, which was 42.5 inches.
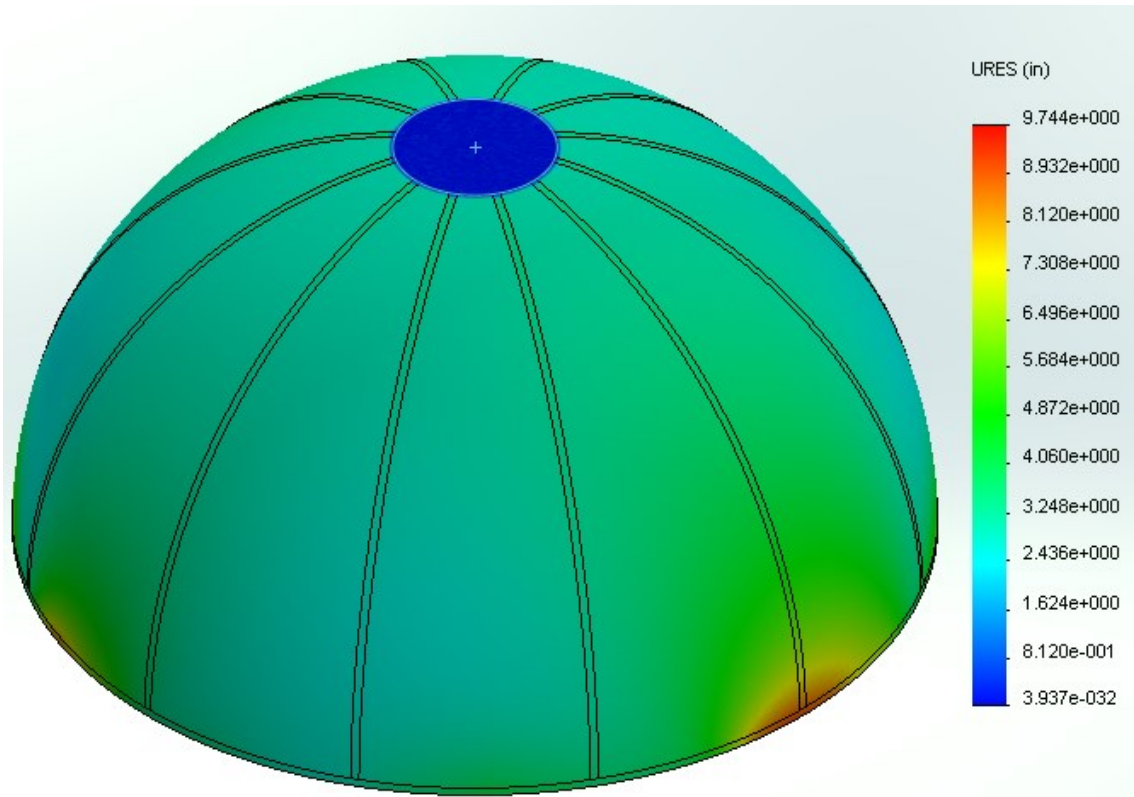
Figure 49: Resultant Displacement for Static Tensile FEM of Thrust Structure and Pellet Injector Interface

The maximum resultant displacement from this model is 9.74 inches. The model without the thrust structure strapping has a maximum resultant displacement of 42.5 inches.

5.2.2 Reaction Chamber, Thrust Structure, and Pellet Injector Assembly Static Compressive (Ignition Failure) Loading

Compressive loading of this assembly is now explored. Figure 50 shows the initial conditions and mesh for this model.
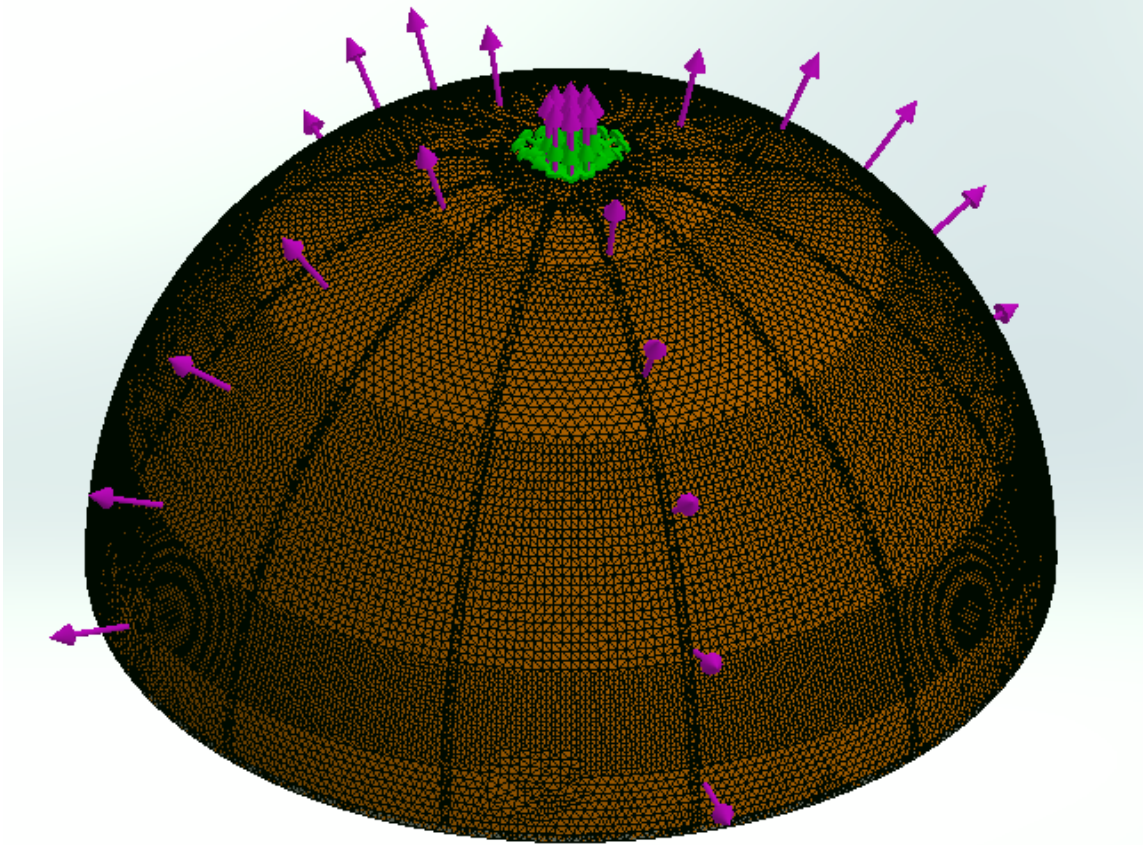
Figure 50: Initial Conditions and Mesh of Thrust Structure and RC Interface Compressive Loading Configuration

This model also consists of 91,320 nodes, 44,760 elements, and 547,512 degrees of freedom. The maximum von Mises stress, stress distribution, and resultant displacement are equal to that of the tensile loading case of 5.2.1, and are so omitted here.

5.3 Reaction Chamber and Thrust Structure Assembly Finite Element Model for Frequency Analysis

A modal analysis was then conducted to explore the assembly's natural frequencies and modes. This assembly is fixed at the pellet injector interface, to simulate its connection conditions with the rest of the starship. The first thirty natural frequencies are calculated. Figure 51 shows the mesh, fixture condition, and first seven natural

frequencies of this assembly. This finite model consists of 74,621 nodes, 36,149

elements, and 447,078 degrees of freedom.
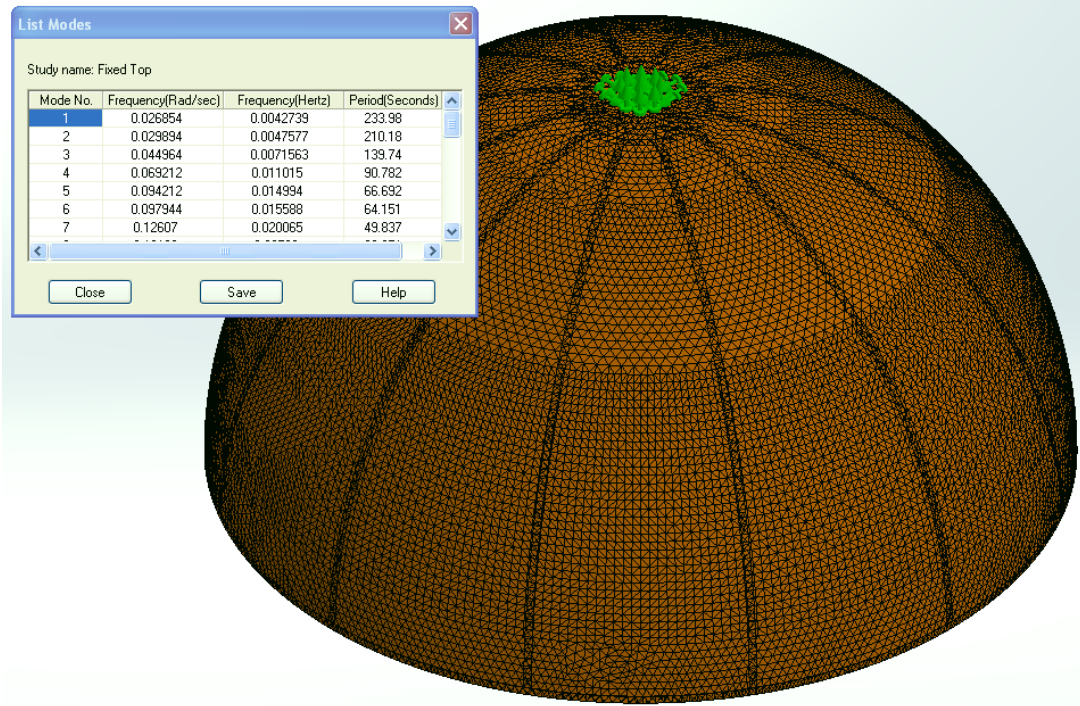
Figure 51: Frequency Analysis of Reaction Chamber and Thrust Structure Fixed at Pellet Injector Interface

We know that stiffening a structure will increase its natural frequency. Also, as more

mass is added to a system, the frequencies would lower as well. In our system, the thrust

structure provides more stiffness to the system, but the added mass to the system is also

significant, thus resulting in the lowering of the frequencies. Table 6 shows a weight

summary of the components of the assembly.

Part Name	Material	Thickness (in)	Weight (Each- lbs)	Total Weight (lbs)
Reaction Chamber	TZM Alloy	0.043	387325	387325
Pellet Injector Interface	TZM Alloy	0.100	14239	14239
Lateral Thrust Structure Brace (QTY 12)	TZM Alloy	0.100	3550	42602
Bottom Thrust Structure Brace	TZM Alloy	0.100	32950	32950

Table 6: Reaction Chamber and Thrust Structure Property Summary

There is a total of 89,791 pounds added to the assembly, which is approximately a 23 percent increase in weight from the Reaction Chamber by itself. Table 7 shows the first thirty natural frequencies of this structure.

Mode No.	Frequency (Hz)	Mode No.	Frequency (Hz)	Mode No.	Frequency (Hz)
1	0.0042	11	0.0322	21	0.0760
2	0.0047	12	0.0393	22	0.0762
3	0.0071	13	0.0394	23	0.0870
4	0.0110	14	0.0396	24	0.0872
5	0.0149	15	0.0467	25	0.0987
6	0.0155	16	0.0483	26	0.0989
7	0.0200	17	0.0563	27	0.1103
8	0.0256	18	0.0564	28	0.1125
9	0.0257	19	0.0656	29	0.1244
10	0.0321	20	0.0661	30	0.1249

Table 7: Modal Analysis Natural Frequency Results of Reaction Chamber and Thrust Structure Fixed at Pellet Injector Interface

The first natural frequency is 0.004 Hz. This is safely removed from the 250 Hz detonation rate of the propulsion system.

6. Reaction Chamber, Thrust Structure, Induction Loop, Field Coils, and Pellet Injector Interface Fixed at the Pellet Injector Interface (Top)

6.1 Reaction Chamber, Thrust Structure, Induction Loop, and Field Coil Assembly Shell Model

In this chapter, the Induction Loop, Field Coils (1 through 4), and supporting structure for those elements are added to the model. This encompasses all the parts below the parabolic reflector interface for this study. Figure 52 shows the assembly model with all these new parts included.
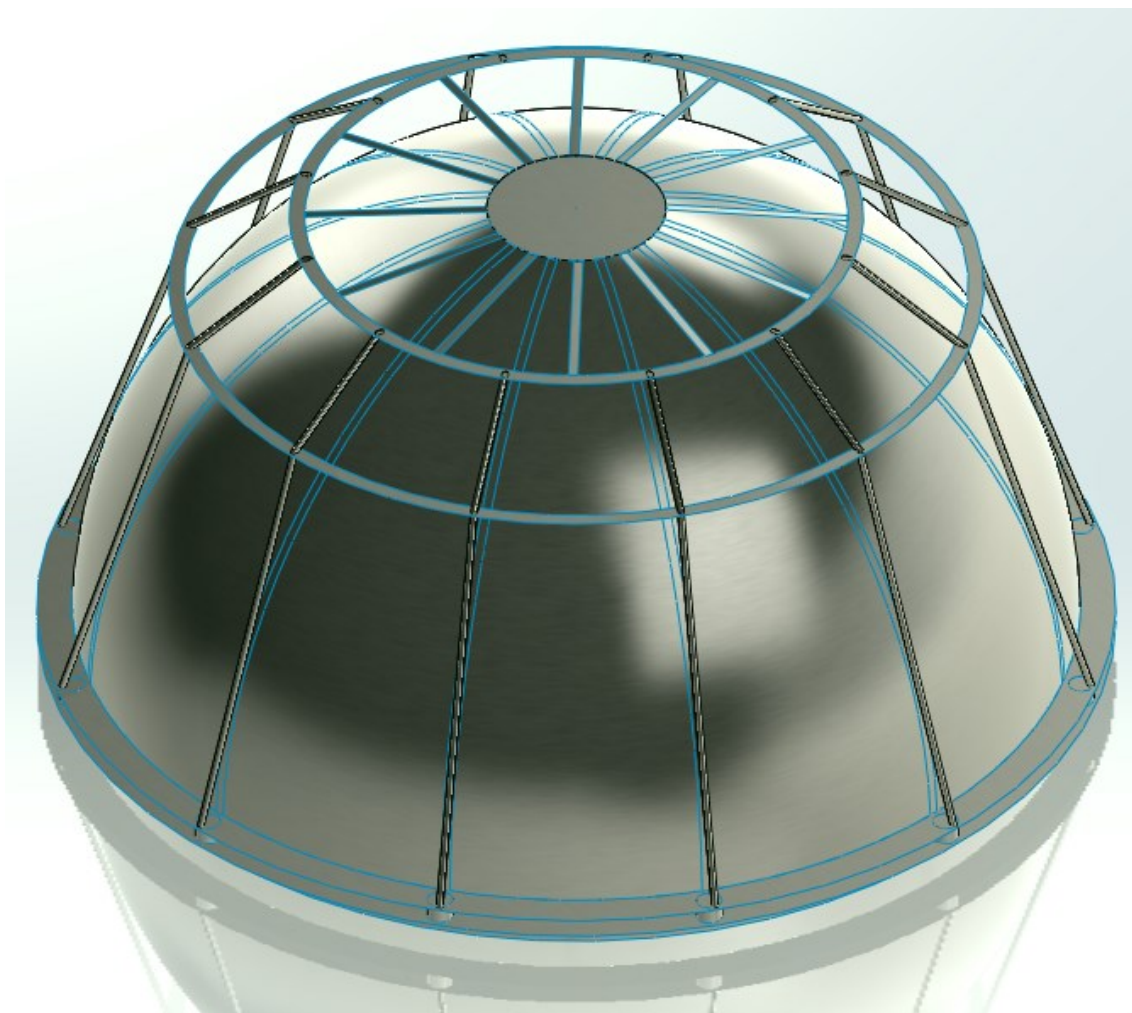
Figure 52: Reaction Chamber with Thrust Structure, Induction Loop, and Field Coils Isometric View

The next figure, Figure 53, shows an exploded view of this assembly so the additional parts can be clearly seen.
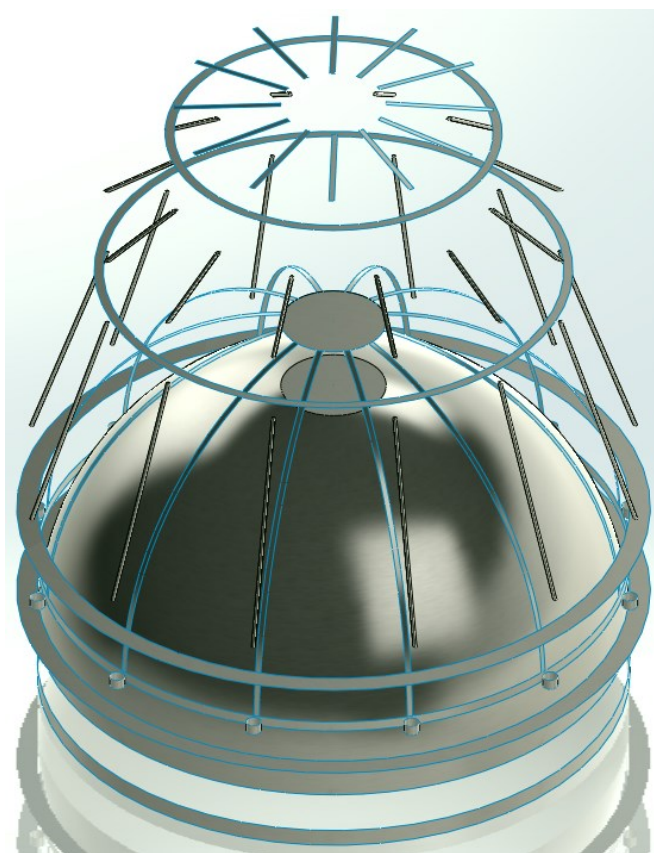
Figure 53: Reaction Chamber with Thrust Structure, Induction Loop, and Field Coils Exploded View

There is an addition of the Induction Loop to the aft (bottom) end of the reaction chamber. Also on the aft end are the additions of Field Coils 3 and 4, with their supporting structure. The supporting structure consists of 12 struts. This is also true for the supporting structure between Field Coils 3, 2, and 1, which are also tubular struts. The supporting structure between Field Coil 1 on the forward (top) end and the pellet injector interface consists of 12 braces, similar to those used in the thrust structure. These new parts are all modeled with the material properties of Extra-low-interstitial Titanium

(TI-5Al-2.5Sn, ELI). The modulus of elasticity for the titanium is 16 million psi with the

Poisson ratio as 0.31. Figure 54 shows a graphic detailing the new parts.
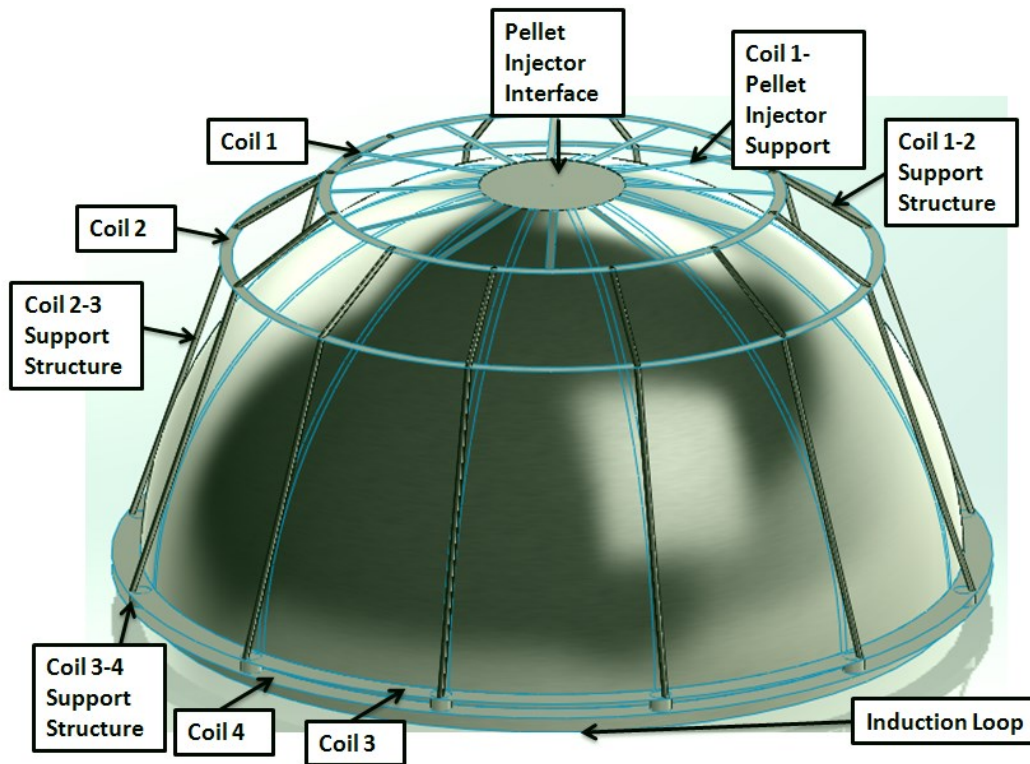
Figure 54: Reaction Chamber with Thrust Structure, Induction Loop, and Field Coils Detailed View

Table 8 shows the weight and material properties breakdown for the items of this

assembly, as mass is an important consideration for any spacecraft.

Part Name	Material	Thickness (in)	Weight (Each- lbs)	Total Weight (lbs)
Reaction Chamber	TZM Alloy	0.043	387325	387325
Pellet Injector Interface	TZM Alloy	0.100	14239	14239
Lateral Thrust Structure Brace (QTY 12)	TZM Alloy	0.100	3550	42602
Bottom Thrust Structure Brace	TZM Alloy	0.100	32950	32950
Coil 3 and 4 Support (QTY 12)	Ti-5Al-2.5Sn	0.250	914	10966
Coil 3	Ti-5Al-2.5Sn	0.330	94252	94252
Coil 4	Ti-5Al-2.5Sn	0.400	113194	113194
Induction Loop	Ti-5Al-2.5Sn	0.250	60114	60114
Coil 2	Ti-5Al-2.5Sn	0.070	6669	6669
Coil 1	Ti-5Al-2.5Sn	0.800	53255	53256
Coil 2 and 3 Support (QTY 12)	Ti-5Al-2.5Sn	0.250	5002	60027
Coil 1 and 2 Support (QTY 12)	Ti-5Al-2.5Sn	0.250	1790	21482
Coil 1 and Pellet Injector Support (QTY 12)	Ti-5Al-2.5Sn	0.100	414	4972

Table 8: 1st Stage Components Property Summary

6.2 Reaction Chamber, Thrust Structure, Induction Loop, and Field Coil Assembly Finite Element Model for Static Loading

With the addition of all these new components, the assembly and finite element model become increasingly complex. Contact conditions have to be explicitly defined as there is a mixture of solid and shell elements in the model. Also, care must be taken to assign correct properties to the shell elements. A significant amount of time is spent pre-processing the model to ensure an accurate simulation.

6.2.1 Reaction Chamber, Thrust Structure, Induction Loop, and Field Coil Assembly Static Tensile (Operational) Loading

First, the operational loading of this assembly is explored. Figure 55 shows the initial conditions and mesh for this assembly model.
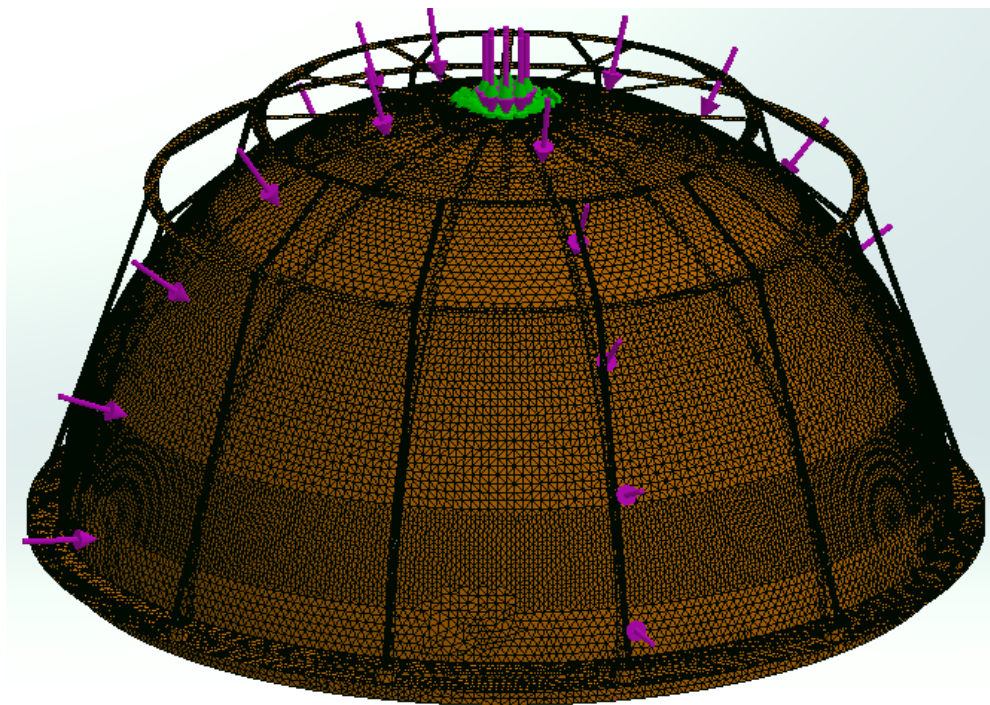
Figure 55: Initial Conditions and Mesh of Thrust Structure, Induction Loop, and Field Coil Tensile Loading Configuration

The magenta arrows show the direction of the tensile loading, the same as all the other models. The initial conditions are unchanged and the loading is the same. This finite element model consists of 186,051 nodes, 90,718 elements, and 1,244,802 degrees of freedom. Figure 56 shows the resultant von Mises stress from this loading.
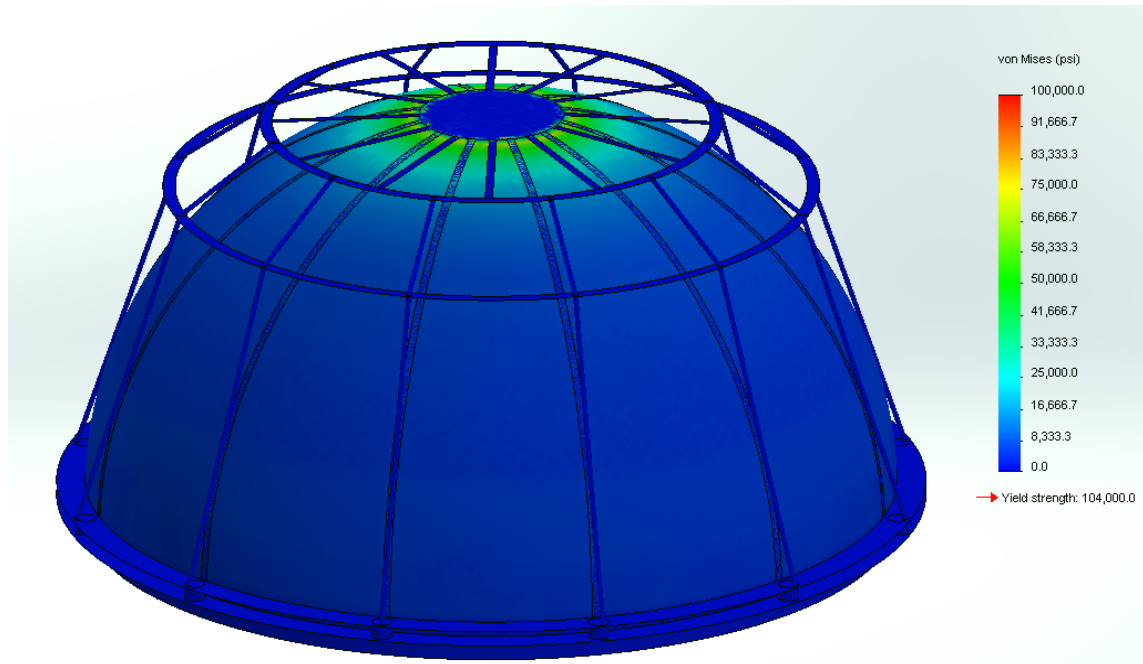
Figure 56: von Mises Stress Results for Static Tensile FEM of Thrust Structure, Induction Loop, Field Coils, and Reaction Chamber

The highly stressed area around the pellet injector interface has an average stress of

58,295 psi. This is under the 0.2% offset yield strength of both TZM and Titanium used

in this assembly. For reference, the room temperature 0.2% yield strength of the TZM is

100 ksi and for the Titanium is 104 ksi. Titanium alloy has a ultimate tensile strength

(UTS) ratio of 1.03 at a temperature of 20 K. The UTS ratio is the ratio between the

ultimate tensile strength at room temperature to the desired temperature. Therefore, the

full mechanical properties may be assumed for analysis in space.

Table 9 shows a summary of the finite element models of the different cases.

Case	Components	Fixture Condition	Loading	Elements	Nodes	DOF	Avg Stress (psi)
1	Reaction Chamber	Bottom Periphery	Tensile	17369	34974	207024	3087
2	Reaction Chamber and Injector Interface	Top Injector Face	Tensile	19920	40310	227307	63076
3	Reaction Chamber, Injector Interface, and Thrust Structure	Top Injector Face	Tensile	44760	91320	547512	59890
4	Reaction Chamber, Injector Interface, Thrust Structure, and Truss Structure	Top Injector Face	Tensile	90718	186051	1244802	58295

Table 9: FEM Summary for Analysis Cases

The average stresses presented in Table 9 are taken around the interface of the pellet injector to the reaction chamber.

The next figure shows the resultant displacement from this loading. This is shown in the deformed scale, so that the effects of the loading can be studied.
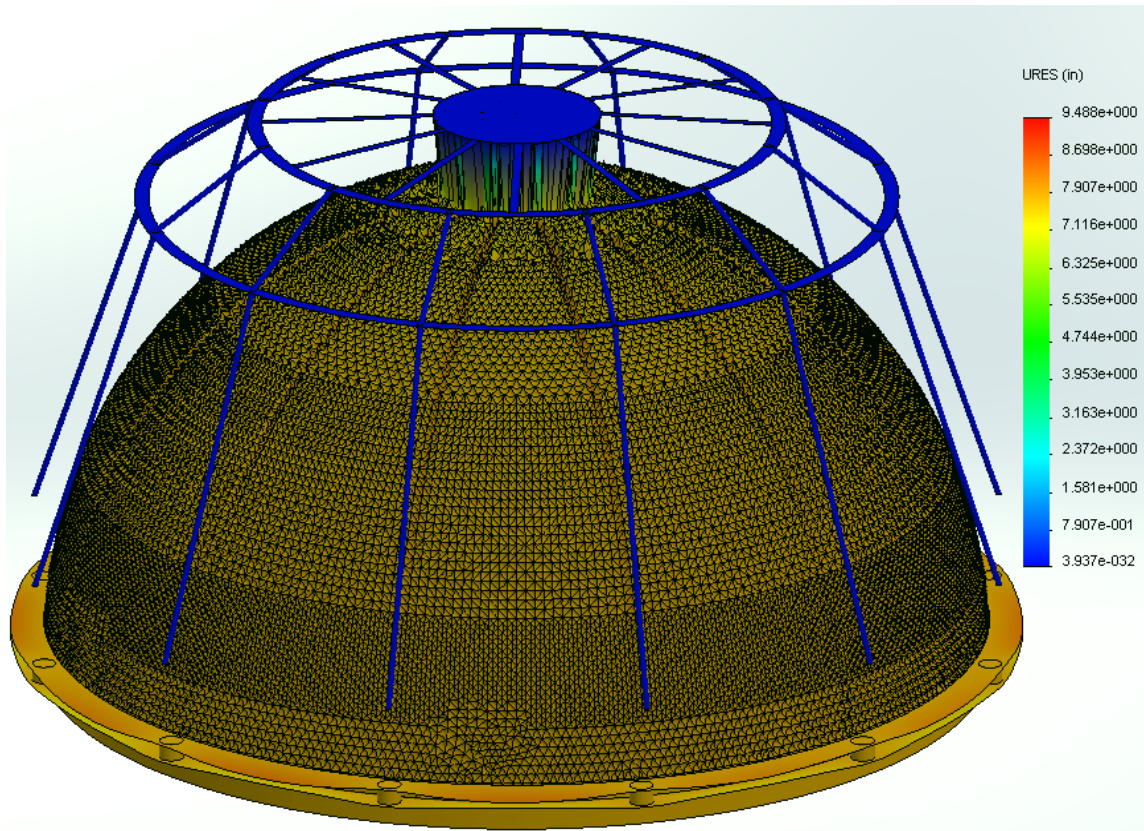
Figure 57: Resultant Displacement for Static Tensile FEM of Thrust Structure, Induction Loop, Field Coils, and Reaction Chamber

This figure shows that the operational loading wants to 'pull' the reaction chamber from its structure. However, due to the nature of the finite element model, the supports between Field Coils 2 and 3 would actually offer more rigidity to the structure than shown. Therefore, this model is more conservative in nature.

6.2.2 Reaction Chamber, Thrust Structure, Induction Loop, and Field Coil Assembly Static Compressive (Ignition Failure) Loading

The compressive loading on this assembly is studied next. Figure 58 shows the initial conditions and mesh for this configuration.
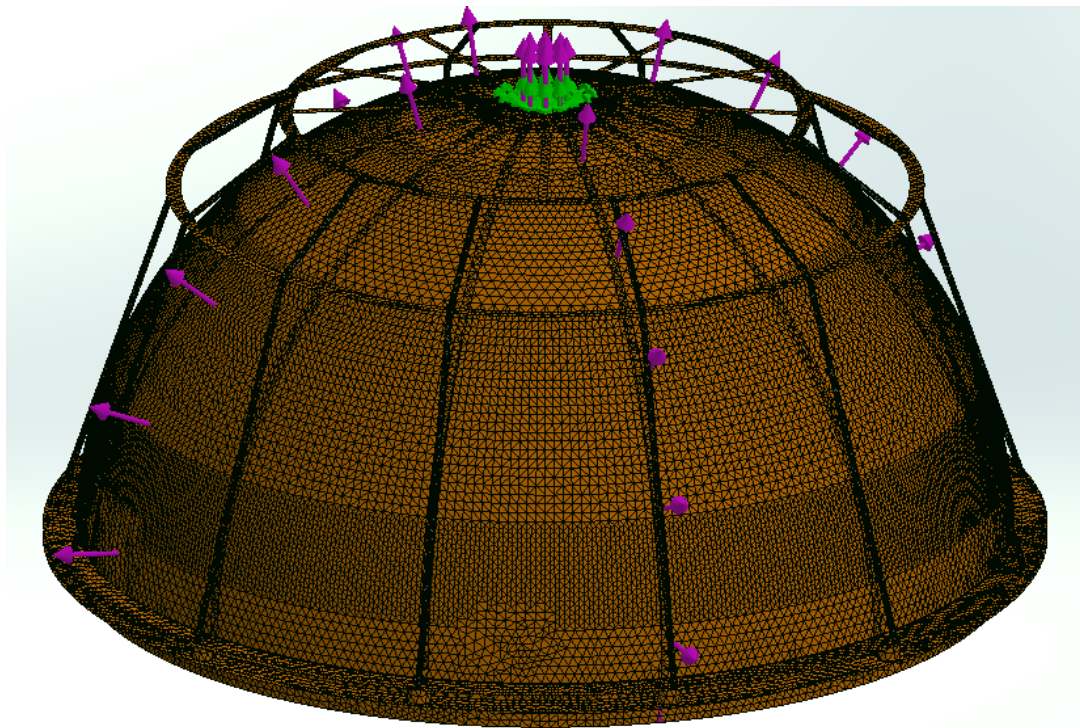
Figure 58: Initial Conditions and Mesh of Thrust Structure, Induction Loop, and Field Coil Compressive Loading Configuration

The nodes, elements, and degrees-of-freedom are the same as the previous subsection.

Here, only, the direction of loading is altered for this configuration. The maximum von

Mises stress, stress distribution, and resultant displacement are equal to that of the tensile loading case of 6.2.1, and so are omitted here.

6.3 Reaction Chamber, Thrust Structure, Induction Loop, and Field Coil Assembly Finite Element Model for Frequency Analysis

A modal analysis was then conducted to explore the assembly's natural frequencies and modes. This assembly is also fixed at the pellet injector interface, to simulate its connection conditions with the rest of the starship. The first thirty natural frequencies are calculated. Figure 59 shows the mesh, fixture condition, and first five natural frequencies of this assembly. This finite model consists of 212,203 nodes, 103,650 elements, and 1,405,410 degrees of freedom.
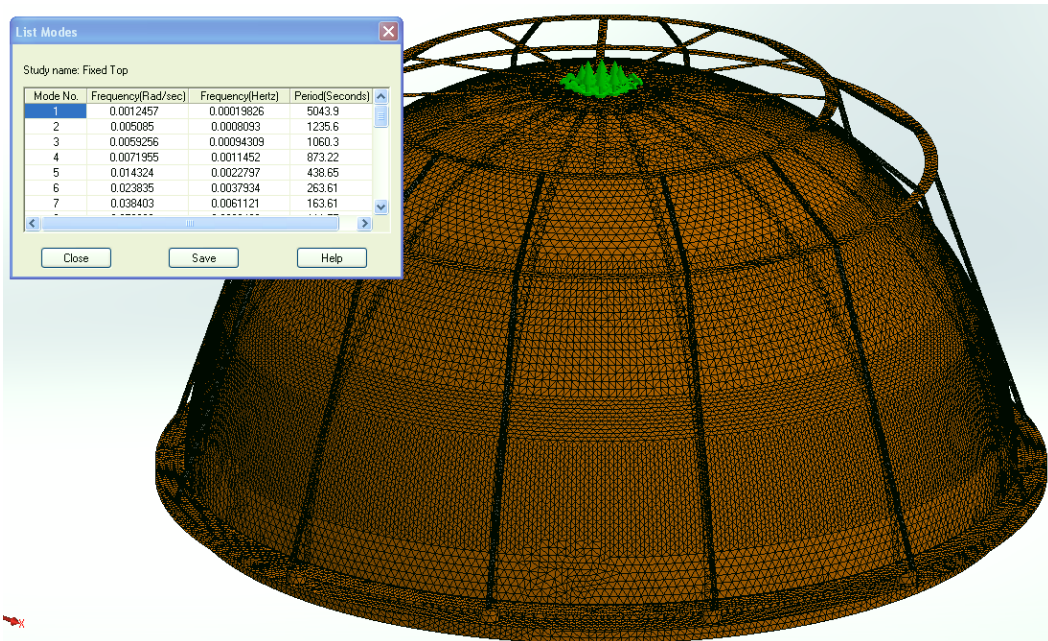
Figure 59: Frequency Analysis of Reaction Chamber, Thrust Structure, Induction Loop, and Field Coil Fixed at Pellet Injector Interface

There is a total of 424,932 pounds added to the assembly, or approximately an 89 percent

weight increase from the model of the previous chapter. Table 10 shows the natural

frequency summary for the first thirty modes.

Mode No.	Frequency (Hz)	Mode No.	Frequency (Hz)	Mode No.	Frequency (Hz)
1	0.0002	11	0.0162	21	0.0349
2	0.0008	12	0.0191	22	0.0368
3	0.0009	13	0.0192	23	0.0401
4	0.0011	14	0.0206	24	0.0402
5	0.0022	15	0.0219	25	0.0407
6	0.0038	16	0.0254	26	0.0410
7	0.0061	17	0.0255	27	0.0411
8	0.0089	18	0.0309	28	0.0412
9	0.0123	19	0.0309	29	0.0433
10	0.0161	20	0.0348	30	0.0479

Table 10: Modal Analysis Natural Frequency Results of Reaction Chamber, Thrust Structure, Induction Loop, and Field Coil Fixed at Pellet Injector Interface

The natural frequencies are very low in magnitude with the fundamental frequency at

0.0002 Hz.

A sensitivity analysis was performed on this configuration of the finite element

model with regards to the accuracy of the frequency for the modal analysis. The

resolution of the mesh was changed, resulting in 165, 987 nodes, 80,986 elements and

1,120,386 degrees of freedom. Table 11 shows the natural frequency summary for the

first thirty modes of this iteration.

Mode No.	Frequency (Hz)	Mode No.	Frequency (Hz)	Mode No.	Frequency (Hz)
1	0.0001	11	0.0162	21	0.0309
2	0.0004	12	0.0162	22	0.0348
3	0.0008	13	0.0197	23	0.0349
4	0.0009	14	0.0197	24	0.0368
5	0.0012	15	0.0206	25	0.0368
6	0.0038	16	0.0219	26	0.0404
7	0.0061	17	0.0255	27	0.0409
8	0.0089	18	0.0255	28	0.0410
9	0.0089	19	0.0277	29	0.0412
10	0.0123	20	0.0277	30	0.0413

Table 11: Sensitivity Modal Analysis Natural Frequency Results

Comparing the results of Table 10 and Table 11 shows a relative accuracy of the modal

frequencies to the hundredths decimal place.

7. First Stage (Partial) Assembly Interface to Parabolic Reflector

7.1 Interface to Parabolic Reflector Configuration Model

This chapter adds the actuator interface and parabolic reflector to the assembly model. These parts are added as a concept to what the interface may look like, but are not thoroughly studied here or analyzed via finite element modeling. Figure 60 shows an isometric view of the overall assembly model of this configuration.
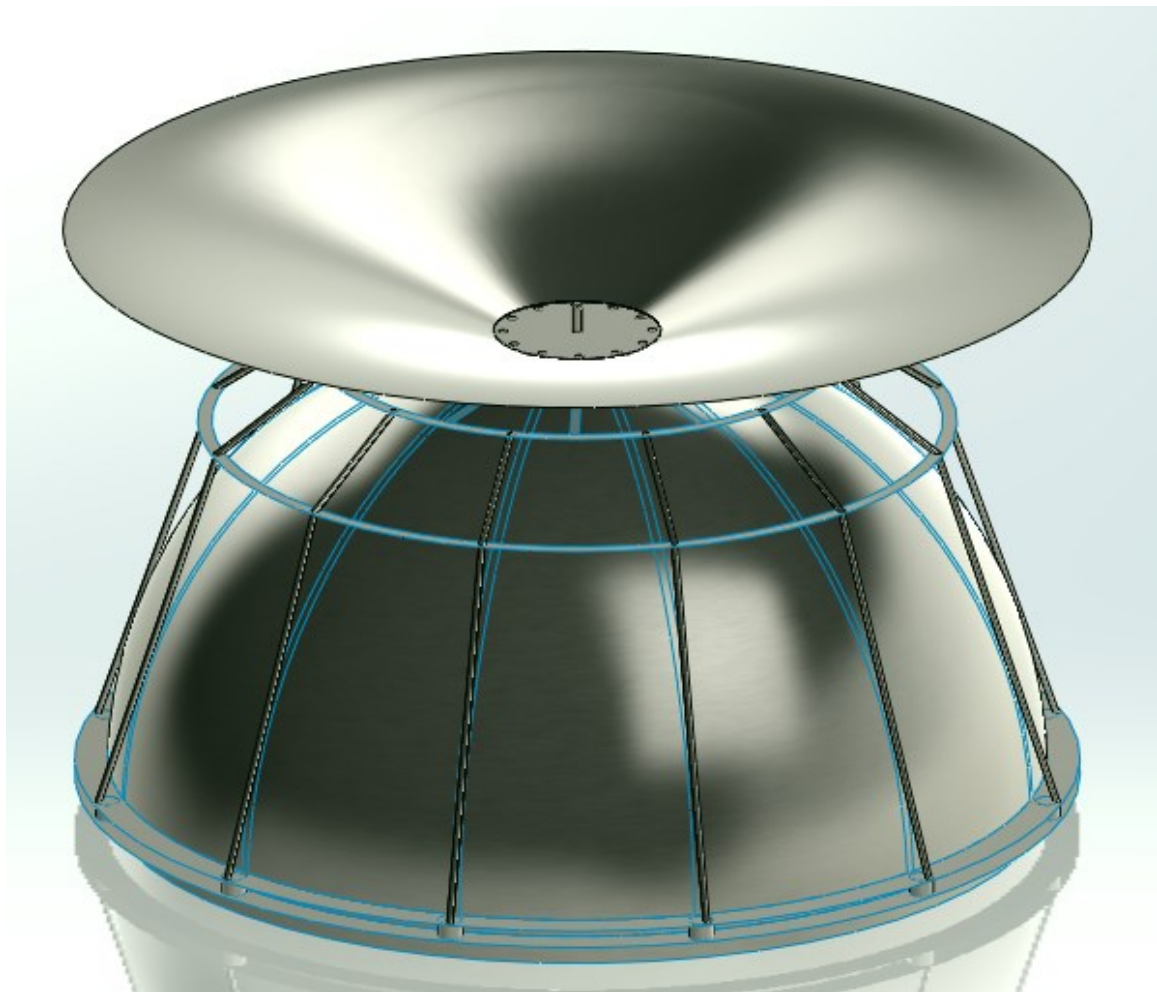
Figure 60: First Stage (Partial) Assembly Isometric View

The next figure shows a right side view of this model.
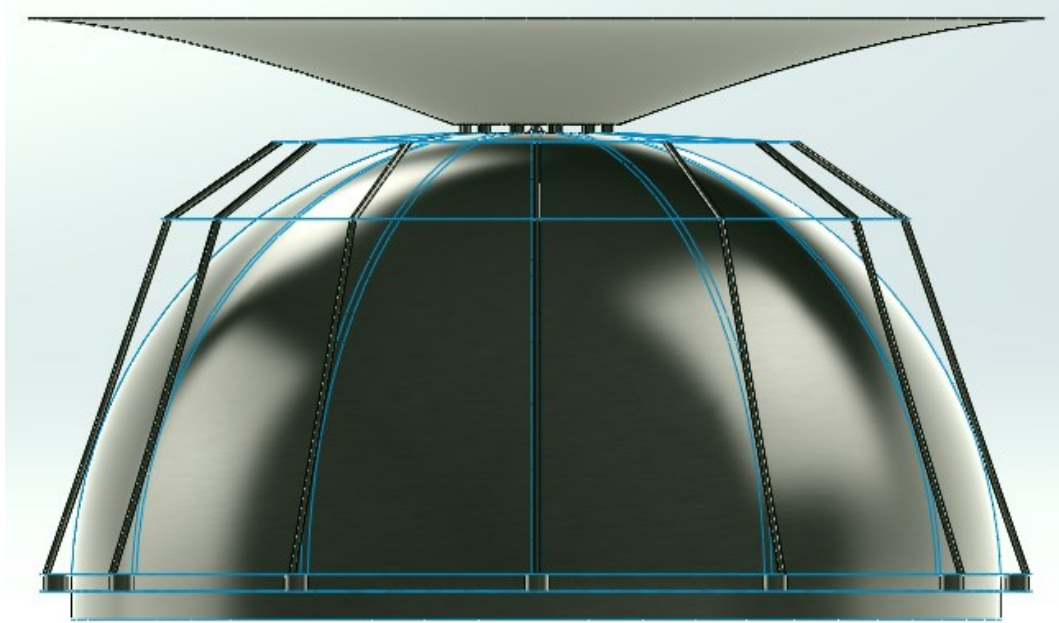
Figure 61: First Stage (Partial) Assembly Right Side View

Figure 62 shows an exploded view of this assembly.

Figure 62: First Stage (Partial) Assembly Exploded View

The additional parts and design will be explored in the next subsections.

7.2 Actuator Design and Interface

The actuator design and interface stems from that proposed in the Project Daedalus study [1]. Figure 63 shows a zoomed in side view of the actuators and its interface to the reaction chamber/thrust structure and to the parabolic reflector.
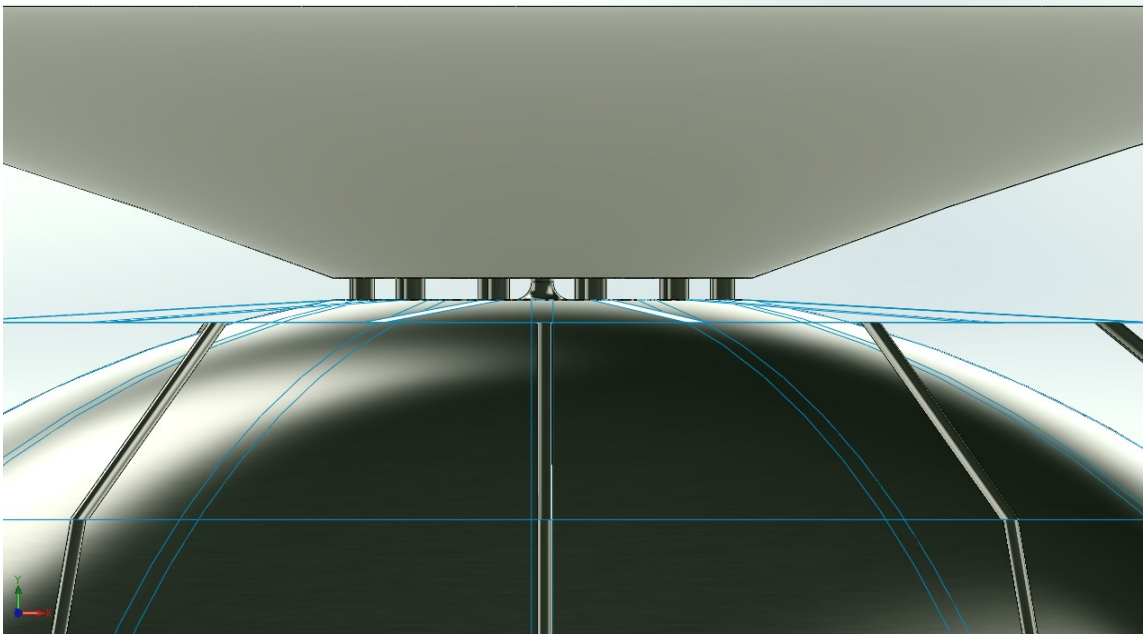
Figure 63: Side View of Actuators and Interface

There are twelve actuators, represented by hollow tubes around the periphery of the pellet injector interface (the pellet injector itself can be seen in the center in the figure above). These hollow tubes represent the gas pressurized container with bellows that house the actuator jacks. The next figure, taken from the Project Daedalus study, shows the mechanism inside the container that would provide for course correction.
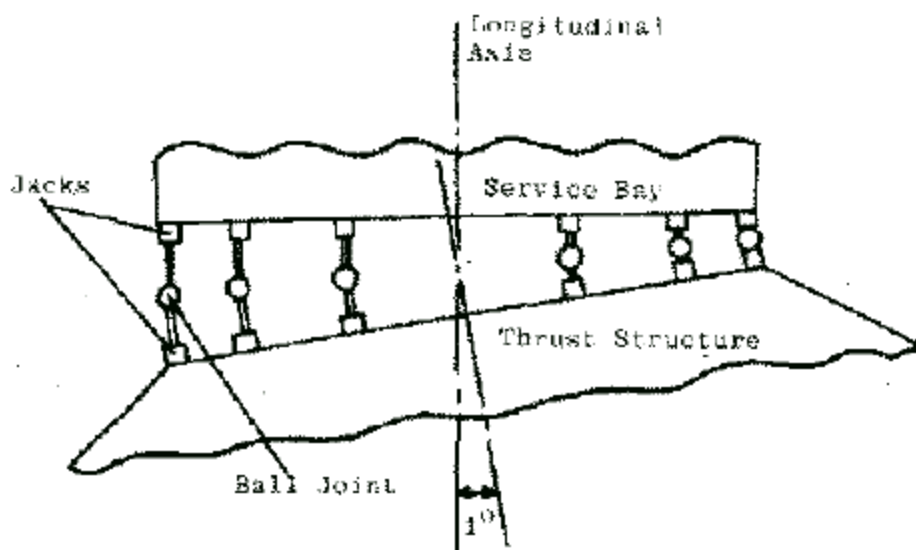
Figure 64: Thrust Vector Control System [1]

The mechanism consists of electrically driven ball screw actuators that can provide one degree of movement through the spacecraft's longitudinal axis. This proposed actuator design would provide movement of the reaction chamber and supporting structure, as would be required for course correction of the spacecraft. Redundant controls will need to be implemented in case one of the actuators fails, so as not to leave the overall course-correction mechanisms inoperable.

7.3 Pellet Injector Design and Interface

The pellet injector is connected directly to the interface plate on the reaction chamber. This would be attached via electron beam welding with fillet reinforcement to increase the weld efficiency to 100%. The fillet weld size would be determined during detailed design and calculations. Figure 65 shows a close-up view of the pellet injector and its interface to the reaction chamber.
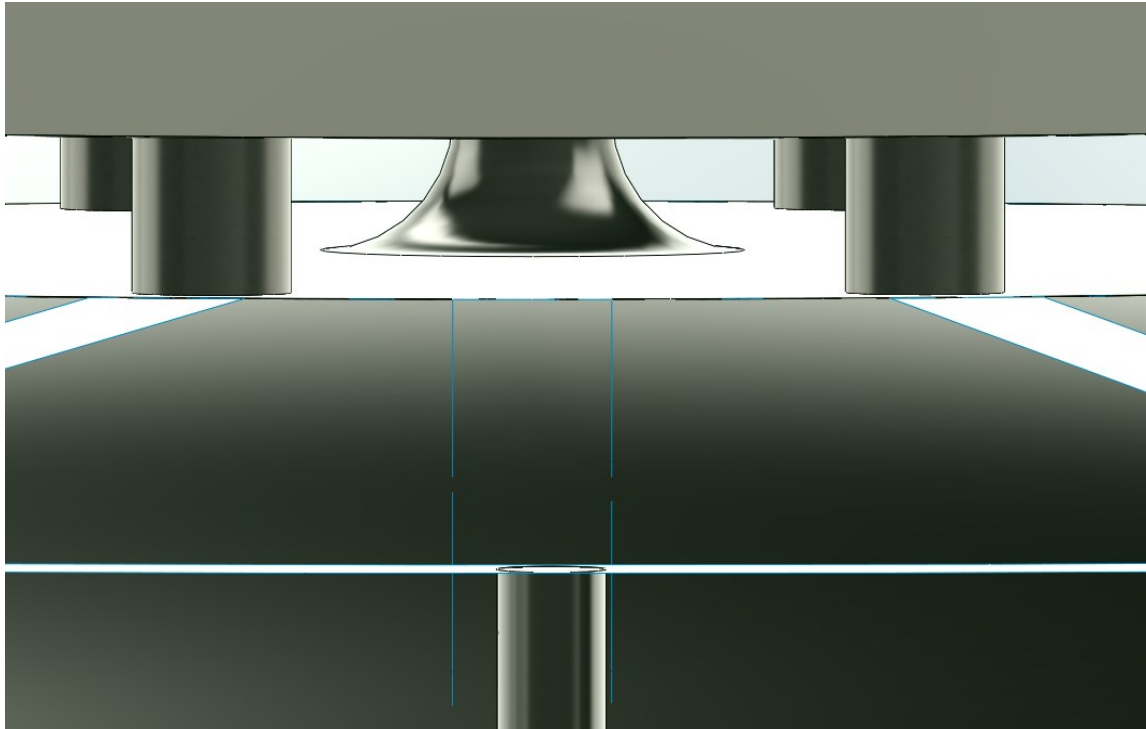
Figure 65: Pellet Injector and Interface to Reaction Chamber Thrust Structure Plate

The pellet injector can be seen gradually sloping down to the 0.010 inch thick thrust structure plate that is joined to the reaction chamber. This is representative of the fillet weld and connection to this plate. The next figure shows the pellet injector interface through the parabolic reflector.
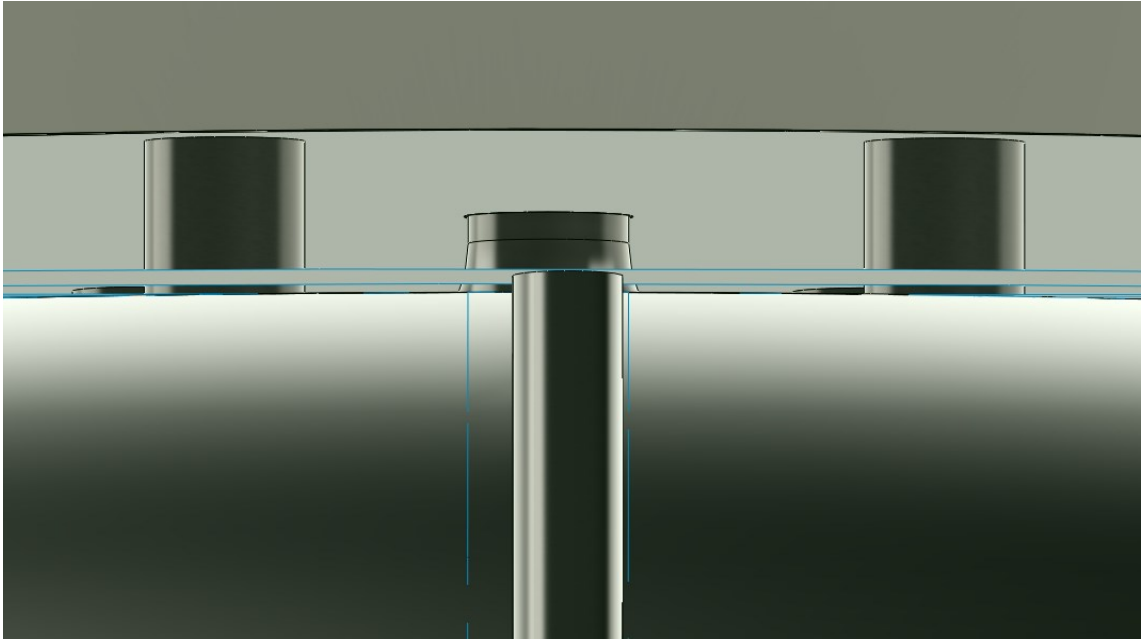
Figure 66: Pellet Injector and Interface through Parabolic Reflector

There is a clearance hole through the parabolic reflector for the pellet injector to feed

through. This clearance hole would be slightly bigger to allow for the one degree range of

motion for the actuator course-corrections. Figure 67 shows a top view of the pellet

injector feeding through the parabolic reflector. Although nothing above the parabolic

reflector is modeled or shown, this pellet injector would interface to a storage tank.
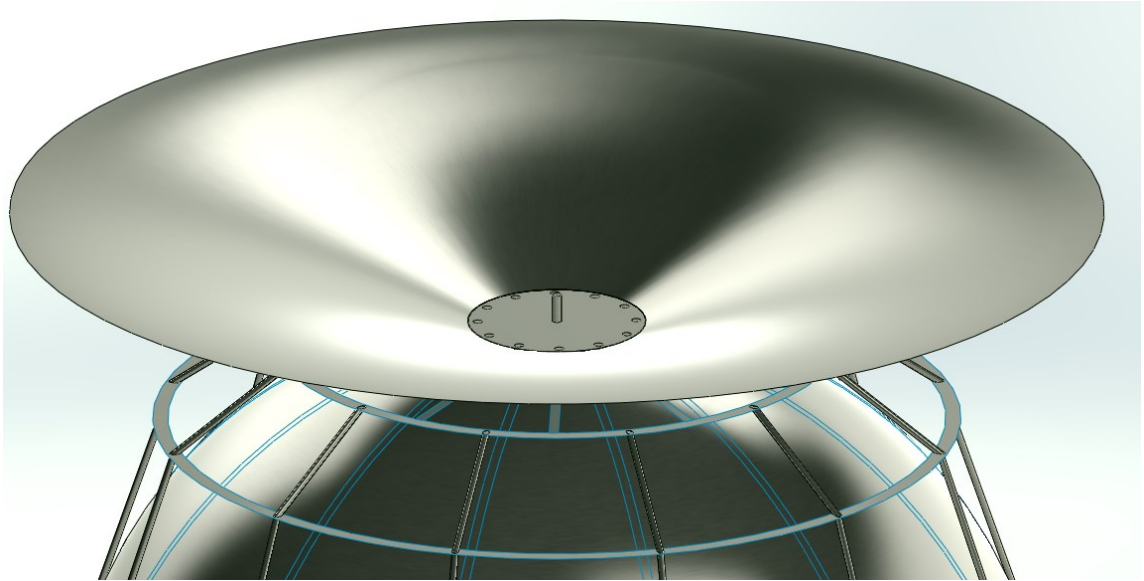
Figure 67: Pellet Injector Interface through Parabolic Reflector

The inner diameter of the pellet injector is kept true to the Daedalus pellet diameter

dimensions (1.580 inches). These parameters are taken from the Daedalus team's trade

studies into the nuclear fuel and propulsion.

8. Manufacturing and Testing Considerations for the Reaction Chamber and Supporting Thrust Structure

8.1 Reaction Chamber Material Specification

The material for the reaction chamber must be very robust. Necessary properties for this material, as outlined in Chapter 2, include a low density, high temperature capability, and very high electrical conductivity [1]. Present-day materials were researched, of which TZM alloy was picked as a starting alloy. The commercial-grade governing specification is ASTM B386, of which there are two different production processes of the TZM alloy with the same chemical composition. Type 363 is a vacuum arc-cast TZM and Type 364 is a powder metallurgy TZM. The impacts of these two production processes are explored.

8.1.1 Vacuum Arc-Cast TZM vs. Powder Metallurgy TZM

Most TZM alloys produced today are by sintering molybdenum powder via powder metallurgy methods. However, vacuum arc casting provides advantages over powder metallurgy when low gas content is desired [10]. Improvements in technique have made the gas content of sintering ingots about the same as vacuum arc-casting. Nevertheless, vacuum arc-casting would be the more conservative production choice as the chemical composition of TZM is very crucial in the anticipated operating environments.

Powder metallurgy products also exhibit tendencies to chip at the edges and develop pitted surfaces during finishing operations [10]. This fact also leads to the choice of vacuum arc-cast TZM as the preferred present-day choice of material.

8.1.2 Optimum Condition TZM vs. Recrystallized Condition TZM

A literature review of refractory materials shows research by the Southern Research Institute (SRI) on the different properties of optimum condition TZM and recrystallized condition TZM [8]. Tensile properties were measured from room temperature up to 3000 degrees Fahrenheit. As temperature increases, tensile and yield strengths are expected to drop significantly from the strengths quoted in specifications, which typically measure ideal conditions at room temperature.

Testing conducted by SRI is of particular interest as the operation temperature of the reaction chamber is estimated to be 1600 degrees Kelvin, or 2420 degrees Fahrenheit. This will provide an important correlation between the finite element model stress results (which are simulated at R.T.), compared to expected mechanical properties at the Icarus operating temperature.

Optimum condition in the study by SRI is hot-warm rolled and annealed for 1 hour at 2300 degrees Fahrenheit. The recrystallized condition occurs through heating at 2475 degrees Fahrenheit in a vacuum for one hour [8]. The minimum recrystallization temperature as stated by ESPI metals is 1652 degrees Fahrenheit [10]. A literature review states different recrystallization temperatures of TZM based on the source. It can be concluded, however, that the Icarus operating temperature of 2420 degrees Fahrenheit will be in the recrystallization temperature range for TZM, leading to crystal grain growth. ESPI metals [11] as well as work done by Nagae et al. [12] point towards the embrittlement of recrystallized TZM. The dynamic stresses on the reaction chamber will require a ductile material at elevated temperatures.

In the empirical study by SRI, for 0.040 inch TZM sheet in the optimum condition at 2500 degrees Fahrenheit, the average yield stress at 0.2% offset was 35.4 ksi. The average ultimate tensile strength was 41.7 ksi, with the average elongation in one inch being 10% [8].

Respectively, for 0.040 inch TZM sheet in the recrystallized condition at 2500 degrees Fahrenheit, the average yield stress at 0.2% offset was 15.1 ksi. The average ultimate tensile strength was 22.9 ksi, with the average elongation in one inch being 27% [8].

These test results from SRI indicate that optimum condition TZM provides a factor of 2.34 times greater yield strength than recrystallized TZM. However, the results also indicate that the average elongation of the recrystallized TZM is 2.7 times greater than that of the optimum condition. These results suggest that the recrystallized TZM provides greater ductility and less yield strength than the optimum condition. This is contradictory to other sources and studies, and will need to be investigated thoroughly experimentally for the Icarus operating temperatures and conditions.

8.1.3 Internally Nitrided TZM

There has been recent work by Nagae et al. in the conditioning of commercial-grade TZM for use in high temperature situations [12]. They have experimented with internally nitriding, specifically in two-step and four-step processes, commercial-grade TZM.

Testing done by Nagae et al. shows greater ductility in a four-step nitride TZM after recrystallization. This is compared to a recrystallized TZM specimen and a four-step nitride TZM specimen. Their testing also led to their conclusion that four-step nitriding of

TZM leads to yield strengths that are 2.6 times as large as the recrystallized specimen at 1773 degrees Kelvin. This is promising research. If TZM does show lower ductility and embrittlement at recrystallization temperatures, four-step nitrided commercial-grade TZM after recrystallization would be the best present-day material for use in the Reaction Chamber, offering better ductility and yield strength than the other TZM forms. However, this would be cautioned with the need for extensive testing of this form of alloy with the Icarus temperatures and properties of interest. There is no literature on the effects of the internal nitriding process to the electrical conductivity characteristics of TZM.

8.2 Reaction Chamber Modularity

At over 328 feet in diameter with a 0.043 inch wall thickness, the reaction chamber should not be manufactured as one solid sheet. Present-day manufacturing capabilities would not be able to make this one solid sheet formed to shape either. For manufacturing and maintenance considerations, the TZM alloy composing the reaction chamber should be joined (welded) together from multiple sheets.

In the Project Daedalus study, it is planned for a system of robotic 'wardens' to service the starship during its interstellar journey [1]. These wardens would be able to repair and replace parts. If the reaction chamber were theoretically to be made of one solid piece, a failure at a singularity could compromise the whole starship. However, use of several sheets formed and welded together will make the design modular, and enable the wardens to repair/replace failure or concern points.

Care must be taken where the reaction chamber is sectioned and joined by welding. It should not be joined in high stress areas, as it could lead to potential weld

failure. For instance, the reaction chamber should not be cut into slivers (similar to a pie) with the vertex coming together at the pellet injector interface, as this is a stress concentration area. Figure 68 shows a modular design of the reaction chamber that should not be considered, as it joins at the stress concentration point of the pellet injector interface.
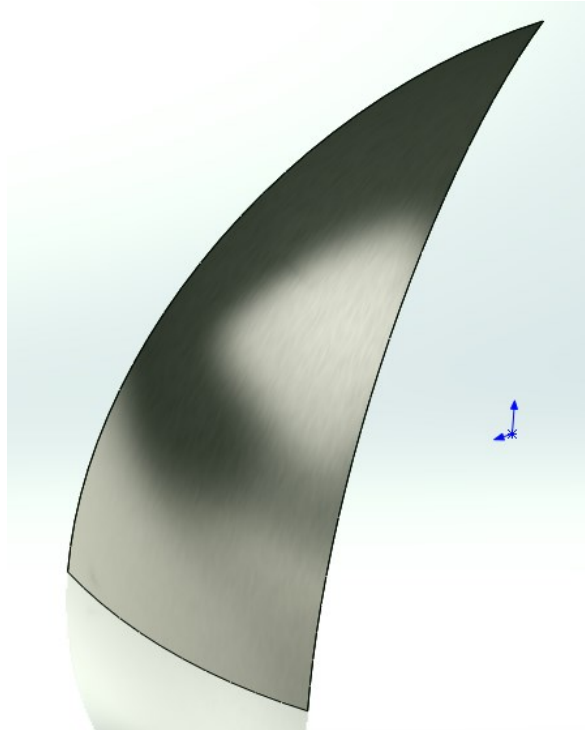
Figure 68: Modular Reaction Chamber Design that Produces Increased Stress Concentration at Weld Vertex

Rather, the sheets for the reaction chamber should be joined at low stress areas and reinforced (fillet or otherwise) as necessary to achieve 100% efficiency. As actual assembly of this spacecraft is still years in the future, a breakdown of the first stage spacecraft configuration into individual assembly parts (i.e. the reaction chamber broken up into X amount of sheets as opposed to one part) is not attempted.

8.3 Welding Considerations

There is only one form of welding that should be considered for the Icarus starship, high energy density welding. There are two forms of high energy density welding currently available, laser beam welding and electron beam welding. Both of these forms will produce full-penetration welds with narrow fusion and heat affected zones as well as little distortion.

8.3.1 Electron Beam Welding vs. Laser Beam Welding

Laser beam welding would not be an adequate welding process for the Icarus starship. The laser beam used in this welding process would be highly reflective against the refractory TZM material. Also, contaminants may be introduced in this process as it does not have to be performed in a vacuum.

Electron beam welding would be the only currently available process of consideration for the Icarus starship. This process would provide a narrow heat-affected zone, narrow fusion zone, and little distortion. This process requires a vacuum environment, which would work well for the Icarus assembly as that starship would have to be assembled in a space environment. This vacuum-environment would prevent the introduction of contaminants into the weld.

Research was conducted in the 1960s by the Navy Materials Laboratory in Philadelphia, PA [13] on the electron beam welding of refractory metals. Sheets of Ti-Mo alloy in thickness of 0.030 inches, 0.060 inches, and 0.125 inches were welded and studied. This was before TZM was available for study, but should be a good starting point for the efficiency and behavior of the EBW of Molybdenum alloys.

This study concluded that material alignment is critical and partially fused or undercut welds may result when the electron beam is only slightly off the seam [13]. Their test results indicate that the joint efficiency of their two 0.030 inch Ti-Mo specimens was an average of 65.1%. This efficiency would not be acceptable for the Icarus reaction chamber and would require fillet reinforcement to achieve 100% efficiency of the joint. Also, material and weld alignment would have to be closely and robotically controlled to avoid variances.

8.4 Assembly Considerations

The scale and complexity of the Icarus starship would require many moving elements for the assembly. Of specific mention would be the joining of the reaction chamber and thrust structure by electron beam welding, which requires a vacuum environment. If pieces of the reaction chamber and thrust structure were to be assembled on Earth, they would need to be transported piece-meal to space for assembly, as the Icarus starship is not meant to be launched from Earth's atmosphere. This would also require very special fixtures for vibration and transportation concerns. These facts would lead to assembly and production of the Icarus spacecraft and components in a space environment.

8.4.1 Lunar Base Staging

A lunar staging point would be a good starting point for the assembly of the Icarus spacecraft, with present-day considerations. There would be considerations that must be taken into account for staging on or near the Moon, such as protecting the Icarus components during assembly.

Also, the presence of helium-3 on the Moon for use in the nuclear fuel pellets makes a lunar base an attractive option. If we were able to establish a foothold on the Moon, we would be able to harvest this fuel for the reactions.

Parts could be manufactured/pre-assembled on the Moon and transported to near lunar orbit for final assembly of the Icarus spacecraft. Care must still be taken for transportation and the gravitational effects from the Moon, although much less than if it was from Earth.

8.5 Additive Manufacturing

In the last decade, great strides have been made in the area known as additive manufacturing, or more commonly 3D Printing. This contrasts to the more traditional subtractive manufacturing (i.e. mills, lathes, etc.). Most parts are made with a combination of methods, including CNC milling, extruding, molding, and forging.

NASA recently successfully manufactured a Nickel Alloy rocket engine part for their J2-x engine using additive manufacturing (specifically, selective laser melting) [15]. This is a step forward from traditional additive manufacturing using plastics. This part, and any future parts, have to be fully studied as to impact on properties from using the additive manufacturing process (tensile/compressive strength, hardness, and microstructure).

The attractiveness of additive manufacturing for Project Icarus is apparent, as this will allow for the custom manufacturing of parts both for initial builds, and as replacement parts. One possibility is to have this capability available in the second stage of the Icarus spacecraft. Replacement parts could be readily made in this payload bay by the robotic wardens (whether components are at the end of their service life or failure

scenarios may have occurred). This could significantly reduce added mass on the spacecraft resulting from any spare parts initially planned as part of the payload for the operations and maintenance budget.

There are many areas that require further research, such as using additive manufacturing without reliance on gravitational forces, scaling the additive manufacturing machines in size and weight to something that would be feasible for the Icarus spacecraft to transport, and developing a good cost/benefit ratio for usage of the additive manufacturing machines.

Several decades from now, this may be a feasible item to include as part of the Icarus payload.

8.6 Testing Considerations

With the complexity of the Project Icarus spacecraft, extreme care must be taken before its launch. Since the prototype will be the 'deliverable' unit to use industry terms, as much testing must be accomplished on the spacecraft parts and materials before the launch. Some of these considerations are presented next.

8.6.1 Material Testing and Variances

The materials used in the construction of the Icarus spacecraft must be thoroughly examined before being used in manufacturing, both pre and post manufacturing. This is to account for any variations from specified chemical compositions as per the engineering design teams. This will undoubtedly be a costly endeavor due to the scale of the Icarus spacecraft and the fact that there will be raw material that is rejected due to material variances.

8.6.2 Fatigue Testing

The expected cycles of the Icarus first stage reaction chamber and support structure are 30 billion cycles at 250 Hz over the course of 4.5 years of acceleration. This is magnitudes higher than traditional fatigue cycles/testing.

Some research prescribes to the theory that if stresses are maintained under a certain 'threshold', a material will not fail. However, recent research indicates that there is no fatigue strength 'threshold', and all materials will fail after a certain number of cycles.

Extra care must be taken to reduce stress concentrations and risers on the Icarus spacecraft. Scale model testing should be performed for the specified 30 billion operation cycles on the nominal model. Also, testing should be performed on variance models to deduce the effects of stress concentrations and risers on the scale spacecraft.

8.6.3 Nondestructive Testing of Welded Joints

High energy density electron-beam welding will be used to join most of the parts of the Icarus spacecraft. Some of these joints will be full-penetration, some will be partial-penetration, and some will be fillet reinforced. Non-destructive testing that is adapted to assembly in space must be used to certify the integrity and strength of these joints.

There are a myriad of NDT methods used for Earth-based testing, including visual inspection (VT), dye-penetrant inspection (PT), magnetic testing (MT), amongst others. However, for the materials of the Icarus spacecraft, only certain methods would be viable for the conditions present.

In a study by de Lacy [14] on the NDT for the Space Shuttle, an ultrasonic transmission reflection technique was mentioned for the NDT of coated refractory metals. Nondestructive evaluation methods for the coating required for the reaction chamber include eddy current, thermoelectric monitoring, and electron emission radiography, of which electron emission radiography is mentioned as the most valuable in the article.

For modularity of the spacecraft, in-situ NDT is also an important consideration. This would be performed by the robotic wardens for any parts that require replacement or service as dictated by failure or maintenance schedules. The capability of the wardens to perform Electron Beam Welding (EBW) would also be important for the servicing of the spacecraft's parts.

9. Conclusions and Continuing Work

9.1 Conclusions

This thesis develops for the first time a finite element model of the Icarus spacecraft reaction chamber, pellet injector structure, and stiffening framework. A finite element methodology is presented within the context of a static analysis and a modal analysis for a variety of configurations. Manufacturing and testing considerations are discussed.

The connection between the reaction chamber and the parabolic reflector (i.e. pellet injector interface) should have a sufficient surface area to react to the thrust loads from the nuclear reactions. In this thesis, the loading is uniformly distributed and assumed ideal, which would not be the case in actual operation. This further stresses the point that a larger surface area is needed as a 'fixture' point at the top of the reaction chamber for the reaction loads.

With the miniscule thickness of the reaction chamber as specified (0.043 inches), an integrally backed thrust structure is necessary to support the loading. Again, the finite element models used in this analysis assumed optimal loading. In the event of uneven loading, the integrally backed thrust structure would become more crucial in supporting the reaction chamber structure during operational loading.

Fatigue will play a very important role in the design of the Icarus spacecraft. With the current scheme of operations using nuclear pulse fusion, 30 billion cycles are expected to be incurred on the reaction chamber, which are magnitudes higher than traditional fatigue studies. Care must be taken to limit stress risers and concentrations in

the design, and to keep operating stresses on the spacecraft as low as possible to provide an adequate margin of safety.

Modularity, assembly, and testing of the spacecraft are crucial. The spacecraft must be sufficiently modular as to prevent a failure point from jeopardizing the whole starship, and also allow it to be replaced via the robotic wardens. Assembly of the spacecraft in space is also important, including planning for transportation and protection of the resources used in the assembly of the Icarus spacecraft. Next, testing of the spacecraft, whether on a component basis or at a system's level, becomes important to weed out any flaws before departure. This includes testing of any joints (welded, mechanical, or otherwise) by non-destructive testing. These methods, currently used in production on Earth, will have to be sufficiently adapted to be used in a deep space environment and also adapted to be automated and repeatable.

Last, but not least, material selection and properties for the Icarus spacecraft should come under careful scrutiny. In this thesis, this was started for the material for the reaction chamber. This careful analysis of material selection should include, amongst others, analysis of phase diagrams and variances in chemical compositions, interaction between different materials including expansion/contraction rates, high-cycle fatigue testing, thermal effects from elevated temperatures and radiation. This analysis into the material selection should be multidisciplinary and should include finite element modeling and testing with various permutations of the material and design.

9.2 Continuing Work

As Project Icarus is a forward-thinking design study, there are a lot of areas that will require significant research before interstellar missions become feasible. I will limit this continuing work section to areas that were touched upon in this analysis.

Evaluation and selection of materials to be used in the Icarus spacecraft must be gone through with a fine-tooth comb by a multi-discipline team. This will include assessing any material variances and effect on mission (including whether the material can still be used if there are any variances), assessing material properties at various temperature extremes expected to be encountered, weldability and weld efficiency of materials. Along with the evaluation and selection of materials comes research into variations and different alloys of those materials to improve physical properties (i.e. internal nitriding of commercial TZM alloy to increase yield strength and ductility).

Fatigue cycle testing to the specifications of the Icarus mission should be evaluated analytically and empirically if possible. This includes testing to the specified lifecycle limit under the Icarus operating and failure conditions. This fatigue testing will be a very important factor in determining the suitability of a material for use in the Icarus spacecraft.

Modal, frequency, and dynamic vibration analyses should be performed as the design progresses to ascertain any effects between operational pulse rates and natural modes of the structure. As it is very difficult to damp vibration in space, particular attention should be taken of any resonance reactions. Also, damping in space environments is an increasing area of research and should follow a parallel research path to the Icarus research, as it would be beneficial for the Icarus spacecraft design.

Assembly of the spacecraft should be closely reviewed including transportation of resources, protection of the assembly during construction, testing of the assembly, and modularity. This will require special attention to non-destructive testing methods in a deep space environment to determine the suitability of any welded joints, including permissible rework if any. This non-destructive testing should be automated (robotic) and repeatable, as to not allow for any human operator error.

The thickness of the reaction chamber, as well as whether a double-walled construction joined by ties and internally pressurized, should be closely evaluated. A dynamic compressive load could buckle the structure and should be researched. Such analysis will have a direct effect on mass of the spacecraft, as well as assembly and modularity, so this should be well-researched to determine what is necessary for the mission.

Factors of safety for the Icarus spacecraft should be well-defined, including factors of safety on yield/tensile strength for static operational loading, dynamic operational loading, fatigue loading, thermal loading, and any other defined properties affected from operation.

References

[1] A. Bond. *Project Daedulus.* In A.R. Martin, editor, *Journal of the British Interplanetary Society.* London, England, 1978.

[2] R.K. Obousy, *"Project Icarus: A Technical Review of the Daedalus Propulsion Configuration and Some Engineering Considerations for the Icarus Vehicle"*, Presented at the Advanced Space Propulsion Workshop in Colorado Springs, Colorado (2010).

[3] R.K. Obousy, *"Project Icarus: A 21st Century Interstellar Starship Study"*, Presented at the Tennessee Valley Interstellar Workshop November 28 & 29, Oak Ridge, Tennessee, 2011.

[4] Robert Swinney, Kelvin F. Long and Pat Galea *"Project Icarus: Son Of Daedalus — Flying Closer To Another Star — A Technical Update And Programme Review"*, JBIS 64 No.11/12 pp 358-371 (2011).

[5] ASTM Standard B386, 2003 (2011), "Standard Specification for Molybdenum and Molybdenum Alloy Plate, Sheet, Strip, and Foil," ASTM International, West Conshohocken, PA, 2011, DOI: 10.1520/B0386-03R11, www.astm.org.

[6] ASTM Standard B387, 2010, "Standard Specification for Molybdenum and Molybdenum Alloy Bar, Rod, and Wire," ASTM International, West Conshohocken, PA, 2010, DOI: 10.1520/B0387-10, www.astm.org.

[7] *SolidWorks and SolidWorks Simulation*, Dassault Systemes SolidWorks Corp., 2012, www.solidworks.com.

[8] Southern Research Institute. (1964). *Mechanical and Physical Properties of TZM Molybdenum Alloy Sheet and of Tungsten Sheet* (Bureau of Naval Weapons Contract No. N600(19)59530). Birmingham, Alabama: Clearinghouse for Federal Scientific and Technical Information, CFSTI.

[9] L.B. Lundberg. *A Critical Evaluation of Molybdenum and Its Alloys for Use in Space Reactor Core Heat Pipes.* Los Alamos Scientific Laboratory, Los Alamos, NM, 1981.

[10] ESPI Metals. Molybdenum Arc-Cast. http://www.espimetals.com/index.php/technical-data/109-molybdenum-arc-cast (January 02, 2013).

[11] ESPI Metals. Molybdenum TZM. http://www.espimetals.com/index.php/technical-data/155-molybdenum-tzm (January 16, 2013).

[12] Masahiro Nagae, Tetsuo Yoshio, Jun Takada and Yutaka Hiraoka *"Improvement in Recrystallization Temperature and Mechanical Properties of a Commercial TZM Alloy*

through Microstructure Control by Multi-Step Internal Nitriding", Materials Transactions, Vol. 46, No. 10 (2005) pp. 2129 to 2134.

[13] Edward F. Deesing. *Electron Beam Welding of Refractory Metals* (Bureau of Naval Weapons WEPTASK RRMA 02 018/200 1/R007 05 01). Naval Air Engineering Center Aeronautical Materials Laboratory, Philadelphia, PA, 1963.

[14] T.J. de Lacy. *Nondestructive Testing for Space Shuttle.* General Dynamics/Convair. San Diego, CA, 1970.

[15] John Hewitt. *NASA 3D prints rocket parts – with steel, not plastic.* http://www.extremetech.com/extreme/140084-nasa-3d-prints-rocket-parts-with-stell-not-plastic (April 01, 2013).

[16] *SolidWorks and SolidWorks Simulation Help*, Dassault Systemes SolidWorks Corp., 2012, http://help.solidworks.com/2012/English/SolidWorks/SWHelp_List.html?id=88724c64ce694d23a5c98d1955cdaaae#Pg0.

[17] Warren Young, Richard Budynas, and Ali Sadegh, *Roark's Formulas for Stress and Strain* (2011).

[18] S. Timoshenko, S. Woinowsky-Krieger. *Theory of Plates and Shells*. Second Edition, McGraw-Hill (1959).

[19] Walter D. Pilkey, *Formulas for Stress, Strain, and Structural Matrices.* Second Edition, John Wiley and Sons, Inc., Hoboken, N.J. (2005).